THE CHEMISTRY OF GROUP X TRANSITION METALS AND THEIR REACTIVITY WITH C_{60} AND MALEONITRILEDITHIOLATES.

by

Katy Landis

Submitted in Partial Fulfillment of the Requirements
for the Degree of
Master of Science
in the
Chemistry
Program

SCHOOL OF GRADUATE STUDIES
YOUNGSTOWN STATE UNIVERSITY
AUGUST 1998

6014
3

The Chemistry of Group X Transition Maleonitriledithiolates.

Katy Landis

I hereby release this dissertation to the public. I understand that this dissertation will be housed at the Circulation Desk of the university library and will be available for public access. I also authorize the University or other individuals to make copies of this dissertation as needed for scholarly research.

Signature:

Katy Landis 8/13/98
Student, Katy Landis Date

Approvals:

Larry S. Curtin 8/13/98
Larry S. Curtin, Ph.D., Thesis Advisor Date

8/17/98
Allen D. Hunter, Ph.D., Committee Member Date

Timothy R Wagner 8/13/98
Timothy R. Wagner, Ph.D., Committee Member Date

Peter J Kasvinsky 8/17/98
Peter J. Kasvinsky, Ph.D., Dean of Graduate Studies Date

Abstract

In the early 1990's, Drs. Fagan and Calabrese synthesized and characterized several nickel, palladium and platinum C_{60} complexes. Their work played a major role in defining the chemistry of C_{60}. Electrochemical techniques allowed them to propose a suitable mechanism and establish trends for the pattern of exohedral substitution to the C_{60} cage. The goal of this research is to extend Fagan and Calabrese's studies by bonding spectroscopically and spectroelectrochemically active ligands exohedrally to the C_{60} cage. This should enable the extent of communication between the phosphine ligand, the metal and the C_{60}.

The synthesis of a series of maleonitriledithiolate complexes of nickel, palladium and platinum phosphines having the formulae (dppe)M(mnt) and (PPh_3) M(mnt) (where dppe = $Ph_2PCH_2CH_2PPh_2$, mnt = 1,2-dicyanoethene-1,2-dithiolate and M = Ni, Pd or Pt) from the reaction of Na_2(mnt) and the appropriate (phosphine) MCl_2 is reported. These complexes were characterized by a combination of mass spectrometry, IR, UV-Visible and ^{1}H, ^{13}C and ^{31}P NMR. X-ray diffraction analysis of all three congeners revealed them to be isomorphous. Analysis of the diffraction data reveals that the metal centers are all square planar. In addition, characterization of the dppe complexes by single crystal X-ray diffraction reveals that the planar mnt ligands are tilted slightly away from the metal square planes.

A series of (C_{60})M(dppf) complexes (where dppf = 1-1'*bis*(diphenylphosphino) ferrocene and M = Ni, Pd or Pt) were synthesized and characterized using IR, UV-Visible and ^{13}C and ^{31}P NMR spectroscopy. The synthesis of these complexes are novel because the metal is reduced *in-situ*. These complexes are stable in air. The ^{31}P NMR revealed that the phosphorus is coordinated with the respective metal center and the ^{13}C NMR demonstrated the substitution of the C_{60} cage. Cyclic voltammetry was also performed on these complexes. The dppf ligand is irreversible chemically and electrochemically. The cathodic electrochemistry correlates well with that of Fagan and Calabrese's complexes. There are two cathodic waves which are chemically reversible, electrochemically quasi-reversible and are shifted with respect to E^0.

Acknowledgements

The first person that I must thank is my mother. She has made many sacrifices in her life for my sister and I, most of which are unknown to us. Her unrelenting support and encouragement has been, on many occasions, the beacon of light in a sea of darkness. Thank you.

My family has also supported me in many ways. My sisters, Liz and Anne, are my friends whose unconditional love and support are one of the constants in my life. Barb, being the excellent godmother that she is, is always watching out for me, caring for me in her silent way. My Uncle Donald has been a source of guidance for me. My twin sister Mary Louisa and her husband, Rob always give me a good laugh when I needed it and have been a loyal confidants. I want to express my sincere gratitude and love to all of my family.

I would also like to thank my friends. Francesca and Bill Filler have been my friends since my Temple days. I have found that working with Fran has been one of the most rewarding things that I have done in my life. I have learned a lot from her and thank her for her guidance. I would like to thank my friends from YSU: Julie Angelot, Chris Lowe, Greg Ciszewski and Marty Moore. They have helped make the transition to Youngstown easier and have added fun and humor to my life as a graduate student. I will miss them all after graduation.

The Curtin research group has also played an important role in my life and in my research. I will always be thankful for working with them and wish them all the best in life. Thank you, Mike, Jeff, Mary and Colleen.

I would also like to acknowledge the Chemistry department at YSU, especially Dr. Allen Hunter and Dr. Timothy Wagner for their guidance in research and for the contributions to our publication in Inorganica Chimica Acta, Dr. Sherri Lovelace for her friendship and suggestions in research, Dr. Renee Falconer for her friendship and providing an open mind when needed, Sue Viglione for her help. I would like to thank Carrie Slagle for her friendship. I have benefited from knowing her.

I would also like to thank YSU for their support, the Ohio Board of Regents and the National Science Fondation for the money necessary to maintain a research-oriented graduate school. I would also like to thank Dr. Robin McCarley at Lousiana State University for the mass spectrometry work that he has done for the Curtin research group. I would also like to thank Carrie Slagle for the ICP / AA work that was performed on this project.

The one person who deserves the most acknowledgement for this work is my advisor, Dr. Larry Curtin. He has always been an ideal advisor for me. He shares his office and computers with his group members, provides a supportive learning environment by always being there when he is needed. He has stood by my side in my failures and has celebrated my successes with me. He has provided me with the freedom to design and lead my own project, but has guided me and supported me every step of the way. Most of all, he has helped become a scientist and an individual, not just a graduate student with a project. I have been very lucky and I am thankful for the advisor that I was fortunate enough to work with. It has been a privilege and an honor to work for Dr. Curtin.

On a more personal note, I would like to thank Bone for his friendship. We have shared a lot of good times together, such as cutting out early on a Tuesday afternoon to go buy lottery tickets in West Virginia, barbequeing over an atom-splitting fire, the lost sweatshirt, long lunches, and most of all accompanying him to take his driver's test. Thank you, Bone, for your friendship.

Lastly, I would like to thank my husband, Chuck. His love and support have played an important part in my life and I am thankful that I was able to share graduate school as well as my life with him. I realize that I have been selfish and at times a prima donna in the lab, and I am glad that he has been able to tolerate me at home and at school. Thank you for the laughter, fun and love that has helped so much in school. This thesis is as much yours as it is mine.

Table of Contents

Title Page i

Signature Page ii

Abstract iii

Acknowledgements iv

Table of Contents vi

List of Tables ix

List of Figures x

Dedication xiii

Chapter 1 1 - 41

- 1.1 Literature Review 1 - 15
  - The history of C_{60}
  - Related exohedral metal-C_{60} compounds.
  - Applications of C_{60}
- 1.2 Cyclic Voltammetry 15 - 27
  - Electrochemistry of C_{60}
  - The electrochemistry of Fagan and Calabrese's complexes
- 1.3 Maleonitriledithiolates 27 - 33
- 1.4 Research proposal 34 - 37
  - Origination of the target complex: $(C_{60})M(mnt)$
  - Origination of the target complex: $(C_{60})M(dppf)$
- References Cited 28 - 40

Chapter 2 41 - 81

2.1 Introduction 41 - 42

2.2 Experimental Section 42 - 51

General experimental procedures

Synthesis of the (phosphine)M(mnt) complexes

Synthesis and Characterization of maleonitriledithiolate complexes of C_{60}

2.3 X-ray Diffraction Analysis 51 - 52

X-ray diffraction analysis of the title compounds

2.4 Results and Discussion 51 - 75

Synthesis and characterization of the (phosphine)M(mnt) complexes

X-ray crystallographic characterization of the (phosphine)M(mnt) complexes

Synthesis of C_{60}-(mnt)

2.5 Conclusions 75 - 78

References Cited 79 - 81

Chapter 3 82 - 107

3.1 Introduction 82 - 84

3.2 Experimental section 84 - 91

General experimental procedures

Synthesis of the 1,1'-(diphenylphosphino)ferrocene metal dichlorides

Synthesis of the 1,1'-(diphenylphosphino)ferrocene metal C_{60} complexes

3.3 Results and Discussion 91 - 104

Synthesis and characterization of the (dppf)M(C_{60}) complexes

Spectroscopic data

Electrochemistry

3.4 Conclusions 104 - 106

References Cited 107

Bibliography 108-111

Appendix 112

List of Tables

Table 2.1: IR data for the intermediate complexes and their starting materials. 59

Table 2.2: UV-Vis data for the intermediate complexes and their starting materials. 60

Table 2.3: ^{1}H NMR data for the intermediate complexes and their starting materials. 61

Table 2.4: ^{13}C NMR data for the intermediate complexes and their starting materials. 62

Table 2.5: ^{31}P NMR data for the intermediate complexes and their starting materials. 63

Table 2.6: Crystal data and and structure refinement. 66

List of Figures

Figure 1.1: Accepted structure of C_{60} (buckminsterfullerene). 2

Figure 1.2: Proposed structures for C_{20}, C_{70}, C_{80} and $C_{120.}$ 3

Figure 1.3: Diagram of the 5'-6' bonding site and 6'-6' bonding site on the cage of C_{60}. 5

Figure 1.4: Examples of exohedral organic complexes of C_{60}. 8

Figure 1.5: Monomers used in forming C_{60}-based polymers. 9

Figure 1.6: Metal binding to C_{60}. 11

Figure 1.7: The synthesis strategy used by Fagan and Calabrese. 12

Figure 1.8: Orbital compatibility diagram. 13

Figure 1.9: The cyclic voltammetry experiment. 20

Figure 1.10: Cyclic voltammetry of C_{60}. 25

Figure 1.11: Cyclic voltammetry of Fagan and Calabrese's products. 26

Figure 1.12: The structure of sodium maleonitriledithiolate. 28

Figure 1.13: The synthesis of sodium maleonitriledithiolate. 30

Figure 1.14: The structures of TTF and BEDT-TTF. 31

Figure 1.15: Crystal structure of $Ni(mnt)_2^{2-}$. 32

Figure 1.16: Nondegenerate orbitals of $Ni(mnt)_2^{2-}$. 33

Figure 2.1: List of compound numbers. 44

Figure 2.2: Synthesis of intermediates. 45

Figure 2.3: Synthesis of C_{60}-metal-mnt. 49

Figure 2.4: Synthesis of C_{60}-mnt. 50

Figure 2.5: IR of (dppe)Pd(mnt). 54

Figure 2.6: UV-Vis of (dppe)Pd(mnt). 55

Figure 2.7: ^{1}H NMR of (dppe)Pd(mnt). 56

Figure 2.8: ^{13}C NMR of (dppe)Pd(mnt). 57

Figure 2.9: ^{31}P NMR of (dppe)Pd(mnt). 58

Figure 2.10: Mass Spectrum fragments of (dppe)Ni(mnt). 65

Figure 2.11: ORTEP plot for (dppe)Ni(mnt) complex, 50% ellipsoids, perspective view. 69

Figure 2.12: ORTEP plot for (dppe)Pd(mnt) complex, 50% ellipsoids, view in the square plane. 70

Figure 2.13: ORTEP plot for (dppe)Pt(mnt) complex, 50% ellipsoids, view in the square plane. 71

Figure 2.14: Unit cell of (dppe)Pd(mnt). 72

Figure 2.15: Mass Spectrum of C_{60}-mnt. 73

Figure 2.16: Thermal gravimetric analysis of C_{60}-mnt. 74

Figure 2.17: UV-Vis of C_{60}-mnt. 76

Figure 2.18: IR of C_{60}-mnt. 77

Figure 3.1: Structure of diphenylphosphino ferrocene. 83

Figure 3.2: Structure of (dppf)M(C_{60}). 85

Figure 3.3: List of compound numbers. 88

Figure 3.4: Synthesis of (dppf)MCl_2 89

Figure 3.5: ^{31}P NMR of (dppf)Pd(C_{60}). 93

Figure 3.6: ^{13}C NMR of (dppf)Pd(C_{60}). 95

Figure 3.7: UV-Vis of (dppf)Pd(C_{60}). 96

Figure 3.8: IR of (dppf)Pd(C_{60}). 98

Figure 3.9: Anodic Voltammetry of (dppf)Pd(C_{60}). 99

Figure 3.10: Cathodic Voltammetry of (dppf)Pd(C_{60}). 100

Figure 3.11: Multiple Scan Rates of (dppf)Pd(C_{60}). 103

Figure 3.12: Electrochemical Irreversibility of (dppf)Pd(C_{60}). 105

This thesis is dedicated to my mother, who worked so hard to help me through school and to the "men" in my life. My husband, Chuck, who has also put a lot of hard work in this thesis and to my advisor, Larry, who has given me the freedom to grow both scientifically and personally.

Thank you.

Chapter 1

Introduction

1:1 Literature Review

1:1.1 The History of C_{60}.

Fullerene science and technology has become one of the most exciting branches of chemistry in the past decade. Smalley and Kroto's discovery of fullerene catapulted this field of chemistry to the forefront of industrial technology and academic interest. The increasing availibility of C_{60} has opened new frontiers for scientists to explore.

Buckminsterfullerene (C_{60}) is classified as the third allotrope of carbon, diamond and graphite being the other two.[1] The existence of a third allotrope of carbon was speculated about for many years prior to the initial discovery of C_{60}. In 1970, the Japanese team of Osawa and Yoshida proposed an unusual soccer ball shaped model as the structure of C_{60} and included it in their book on aromatic compounds. They theorized that this structure would be extraordinarily stable and would possess qualities similiar to those of aromatic molecules.[2] By the mid-1980's, laser vaporization cluster techniques were developed by Smalley, allowing for the simulation of stellar nucleation conditions. By exploiting this new technique, Smalley, et al., were able to make reasonable speculations about the structural nature of buckminsterfullerene (Figure 1.1).[3]

The most common form of fullerene is C_{60}, although the term fullerene refers to a class of compounds with even numbers of carbon atoms that range in size from twenty to an infinite number. In the latter case, the carbons form extended sheets of fullerenes, called Bucky tubes. The proposed structures for several fullerenes are given in Figure 1.2. Fullerenes were named after Buckminster Fuller, who first utilized a geodesic dome pattern in architectural designs.[4]

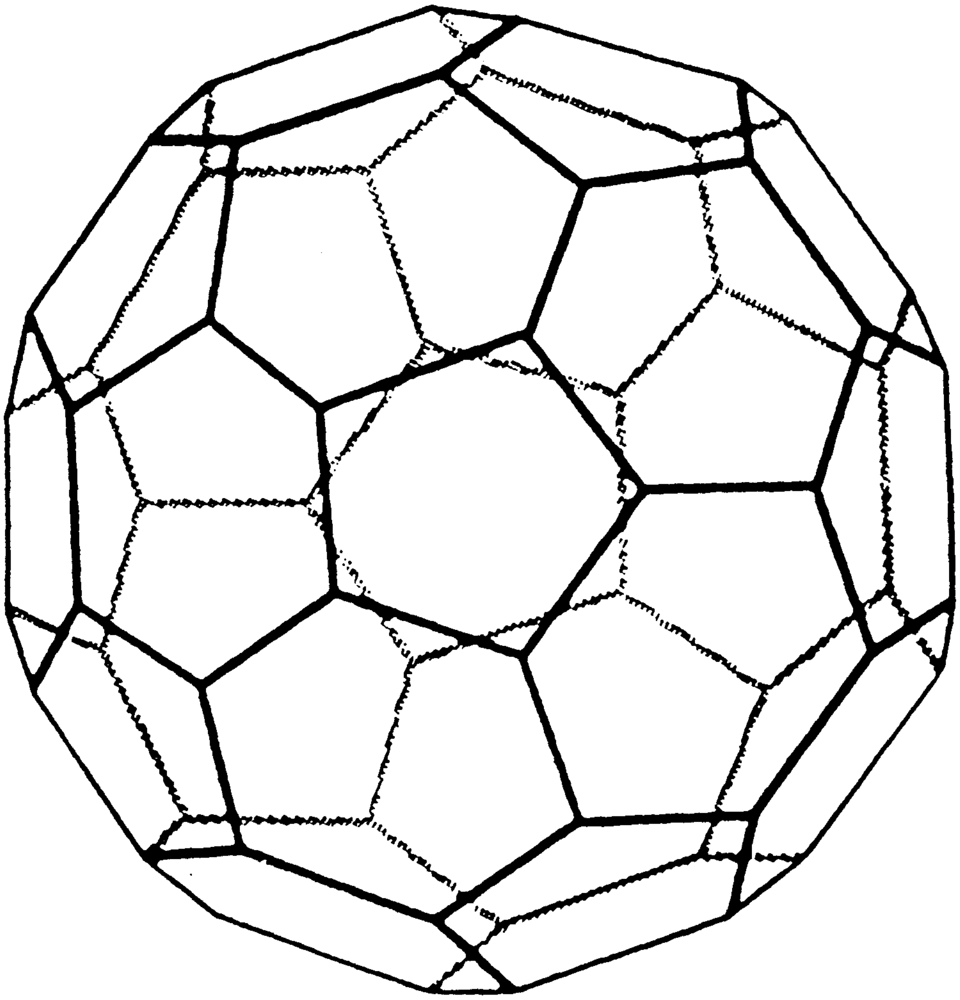

Figure 1.1: Accepted structure of C_{60} (Buckminsterfullerene).

Landis, M.L. Master's Thesis, Temple University, 1996.

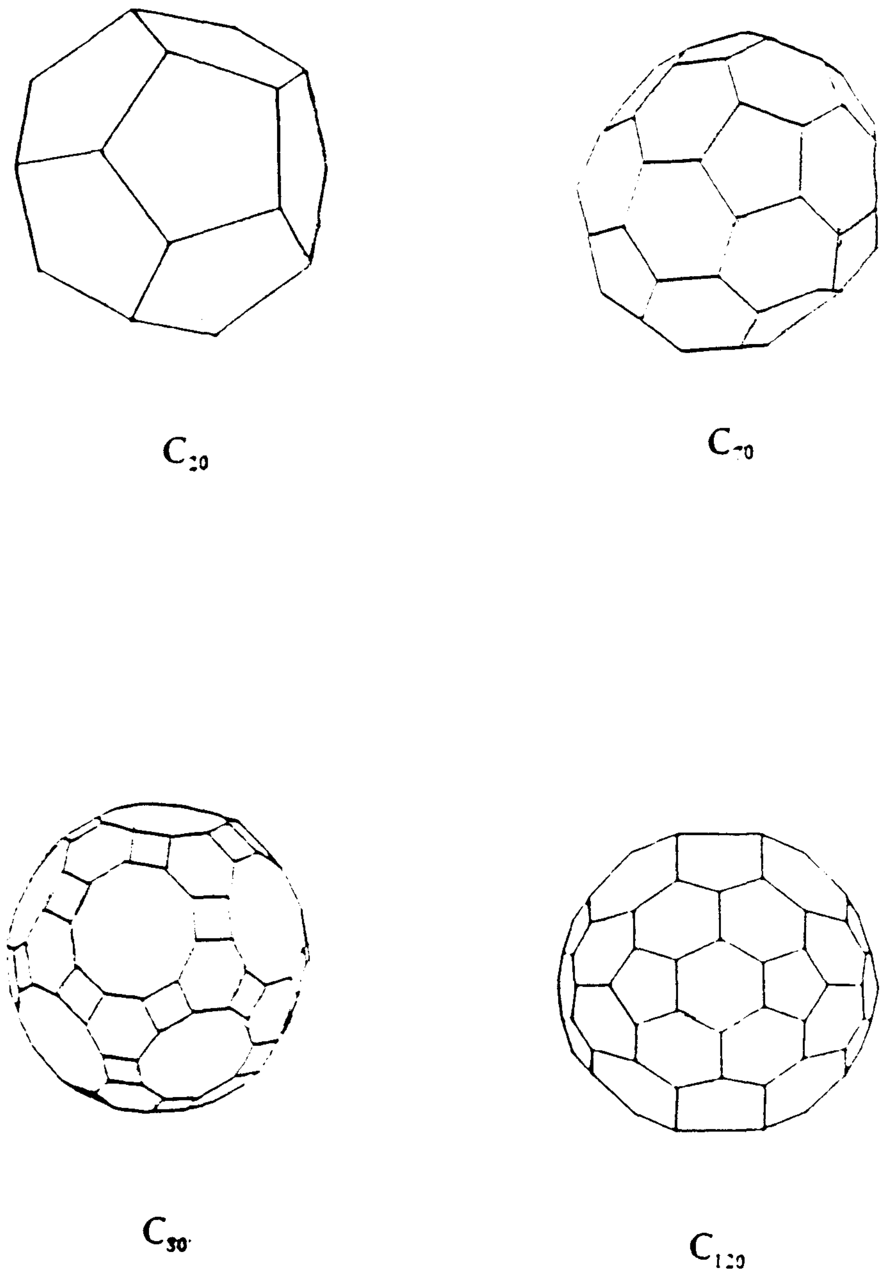

C_{20} C_{70}

C_{80} C_{120}

Figure 1.2: Proposed structures for C_{20}, C_{70}, C_{80}, and C_{120}.

Landis, M.L. Master's Thesis, Temple University, 1996.

C_{60} was first isolated in the vapor phase by Smalley, Kroto and Curl. They proposed that it had an unusual geodesic dome-like pattern that consisted of twelve pentagonal faces and twenty hexagonal faces. The model proposed by Kroto for C_{60} (Figure 1.1) became universally accepted by the scientific community after it's structure was confirmed via single crystal X-ray diffraction analysis.[5]

The highly symmetrical icosohedral geometry of C_{60} gives rise to unique electronic properties. All of the carbon atoms in C_{60} are equivalent and form one double bond and two single bonds with their neighboring carbons. The frontier orbitals of C_{60} are uniquely characteristic. The h_u HOMO displays a five-fold degeneracy, while the t_{1u} LUMO is triply degenerate.[6] Ultraviolet photoelectron spectroscopic (UPS) studies of C_{60} revealed it to be a closed shell species with an appreciable HOMO-LUMO gap of 1.5 - 2.0 eV.[6] C_{60} is also known to have the lowest electron affinity (2.6 - 2.8 eV) of any carbon cluster. The close correlation between the UPS data and most previous electronic structure calculations strongly supports the spheroidal shell model for the soccer ball shaped C_{60}.

There are two main classes of substituted C_{60} complexes. The large space inside of the central cavity affords the opportunity for insertion of a variety of atoms and small molecules inside the C_{60} cage. These complexes are called endohedral complexes. Exohedral complexes of C_{60} are compounds in which substituents are bonded to the exterior of C_{60}. There are two types of bonding sites on the C_{60} cage, one across the 6-6' bonding site and one across the 5-6' bonding site (Figure 1.3). The presence of two bonding sites is fortuitous because it allows for a wide variety of substituents to be attached in an exohedral fashion. Organic substituents, such as azides, favor bonding across the 5-6' sites as they have the appropriate bond length to preserve the geometry of the organic ligand.[7] Transition metals and other inorganic substituents display a preference to bond across the 6-6' sites because their geometries allow for backbonding to the *d* orbitals of C_{60}.[8] C_{60}-containing polymers are also included with the exohedral

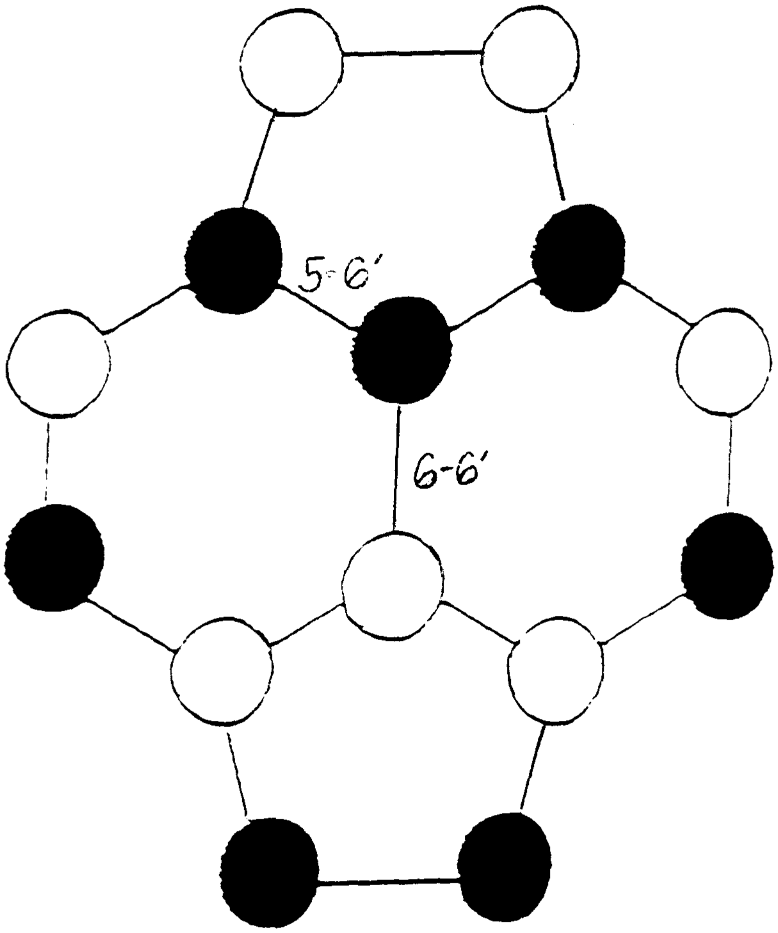

Figure 1.3: Diagram of the 5-6' Bonding Site on the Cage of C_{60}.

Landis, M.L. Master's Thesis, Temple University, 1996.

class of complexes. In addition, alkali metal doped C_{60} materials have been extensively studied for their superconducting properties.

Metal containing endohedral complexes were studied by Heath et al.[9] The metal atoms were directly encapsulated in the interior of the C_{60} cage. Other substituents, such as halogens, alkali metals, and small organic molecules have also been incorporated into the C_{60} sphere.[9] The enthusiasm over this area of fullerene science is primarily due to the ability to study metal atoms in an undisturbed environment. Metal atoms inside of a fullerene cage have the advantage of being free from ligand and/or solvent effects and can therefore exist in their formal oxidation state. The properties of metals under these unique conditions can be determined spectroscopically.[9]

Characterization of endohedral complexes of C_{60} has proven to be problematic for several reasons. The largest drawback in the study of endohedral metal complexes of C_{60} is that their solubilities are very limited in most solvents. Thus, isolation and purification is difficult. In addition, the synthetic mechanism is not well understood providing further obstacles in the rational design and characterization of endohedral C_{60} complexes. This division of C_{60} chemistry is still widely studied and the promise of pure endohedral metal complexes is eagerly anticipated by both synthetic chemists and spectroscopists.

Exohedral complexes have a number of significant advantages over endohedral complexes. The primary advantage is that exohedral ligand attachment generally imparts increased solubility, yielding compounds that are easily purified. Thus, materials for single crystal X-ray analysis can be obtained, allowing unambiguously structural determinations of the complexes. Exohedral complexes are also generally easier to characterize because the ligands typically are spectroscopically active. In addition, there are a greater variety of complexes available because of the different bonding modes that are present on the cage of C_{60}.

Dr. Amos Smith and other scientists have synthesized and attached organic ligands, such as alkyls, carbenes, oxygen and carbynes to the exterior of the fullerene cage[9]. The primary organic reactions, such as hydrogenation, halogenation, amination and epoxidation are the most frequently used pathways to exohedrally substitute C_{60} with organic ligands (Figure 1.4).[10]

Fred Wudl and his associates are one of the leading research groups at the forefront of exohedrally substituted C_{60} chemistry. His most valuable contribution was an extensive list of fullerene activity and coordination chemistry. Wudl studied the reactivity of C_{60} with amines, thiolates, phenoxide, cyclopentadiene, furan, isobenzofuran, anthracene and phenyldiazomethane.[11] These studies demostrated the electrophilicity, dienophilicity and dipolarophilicity of C_{60} to the scientific community.[11] His work in the study of the thiolate and amine substituted C_{60} proved to be difficult and remains unpublished materials. Wudl had difficulty with the mixture of compounds and the characterization of the products. These problem still plague fullerene chemists today.

Polymers of C_{60} were also prepared by Wudl and his associates.[12] The main purpose of incorporating C_{60} into polymers is to enhance the polymer's conductivity. Two of the most important C_{60} polymers made by Wudl's group are the PNP and CBP polymers. The PNP polymers are an arrangement of fulleroids that are used as the backbone of the polymer and the CBP polymers are macromolecules with fulleroids dangling off as pendants from the main polymer backbone. The PNP polymers were labeled "pearl necklace" polymers due to their resemblence to pearls neatly strung together and the CBP polymers, with their loosely hanging pendants, are aptly named the "charm bracelet" polymers[12] (Figure 1.5).

The principle problem encountered in this work was limited solubility. Attachment of solubilizing groups would help to alleviate this problem, however, the conductivity of polymers are greatly affected by such substituents. Polymer scientists are currently developing strategies for the attaching ligands that enhance polymer solubility as well as conductivity.

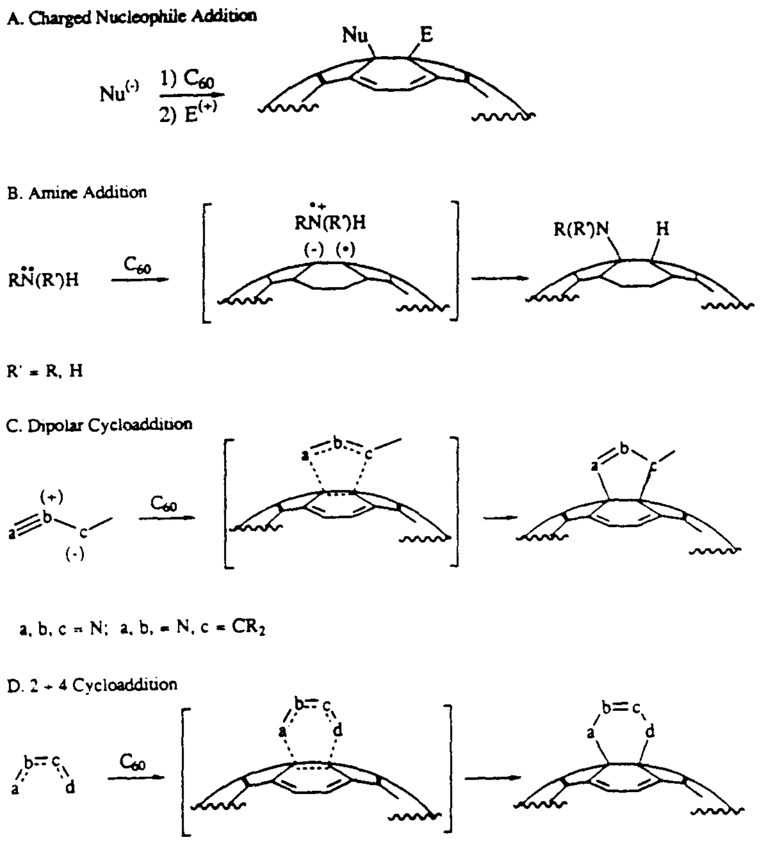
A. Charged Nucleophile Addition
Nu
E
Nu(-)
1) C60
2) E(+)
B. Amine Addition
RN(R')H
C60
RN(R')H
(-) (•)
R(R')N
H
R' = R, H
C. Dipolar Cycloaddition
(+)
a
b
c
(-)
C60
a, b, c = N; a, b, = N, c = CR2
D. 2 + 4 Cycloaddition
a
b
c
d
C60

Figure 1.4: Organic Exohedral C_{60}-Complexes.

Landis, M.L. Master's Thesis, Temple University, 1996.

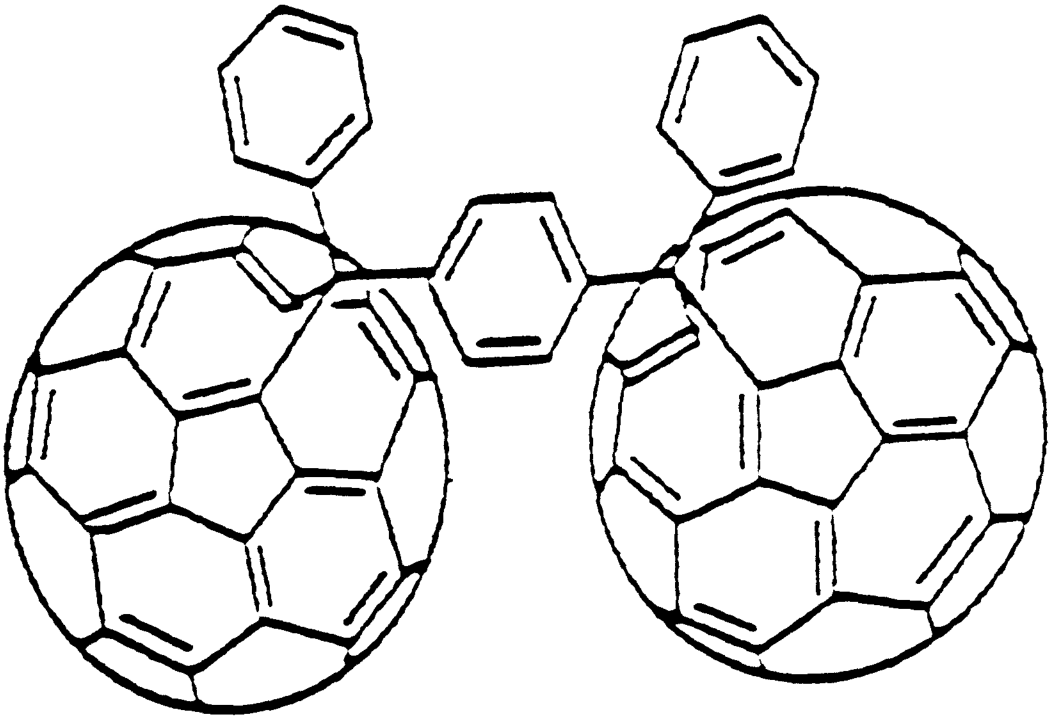

Figure 1.5: Monomer used in Forming C_{60}-Based Polymers.

Wudl, F., *Acc. Chem. Res.*, **1992**, *25*, 157 - 161.

1.1.2 Related Exohedral Metal-C_{60} Compounds.

Development of a large scale synthesis of C_{60} has allowed inorganic and organometallic chemists to explore it's reactivity with low valent transition metals (Figure 1.6). C_{60} was originally believed to be an unreactive sphere and the true chemistry of C_{60} remained ambiguous until Hawkin's osmium tetraoxide complexes were published early in 1991.[13] Also in 1991, Fagan et al. published papers outlining their discovery of exohedrally bonded metal complexes of fullerene. Fagan and Calabrese developed a pilot project that centered on the reactivity of C_{60} with organometallic ruthenium and platinum reagents. They discovered that the binding of ruthenium to planar arenes is very strong and that C_{60} reacted in a very similar fashion. Ruthenium complexes that were originally coordinated with three acetonitrile molecules displaced one acetonitrile upon coordination with C_{60}. These results led Fagan to the conclusion that C_{60} was chemically related to electron-deficient alkenes and that organometallic compounds, such as zero-valent platinum complexes, should form strong bonds to C_{60}. They were able to illustrate that the icosahedral geometry inherent to the C_{60} framework is ideal for dihapto-bonding to a transition metal. This project clearly demostrated that metals could be directly bonded to the C_{60} cage and was the groundwork for their future investigations.[14]

In 1991, Fagan and Calabrese published the single crystal X-ray diffraction profile of an exohedral zero-valent Pt-C_{60} complex of the form $(PPh_3)_2Pt$-C_{60} (Figure 1.7). The single crystal X-ray study demonstrated that the platinum remained platinum in the zero valent state and was bound across the 6-6' bonding site. This was not an unexpected result because the bond distance across the this bonding site is close to that of an electron deficient arene and allows for backbonding to occur (Figure 1.8). Their findings were confirmed via NMR, mass spectrometry and single crystal X-ray diffraction. Analysis of the diffraction data shows that the carbon atoms participating in the metal-C_{60} bond are distorted out of phase with respect to the other carbon atoms. One effect of metal coordination to an alkene is that the four groups attached to the alkene bend back away

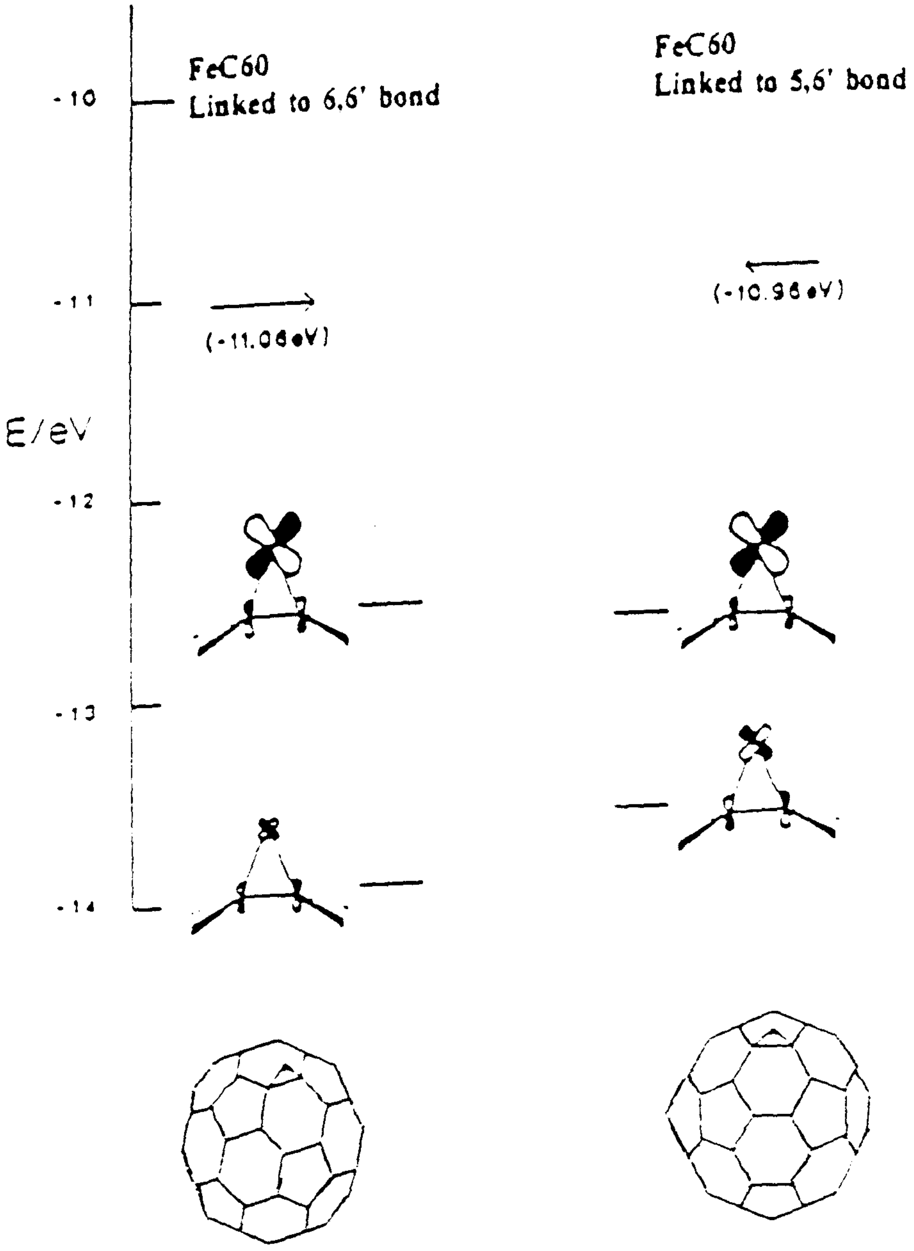
FeC60
Linked to 6,6' bond
FeC60
Linked to 5,6' bond
-10
-11
-12
-13
-14
E/eV
(-11.06eV)
(-10.96eV)

Figure 1.6: Metal Binding to C_{60}.

Landis, M.L. Master's Thesis, Temple University, 1996.

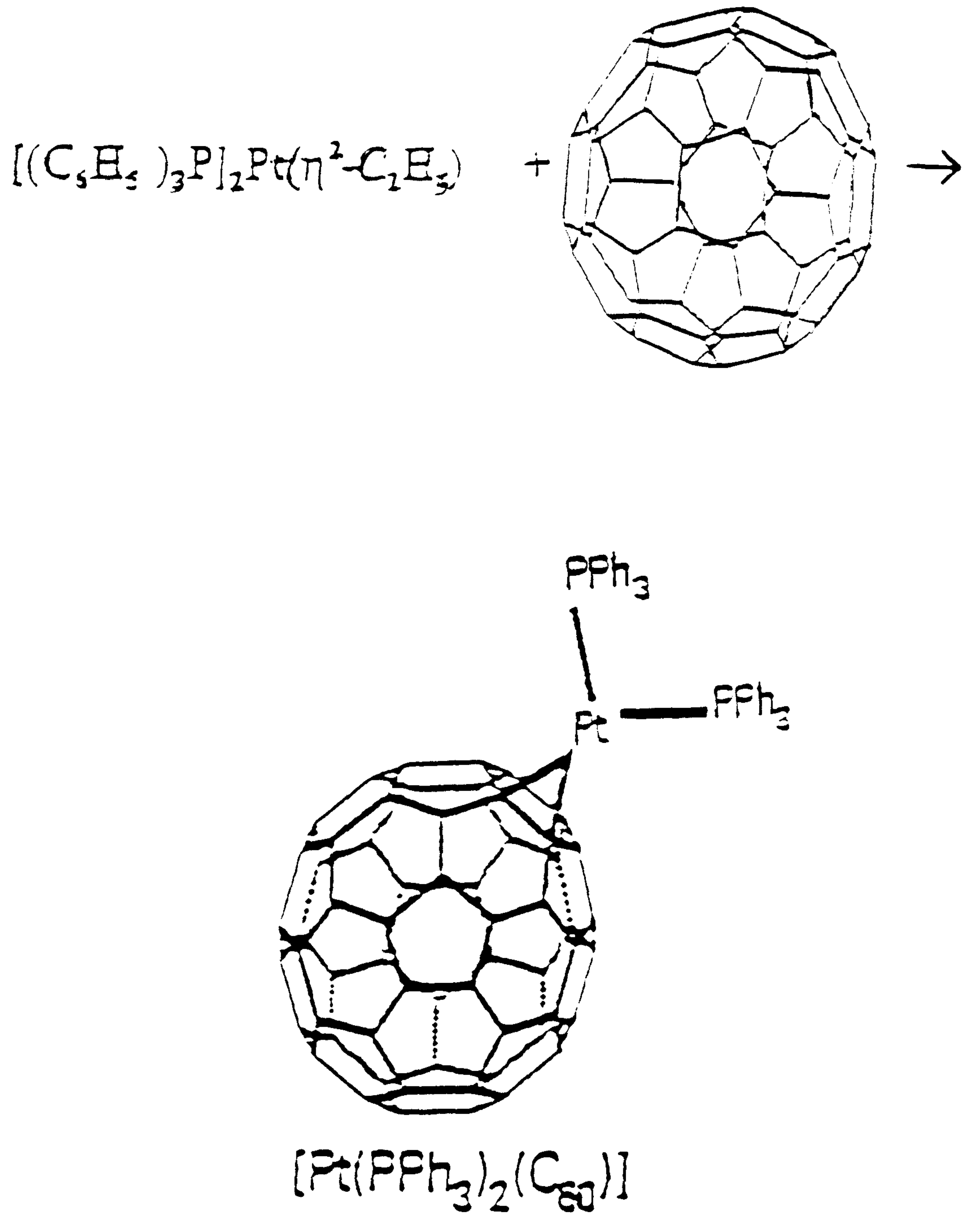
[(C5H5)3P]2Pt(η2-C2H5)
+
→
PPh3
Pt
PPh3
[Pt(PPh3)2(C60)]

Figure 1.7: The Synthesis Strategy used by Fagan and Calabrese.

Fagan, P. J.; Calabrese, J. C.; Malone B., *Science.*, **1991**, 252, 1160 - 1161.

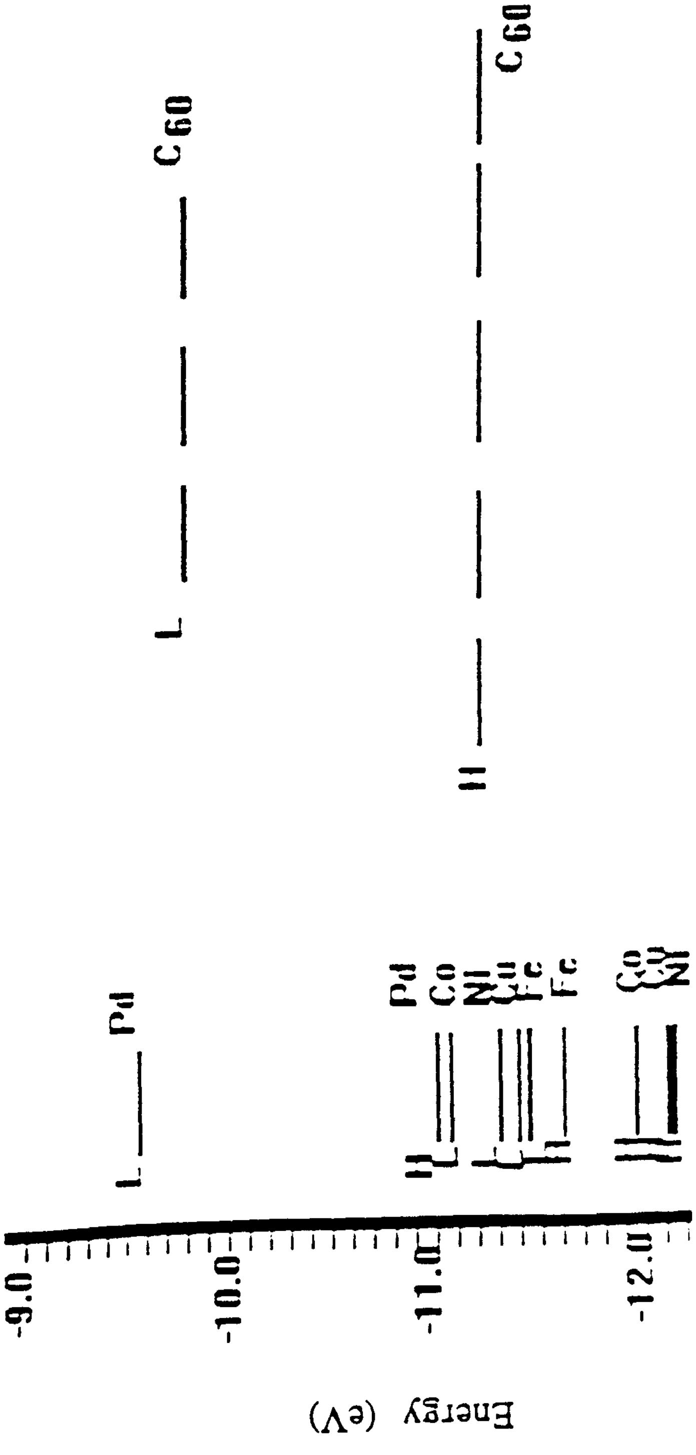
C60
C60
L
H
Pd
Pd
Co
Ni
Fe
Fe
Co
Ni
-9.0
-10.0
-11.0
-12.0
Energy (eV)

Figure 1.8: Orbital Compatibility Diagram.

Landis, M.L. Master's Thesis, Temple University, 1996.

from the metal. The fact that the platinum atom bonds across the 6-6' bonding site is rationalized because the they are shorter than the 5-6' bonds and contain the most double bond character. Platinum atoms are able to pull two carbon atoms out of the sphere and this significantly lengthens the carbon-carbon bond to which it is attached. This effect is less pronounced in the palladium derivative and even less so in the nickel derivative. Upon coordination to the transition metal, the six membered rings in C_{60} become more aromatic-like in nature.[15]

In addition, Fagan and Calabrese synthesized a series of multiply substituted C_{60} complexes by varying the stiochiometric ratios of the reactants. The substituents on the hexa-substituted C_{60} complexes are in an octahedral array. This was determined by single crystal X-ray diffraction analysis. Fagan also established that the subsequent addition of each metal atom causes C_{60} to become more aromatic in nature and the metal fragments become more labile and equilibrate on and off the C_{60} surface. The increase of metal substitution readily decreases the electron affinity of the C_{60} complex which makes the subsequent coordination of other electron-rich metals more difficult. Removal of a double bond from a conjugated system causes a decrease in the energy of the LUMO and consequently lowers the electron affinity of the whole molecule.[16]

1.1.3 Applications of C_{60}.

Potential applications of C_{60} have been extensively explored. One area of interest is that of photo conductors. Doped fullerenes and fullerenes with addenda have lost their center of inversion and can therefore expect to have an 2x response as a non-linear optical material. C_{60} has also been used as a lubricant in an industrial capacity.[18] Other practical applications of C_{60} include: high-surface area catalysts, optical sensors, ferromagnetic complexes, rocket propellants, high-strength microfibers, carriers of radioactive isotopes, semiconductors, high-temperature superconductors, and fullerene-based conductive polymers.[18] These are only some of the infinite examples of the all of the possibilites that have come about in the ever-growing field of fullerene science and technology.[17]

The most promising superconductive materials made from C_{60} are the alkali metal doped fullerides. C_{60} has superconductive properties when complexed with $A_{3-x}B_x$, where A and B = K, Rb, or Cs to form $A_{3-x}B_x C_{60}$. With these complexes, C_{60} is triply reduced and half fill the degenerate LUMO states of C_{60}. This may allow the metal fulleride to behave as a superconductor. Rb_3C_{60} also has the highest transition temperature of lower element materials, and the highest reported T_c of any organic superconductor. While the T_c's for the metal fulleride are still lower than the highest T_c's reported for some copper oxides, these metal fulleride complexes represent an entirely new division of superconductors, because they differ from oxide and organic superconductors chemically, electronically and structurally.[18]

1.2 Cyclic Voltammetry

Cyclic voltammetry is a multifaceted electroanalytical technique which is valuable in the analysis of many different compounds. Organic chemists use it to study biosynthetic patterns and electrochemically generated free radicals. Inorganic chemists find it useful to explore the effects of ligands on the oxidation / reduction states of central metal ions in complexes or in multinuclear clusters. Physical chemists employ this technique to model and obtain information in the study and determination of chemical and electrochemical mechanisms. Analytical chemists find cyclic voltammetry particularly useful as a means of quantifying analyte concentration and in the study of electron transfer pathways (i.e. kinetic) and the identification formal potentials (E°)'s, which are unique properties of compounds.[20]

Cyclic voltammetry has several advantages over many electrochemical techniques which include: the small amount of analyte needed to perform the experiment, a high degree of sensitivity, simple data analysis and interpretation and the relative ease with which the experiment is performed. A typical cyclic voltammetry experiment includes working, reference and counter electrodes, a cell in which the electrodes are contained, an electrolyte solution containing the analyte and a potentiostat. Modern potentiostats typically include a computer with software that controls the potentiostat and aids in the manipulation of data.[21]

The working electrode is the electrode at which the electrochemistry of interest is occurring. The potential of the working electrode is controlled relative to the reference electrode, which has a stable oxidation / reduction potential. A high input impedance is placed between the working and reference electrodes so that current does not flow between them, which would result in an alteration of the potential of the reference electrode. The electrode at which the other half of the redox reaction takes places is the counter electrode. Thus, current flows between the counter and working electrode and not the working and reference electrodes. The most common types of working and counter electrode materials are inert metals that act as electron sources or sinks and do not interfere with the electrochemistry taking place. Gold, platinum, mercury and carbon are typical examples of these electrodes. Typical reference electrodes are saturated calomel, standard hydrogen and silver/silver chloride electrodes. They are employed because of the high stability of their redox potentials. Electrodes are available in a wide variety of shapes and sizes with the most common shapes being circular disks or wires.[22]

Mass transport in electrochemical experiments occurs via three mechanisms: diffusion, hydrodynamic motion and migration. Diffusion is the motion of a species under the influence of a concentration gradient (from high concentration to low concentration). In most electrochemical experiments, diffusion is the primary mode of mass transport in quiescent solution; this dramatically simplifies the data analysis and interpretation. When the solution is stirred, hydrodynamic motion takes place. Although the Nernst layer is still present and diffusion still occurs, the thickness of the Nernst layer decreases due to the replenishment of the analyte near the electrode surface. Migration involves the motion of a charged species in response to a potential gradient at the electrode / solution interface surface. Migration effects are minimized by adding a large excess of a supporting electrolyte to the solution so that most of the electrostatic charge is carried by the electrolyte and not the electroactive species.[23]

Mass transport in electrochemical experiments is described by the *Nernst-Planck* equation:

$$(i/nFA) = J_i(x) = D_i\,(dC_i(x) / dx) - [(z_iF/RT)\,D_iC_i\,(d\phi(x) / dx) + Ci\nu(x)$$

species flux = diffusional term - migrational term + hydrodynamic term

where i is the current in amperes (or C/sec), n is the number of electrons transferred, F is the faraday constant ($9.6485 * 10^4$ C/mol), A is the electrode area in cm^2, $J_i(x)$ is the flux of species i in mol/(sec*cm^2), D is the diffusion coefficient in cm^2/sec, $dC_i(x) / dx$ is the concentration gradient in mol/distance x, z_I is the ion charge, R is the molar gas constant (8.3145 J/(K*mol)), T is the temperature in Kelvin, $d\phi(x) / dx$ is the potential gradient in Volts/distance x, and $\nu(x)$ is the velocity of a species moving in solution in cm/sec. Electrolysis of the analyte depletes its concentration at the electrode surface. If the experiment is done in a unstirred environment with a large excess of supporting electrolyte, diffusion is the principal means of transporting the analyte to the surface of the electrode. Since this is a relatively slow process, it cannot maintain the concentration / distance profile in a steady-state. If this is the case, the depletion zone grows and the rate of mass transport decreases. When the surface concentration of the analyte is driven to zero, mass transport becomes the rate-limiting step.[24]

A voltammogram is generated by applying a linear potential ramp to the working electrode from an initial value to a predetermined switching potential, at a given sweep rate. The potential of the working electrode is controlled relative to the reference electrode. The direction of the scan is then reversed, usually to the initial value. The resulting current is plotted as a function of the applied potential. The potential which is applied to the working electrode can be considered an excitation signal, which is described by the *Nernst equation* for the ratio of oxidized / reduced species.[25]

$$E = E^{\circ\prime} - (RT/nF) \ln([\text{Reduced}]/[\text{Oxidized}]) \quad (\text{at } x = 0)$$

A true appreciation of the information that the voltammogram provides may be realized at the molecular level. At this level, chemical and electrochemical reactions occur at the working and counter electrodes. The half-reactions that occur are indicative of the chemical and electrochemical changes that are taking place in the cell. An electrochemical reaction occurs in response to an interfacial potential difference at the corresponding electrodes. An oxidation occurs when the potential of the working electrode is moved from a potential where no electrolysis is occurring to more positive potentials. In this process, the energy levels of the electrons in the electrode decreases until it is energetically favorable for an electron to be transferred from the analyte to the electrode. When the potential of the working electrode is moved to more negative potentials the energy levels of the electrons increases until the substance becomes reduced.[26] At this point, the energy levels of the electrons in the electrode increases until it is energetically favorable for an electron to be transferred from the analyte to the electrode.

In solution, an electrical double layer, which acts as a capacitor, is formed at the electrode / solution interface. The layer closest to the electrode, the inner layer or Helmholtz layer, contains specifically absorbed solvent molecules and partially desolvated ions. The outer Helmholtz layer consists of fully solvated ions at a distance of closest approach. Thus, the two Helmholtz layers yield a relatively compact layer of charge at the surface of the electrode. The interaction of the ions and the charged metal surface can also include the effects of relatively long-range electrostatic forces. This gives rise to a diffuse layer near the electrode surface in which the concentration of anions or cations is higher than that in the bulk of the solution. The size of the diffuse layer is dependent on the total ionic concentration in the solution and the potential of the electrode. Electrode processes can be affected by the structure of this double layer, especially if the electroactive species is not specifically absorbed to the electrode surface. In this case, the total potential that it is observed by the redox couple is less than the potential at the electrode surface because some of the potential is used in charging the double layer. The physical situation in the solution next to the electrode during a potential scan can be described by concentration-distance profiles. This is a graphical representation of how solution concentrations vary as a function of distance from the electrode surface.[27]

Two forms of current are observed in a voltammogram: faradaic and non-faradaic. Non-faradaic currents are background currents, charging currents, and currents that result from an absorbed species and limit the sensitivity of the experiment. They arise from the motion of ions in the electrolyte as a result of the potential gradient. Faradaic currents arise from electron transfers to or from the analyte. It is the Faradaic current that causes the peaks in the voltammogram. A peak is generated in a typical voltammogram when the surface concentration of the analyte electrode surface has been driven to zero. This is a result of the relatively slow rate of analyte diffusion across the Nernst layer (Figure 1.9).

Fick's fist law correlates the current flux occurring at the electrode surface to the concentration gradient of the analyte (for an unstirred solution).

$$-J_o\,(x,t) = D_o\,[dC_o\,(x,t)\,/\,dx]$$

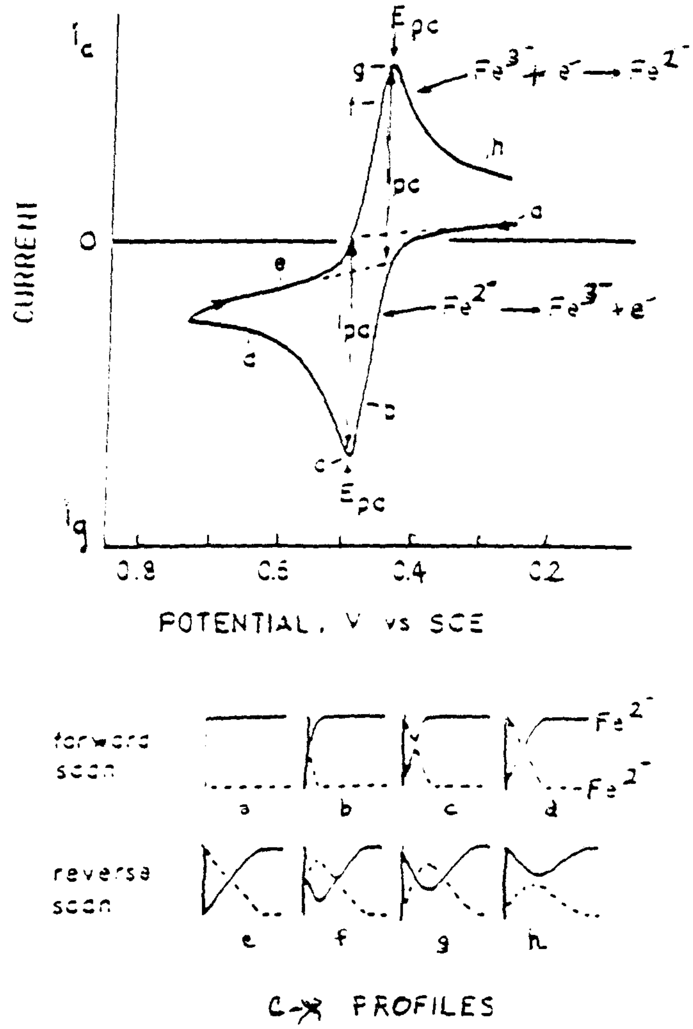

Figure 1.9: The cyclic voltammetry experiment

The currents generated in a voltammogram are also a function of scan rate and therefore vary with time. *Fick's second law* relates the change in analyte concentration with time.

$$dC_o\,(x,t)/\,dt = D_o\,[d^2C_o\,(x,t)/\,dx^2]$$

The change in concentration at location x is determined by the changes in flux into and out of a system that has a given width of dx. This relationship demonstrates how concentration acts as a function of potential and is also dependent on of the surface area of the electrode itself. Thus, the electrochemical reaction taking place in the cell must be considered along with mass transport. To accurately describe this system, the *Nernst-Planck* equation or *Fick's second law* should be applied In the overall process, the instantaneous current is dependent upon three things: the surface concentration, the rate of diffusion and the kinetics of the system. [28]

There are several restraining boundary conditions that must be considered when solving *Fick's laws*. The initial conditions are the semi-infinite and electrode surface boundary conditions. These constraints must be taken into consideration when studying mass transfer in an electrochemical system. The surface boundary conditions represent the bulk concentration of analyte in the solution at t = 0. The semi-infinite boundary conditions are determined by the length of the diffusion pathway. If the distance to the sides of the cell are great enough, this effect is negligible at the electrode surface. Therefore, if the cell is large with respect to the electrode area, then the concentration of the bulk solution reaches a constant value. The electrode surface boundary conditions state that the surface area of the electrode is directly proportional to the concentration gradient at the electrode surface.[29]

The *Butler-Volmer* equation, derived from *Ficks laws*, may be used to approximate how current depends on overpotential. The overpotential is defined as an excess of potential beyond E° of a given system.

$$i = i_o \left[e^{[-\alpha\, nF / RT]\, (E-E^{o})} - e^{(1-\alpha)\, [\, nF / RT]\, (E-E^{o})} \right]$$

where i_o is the exchange current, α is a measure of the slope/symmetry of the energy profiles, and E-E° is the overpotential. The overpotential, related to any given current, translates as the activation energy only; this is because the mass-transfer effects are neglected. The overpotential also reflects the kinetics of the electron transfer, whereas a low exchange current will result in a larger activation overpotential for any given current. The *Butler-Volmer* equation is useful for experiments when the overpotential is small with respect to the ΔG of the electrochemical reaction.[30]

Once the voltammogram has been generated, the redox wave are examined for reversibility. Reversibility may be chemical or electrochemical. Electrochemical reversibility is determined by the rate of electron transfer. If it is rapid enough to maintain an equilibrium of reduced and oxidized forms at the electrode surface, the reaction is considered to be electrochemically reversible. Thus, if an infinitesimal change from E results in driving the net reaction either direction and if the concentration of the analyte at the interface surface continues to stay at an equilibrium.[31] The proper equilibrium ratio is determined by the *Nernst Equation*:

$$E = E^{o\prime} - (RT/nF) \ln ([\text{Reduced}]/[\text{Oxidized}]) \; (x = 0)$$

ΔE_p should be 59/n mV at all scan rates for the electron transfer to be considered reversible. Quasi-reversible electron transfer (slow) kinetics are manifested in ΔE_p shifts that are larger than 59/n mV and overlap on the potential axis typically. If the peaks show no overlap on the potential axis and are greater than 150 mV apart, then they are considered irreversible. An electrochemically reversible redox wave is reversible if the *Nernst equation* is obeyed at E_{app}.

A chemically reversible redox wave is one in which the net cell reaction is driven either forward or backward by changing E. A chemical reaction in the solution that occurs near or at the electrode surface (a homogeneous reaction) may be best described by an electrochemical mechanism. Multi-electron transfers that are coupled with a proton transfer often occur with one electron to one proton at one time and as a succession of reactions. The second electron transfer is dependent upon the rate of the first proton transfer. Thus, it is often important to consider the electrochemical solvents and other experimental factors. These conditions may play a very important role in the determination of the pathway of a reaction.

Charge transfer kinetics can be obtained through the cyclic voltammetry experiment. In a kinetically slow charge transfer, E_p increases with increasing scan rates. Rate constants may be determined by using the *Butler-Volmer* relation:

$$k_f + k_b = k^o \left[e^{[-\alpha\, nF / RT]\,(E-E^o)} - e^{(1-\propto)\,[\,nF / RT]\,(E-E^o)}\right]$$

where k_f is the forward rate constant, k_b is the reverse rate constant, and k^0 is the standard rate constant in 1/sec.[32]

1.2.1 Electrochemistry of C_{60}.

Several voltammetric and differential pulse polarographic studies have been performed on C_{60}. As a result of these experiments, the existence of at least eight oxidation states for C_{60} have been discovered ($C_{60}{}^{n}$: n = 0, 1-, 2-, 3-, 4-, 5-, 6-, and x+

where x has yet to be definitively established). C_{60} has six observable reversible electrochemical reductions in an CH_3CN / toluene solvent system (at 263 K and at a scan rate of 100 mV/s) (Figure 1.10).[33] This phenomena is not totally unexpected, because the LUMO of C_{60} is triply degenerate. The redox waves are regularly spaced at potential interval 400 mV. It has been established via bulk electrolysis by Dubois, et al., that the first four reductions of C_{60} are single electron transfers.[34] Haddon's predictions are strongly supported by Dubois's work, observing reductions of C_{60} from C_{60} to C_{60}^{-6} anion.

1.2.2 The Electrochemistry of Fagan and Calabrese's Complexes.

The electrochemical properties of exohedral C_{60}-metal complexes were investigated through the use of cyclic voltammetry by Fagan, et al.[14] The monosubstituted C_{60} complex displayed three to four single electron reduction waves which were shifted by approximately 400 mV to more cathodic potentials with respect to those of C_{60}'s in the same solvent systems (Figure 1.11). The presence of only three to four waves as opposed to the six that have been reported for C_{60} is due in part to the limitations of the solvent window. The results also demonstrated that reduction of the C_{60}-metal complex is accompanied by a loss of the metal fragment in a classic EC mechanism. The rate of metal dissociation depends upon the metal itself, the ligand that it is attached to, and the extent of the reduction that has occurred. Simulation of the voltammetric data gave quantitative data on the rate of C_{60}-ligand dissociation. The rate constants and reduction potentials were determined by iteration until a good fit was obtained between the experimental and simulated voltammograms. The platinum complexes were best suited for this simulation, with nickel and palladium being more difficult beyond the first reduction peak. The rate constants followed the trend nickel, palladium, platinum, with platinum having the larger rate constants. The rate constants for dissociation for the

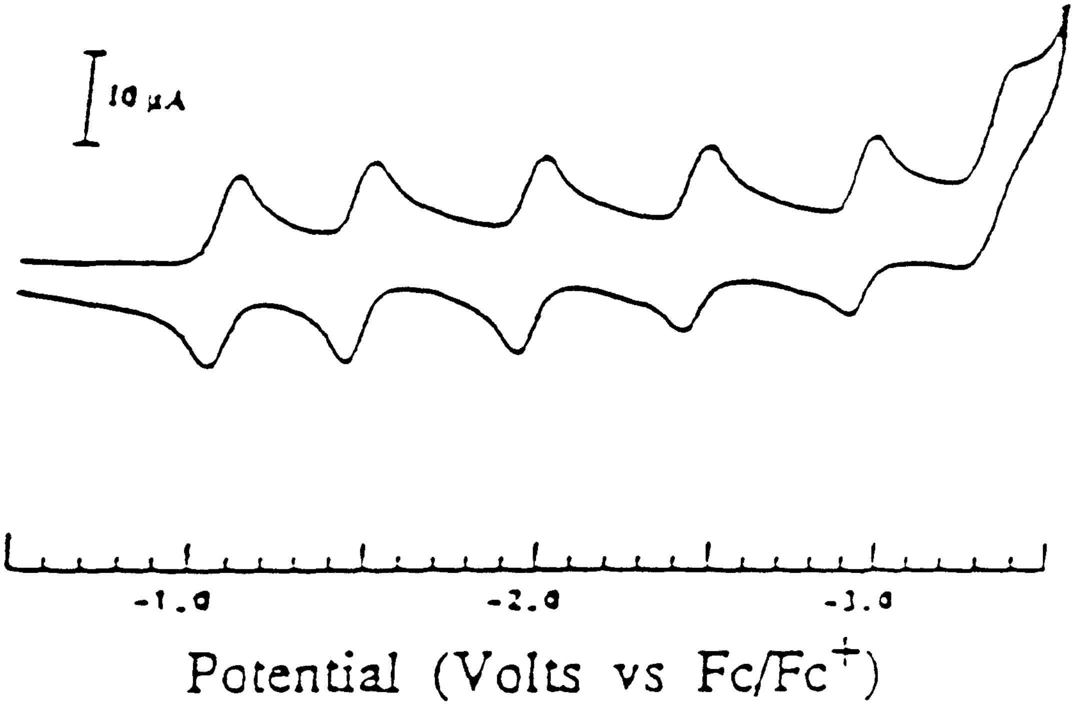

Figure 1.10: Cyclic Voltammetry of C_{60}.

Haddon, R.C., *Chem. Phys. Lett.*, **1989**, *125*, 459.

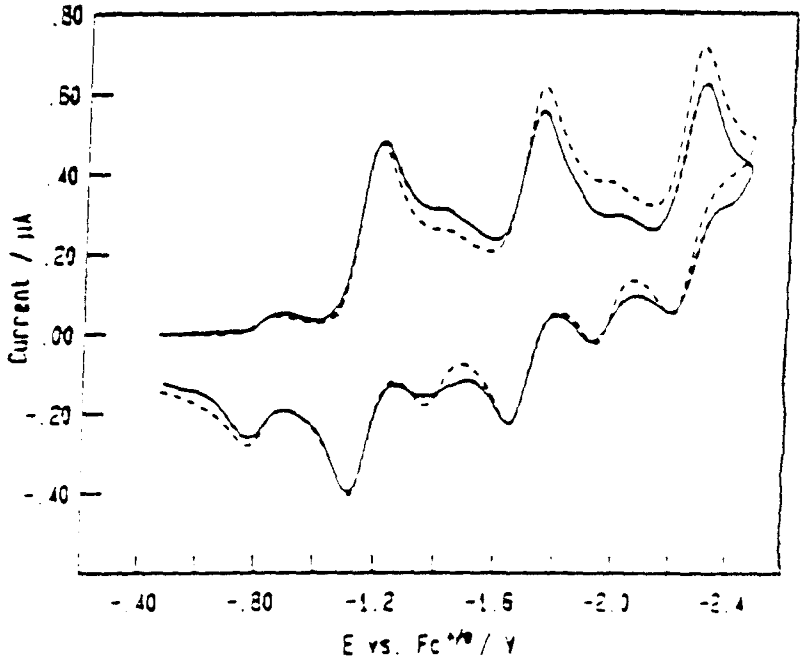

Solid line: Cyclic voltammogram of (Ph$_3$P)$_2$Pt(η^2-C$_{60}$) at 50 V/s (solid) (0.20 M TBAPF$_6$ in tetrahydrofuran, 200 μm diameter platinum disk working electrode, 25 °C). Dashed line: Digital simulation using reversible potentials given in Table I (except $E^0_{MC_{60}^{2-}}$, which is 70 mV more negative) and dissociation rate constants given in Table II. Initial concentration of C$_{60}$ was set at 9% that of the complex. All electron transfer reactions were simulated as close-to-reversible ($k_s \geq 0.1$ cm/s, where k_s is the standard heterogeneous electron transfer rate constant).

Figure 1.11: Cyclic Voltammetry of Fagan and Calabrese's Complexes.

Lerke, S. A., *J. Am. Chem. Soc.*, **1992**, *114*, 7807 -7813.

$(Ph_3P)_2Pt(\eta^2-C_{60})$ complex, for example, was determined to be: $k_1 = 0.006\ s^{-1}$; $k_2 = 0.94\ s^{-1}$; and $k_3 = 105\ s^{-1}$ at 298 K. Surprisingly, the nickel, palladium and platinum complexes are reduced at exactly the same potentials in spite of the fact that the three different metals backbond to different extents. Fagan suggests that this may be due to the electron density from the *d*-orbital "leak"ing back into the remaining double bonds on the C_{60} cage.

The electron affinity of the cluster of carbons is lowered by the coordination of the transition metal ligands to C_{60}. A result of the removal of one of the C=C double bonds from conjugation on the C_{60} cage upon ligand attachment is the addition of electron density to the backbonding $d\pi$-$d\pi$ bond. Increasing the number of metal bonds to the C_{60} successively lowers the electron affinity of the cage, with the reversible potentials for most of these compounds shifting in the cathodic direction. The electron affinity may thus be "tuned" by the number of metals on the complex. The implication of this effect is that the metals act as protecting groups and alter the reactivity of C_{60}, so that it may be more controllable with respect to successive addition reactions.[35]

1.3 Maleonitriledithiolates

Maleonitriledithiolates (mnt) (Figure 1.12) are typical sulfur donor ligands which are capable of forming a wide range of metal complexes. These complexes are stable in air and rich in terms of redox chemistry. Mnt containing complexes have the ability to stabilize the transition metal to which it is complexed to in a variety of oxidation states. They are also ideal for spectroelectrochemical studies because they have high molar absorptivities in the UV-Vis. In addition, the nitrile stretching frequency is sensitive to the extent of π backbonding between the metal and the ligand which may change upon oxidation or reduction.

Metal mnt complexes are closely related in structure to the molecular metal tetrathiafulvalene (TTF) and to the organic super conductor BEDT-TTF. The metal will

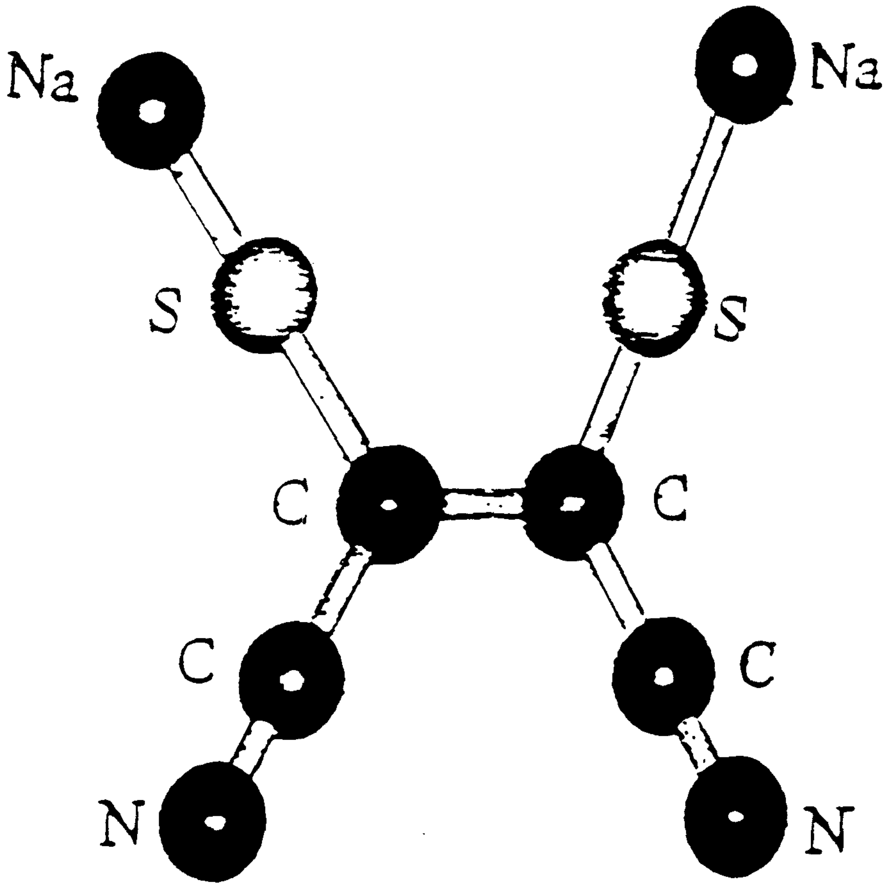
Na
Na
S
S
C
C
C
C
N
N

Figure 1.12: The Structure of Sodium Maleonitriledithiolate,

act as a replacement for the C=C double bond unit to resemble the five membered rings in BEDT-TTF (Figure 1.14). This type of five membered ring tends to be aromatic in inorganic chemistry and may further enhance conductivity and stability of these materials. The applications of mnt-based complexes includes photoconductors, non-metallic conductors and catalysts.[37]

The salt, disodium maleonitriledithiolate ($Na_2S_2C_2(CN)_2$ or Na-mnt) was prepared according to *Inorganic Syntheses*. These salts were prepared in such a fashion for the purpose of establishing that the mnt ligand will adopt the *cis* conformation (Figure 1.13).[38]

In the early 1960's, transition metal chemistry has been the focus of many studies. Metal-mnt chemistry complexes were especially interesting to inorganic chemists due to the fact that the metal may easily stabilize the mnt ligand. The mnt ligand is able to act as a redox center and that the redox changes observed for its complexes entail non-bonding mnt π ligands. In 1966, Williams et al. had synthesized a group of planar four-coordinate, paramagnetic complexes. These complexes were 1,2-dithiolene complexes that utilized Ni and Pd as the coordinating metals (Figure 1.15). The spectral and magnetic properties of these complexes and their anions were studied. As a result of his EPR studies, Williams reports that the $Ni(mnt)_2^-$ complexes have five degenerate orbitals (Figure 1.16). Resonance-raman spectral studies in combination with low temperature absorption spectroscopy were performed by Clark and Turtle on related mnt complexes using nickel, palladium and platinum. They found that the metal to ligand transition causes a greater change in the C=C double bond length than do other ligand to metal transitions. Also the size of the metal increased the extent of the metal to ligand backbonding in the *d* orbital.[41]

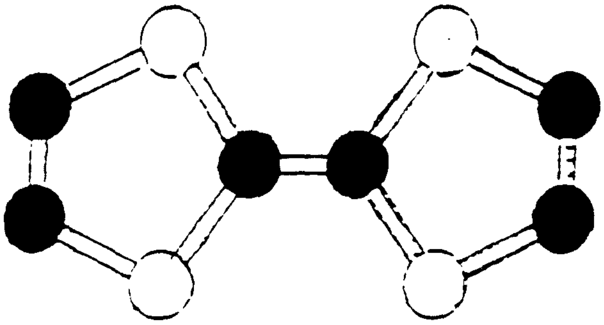

TTF

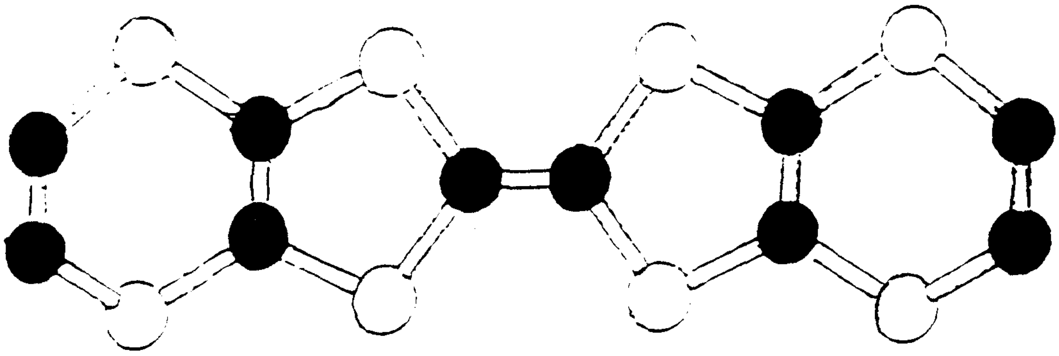

BEDT-TTF

(○ = S, ● = C)

Figure 1.13: The Structures of TTF and BEDT-TTF.

Step no. 1:

$$NaCN + CS_2 + 3HCON(CH_3)_2 \rightarrow$$

$$NCCS_2Na \bullet 3HCON(CH_3)_2$$

Step no. 2:

$$2NCCS_2Na \bullet 3HCON(CH_3)_2 \xrightarrow[H_2O]{}$$

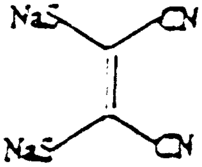

$$+ \quad 6HCON(CH_3)_2 \quad + \quad S_2$$

Figure 1.14: The Synthesis of Sodium Malenitriledithiolate.

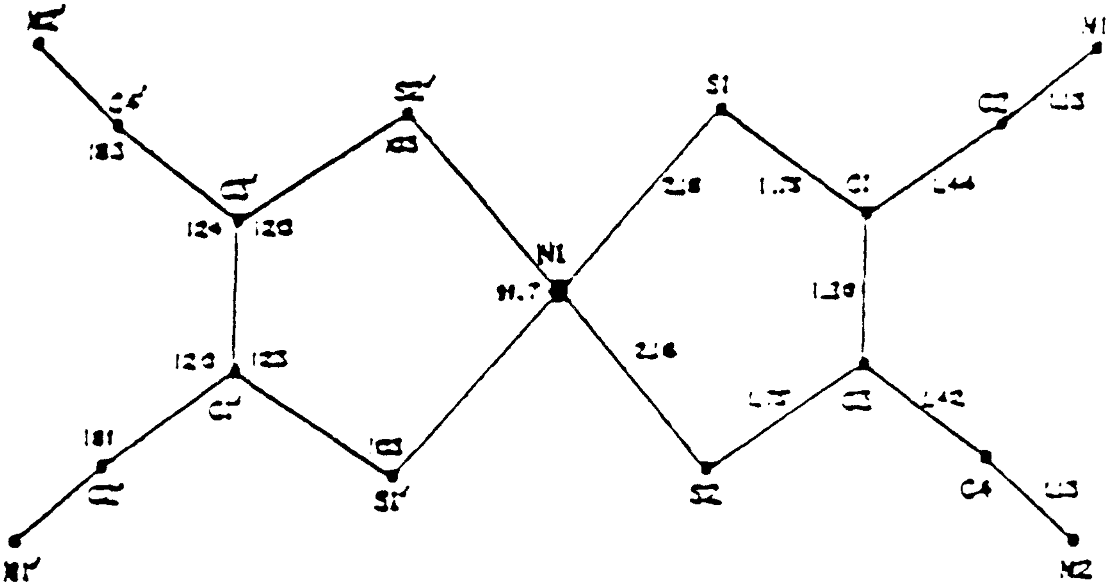
S1
Ni
2.18
2.16
1.39
124
128
123
183
181
S1'
C4
N2

Figure 1.15: The Crystal Structure of Ni(mnt)$_2^{2-}$.

Pearson, R. G. and Sweigart, D. A., *Inorg. Chem.*, **1970**, 9(5), 1167 - 1175.

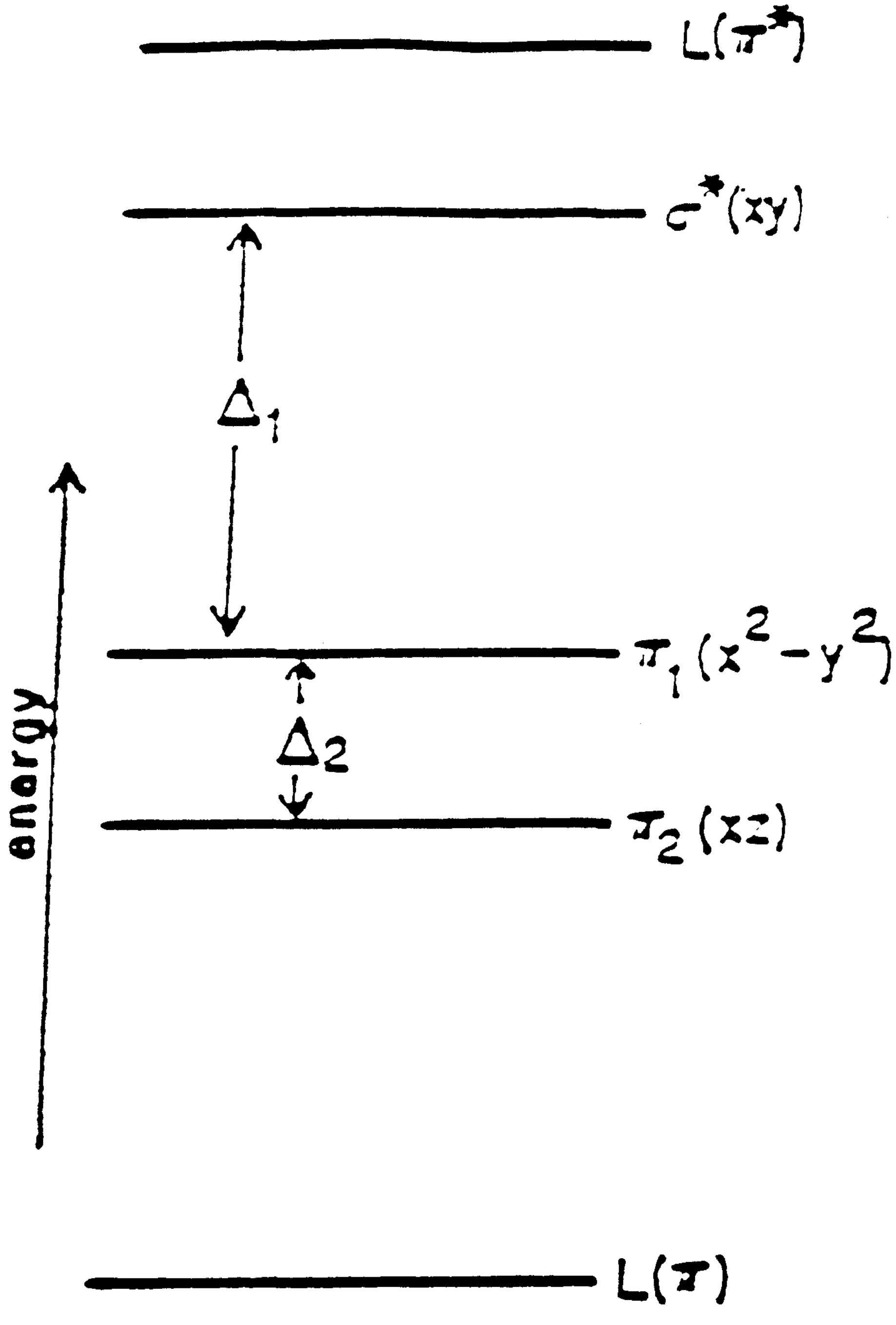
L(π*)
σ*(xy)
Δ1
π1(x2-y2)
Δ2
π2(xz)
energy
L(π)

Figure 1.16: Nondegenerate Orbitals of $Ni(mnt)_2^{2-}$.

Schrauzer, G. N., *Accounts Chem. Res.*, **1969**, *2*, 72 - 80.

1.4 Research Proposal

1.4.1 Origination of the Target Complex C_{60}-Metal-mnt.

Group X metal-mnt ligands were chosen for exohedral attachment to C_{60} to act as spectroscopic, electrochemical and spectroelectrochemical probes of the interactions between the ligand and C_{60}. The electrochemistry of C_{60} and mnt is well documented in the literature and can easily be used as references for the electrochemistry of C_{60}-metal-mnt complexes. The effect of ligand attachment on the E° and reversibility of C_{60}'s reductive electrochemistry will be monitored via cyclic voltammetry. In addition, changes in the voltammetry of the ligand will be used to indicate the interactions between C_{60} and mnt. For many of the coordination compounds, the electronic absorption spectrum provides a convient method for determining the magnitude of the effects of ligands on the *d* orbitals of the transition metal. The combination of these qualities will give rise to the spectroelectrochemical applications of these compounds. Spectroelectrochemistry offers an advantage over traditional electrochemistry in that spectroelectrochemistry information can be obtained as a function of the oxidation state of the complex. The electronic information from the UV-Vis may be used in conjunction with the electrochemical data.

Spectroelectrochemically, this complex has many advantages. The metal-mnt component and the C_{60} have high molar absorbtivities in the UV-Vis. The mnt ligand should supply information regarding any changes in the electronic structures of both C_{60} and the mnt ligand upon coordination of the mnt to the C_{60} cage. The mnt ligand could be an excellent IR probe due to the presence of the C≡N group on the terminal end of the mnt ligand. The nitrile stretching frequency should be highly sensitive to the extent of π backbonding in the mnt ligand and the metal-C_{60} bond. In summary, the benefits of spectroelectrochemistry are that electronic structure data and the type of bonding changes upon successive reduction could be investigated using the UV-Vis and IR probes made possible by the coordination of the mnt ligand.

1.4.2 Creation of the Intermediate Complexes.

Triphenylphosphine M(II)-mnt and (diphenylphosphino)ethane M(II)-mnt were chosen as intermediates in the synthetic design because the phosphines are fairly labile and should easily fall off of the metal, inducing coordination across the 6-6' bonding site of the C_{60} cage. This class of compounds has been previously synthesized, but were never fully characterized. A complete characterization of this series of complexes is one of the goals of this phase of the project. It would be a great benefit to establish the structural environment around the metal center before and after coordination with the C_{60} cage. Also, it is necessary to gather uncoordinated ligand data for the complexes in both the UV-Vis and the IR before making the C_{60} complex. This information will be used as a basis for comparison with the data collected on the C_{60}-metal-mnt complex.

1.4.3 Origination of Target Complex (dppf)M-C_{60}.

The focus of this project was to design new fullerene complexes with novel spectroscopic, electrochemical and spectroelectrochemical properties. 1-1'*Bis* (diphenylphosphino)ferrocene (dppf) was chosen as the ligand for the initial exploration of this type of chemistry. The reasons for selecting dppf were three-fold. The electrochemistry of ferrocene is well documented in the literature, is reversible and appears in the anodic region of the voltammogram, while the C_{60}-metal electrochemistry occurs in the cathodic region. The benefit of this is that the voltammogram is less complicated because the reversibility ferrocene / ferricenium couple does not interfere with the metal-C_{60} electrochemistry. Thus, analysis of the changes in E° and the reversibility of both redox couples is dramatically simplified. Ferrocene is also an electron donor. This may prove to be particularly interesting due to the fact that on the opposite side of the molecule is C_{60}, which is an electron acceptor. This raises the interesting possibility of intramolecular electron transfer which can be probed spectroscopically and electrochemically. In addition, the ferrocene / ferricenium couple have large molar absorptivities and is an outstanding UV-Vis spectroelectrochemical probe. The electroactivity of each component is expected to be enhanced when the ligand, metal and fullerene are complexed together.

The synthetic pathway involves a variation of Fagan and Calabrese's methods.[14] It has already been demostrated that group X metals may be coordinated across the 6-6' bonding site on the C_{60} cage. It is reasonable to assume that metal containing dppf ligands will behave in an analogous fashion. These complexes should be assumed to be air sensitive, due to the fact that zero-valent nickel, palladium and platinum atoms will be coordinated to the C_{60}.

The main goal of this phase of the project is to explore the effects of different phosphorus ligands, such dppf, upon the C_{60}-metal complex through the use of cyclic voltammetry. It is not well known if there is any electronic communication through the phosphorus atoms and if there is, to what extent it occurs. Another area of interest is to identify what effects the addition of an electroactive substituent to the phosphorus ligand might be. A practical way of monitoring these effects would be through cyclic voltammetry. The presence of the ferrocene should be easily detected on the C_{60}-metal complex because of it's characteristic wave in the oxidative direction of the voltammogram.

(41) Clark, R. J. and Turtle, P. C., *J. Am. Chem. Soc. Dalton Trans.*, **1977**, 2142 - 2148.

Chapter 2

The Synthesis and Characterization of Nickel, Palladium, and Platinum Maleonitriledithiolate Complexes: X-Ray Crystal Structures of the Isomorphous Ni, Pd, and Pt ($Ph_2PCH_2CH_2PPh_2$)M(Maleonitriledithiolate) Congeners.

2:1 **Introduction**

Fullerenes, especially C_{60}, are topics of intense investigation because of their unusual chemistry and high symmetry, and their potential for applications as diverse as superconducting materials, novel catalysts, and new biomedical applications[1-5]. The focus of this project, as well as many other inorganic projects that include C_{60}[6-8], is the preparation and characterization of complexes in which the fullerenes are coordinated exohedrally to transition metal centers. One particularly interesting aspect is studying the spectroelectrochemistry of such species[9-12]. Metal sulfur coordination complexes have been extensively studied and are well known to be rich in redox chemistry. Metal maleonitriledithiolate (i.e. mnt or 1,2-dicyanoethylene-1,2-dithiolate) complexes are excellent examples of this[13,14], and were chosen for this purpose. An additional advantage of mnt complexes is that they have large molar absorptivities and are very sensitive to the extent of backbonding present from the metal in the UV-Visible region of the electromagnetic spectrum (which makes them particularly amenable to spectroelectrochemical study in solution and on surfaces) and that their nitrile stretching frequencies in the IR are also sensitive to the extent of communication between the metal and the mnt ligand[15].

As the first stage in this project, a homologous series of (dppe)M(mnt) and $(PPh_3)_2M(mnt)$ complexes (where M = Ni, Pd, and Pt and dppe = $Ph_2PCH_2CH_2PPh_2$) were prepared. It was hoped that these complexes would act as intermediates in the production of exohedrally substituted C_{60} complexes (e g. $C_{60}M(mnt)$). In addition, they were expected to be excellent model complexes for the spectroscopic and electrochemical behavior of $C_{60}M(mnt)$ complexes. Indeed, these phosphine intermediates display some interesting chemistry in their own right. Unfortunately, C_{60} has proven to be unreactive towards the intermediates and we were unable to obtain the $(C_{60})M(mnt)$ complexes from the proposed route[16].

2:2 **Experimental Section**

2:2.1 General experimental procedures.

The general procedures used have been described in detail previously[16-18]. Unless otherwise noted, all reactions and any subsequent manipulations were conducted at ambient temperatures using conventional techniques for the manipulation of inorganic compounds[19]. Where required, anaerobic and anhydrous conditions were maintained by using a prepurified argon atmosphere and a combination of vacuum-line and inert-atmosphere glove box techniques. Unless otherwise noted, all chemicals were purchased from the Aldrich or Fisher Chemical Companies and were of reagent grade or comparable purity. Where necessary, these reagents were purified before use[20]. $Na_2(mnt)$ was prepared by published procedures[21]. Dinitrogen and argon were of 99.999 % purity and were not further purified. Solvents were dried and deaerated by standard procedures and stored under dinitrogen or argon[20].

IR spectra were recorded on a Perkin-Elmer 1600 FT-IR spectrometer and mass spectra were obtained with a Finnigan 1020 GC/MS spectrometer. The ^{1}H NMR, ^{13}C NMR and ^{31}P NMR were recorded on a Varian Gemini-2000 400 MHz NMR spectrometer with reference to the deuterium signal of the solvent employed.[1] Chemical shifts are reported in parts per million down field from tetramethylsilane. Electronic spectra were recorded on a Hewlett Packard 8452A diode array UV-Visible spectrophotometer with wavelengths reported in nm. X-ray diffraction data was collected on a Siemens P4 automated diffractometer.

2:2.2 Synthesis of the (phosphine)M(mnt) complexes.

All of the (phosphine)M(mnt) complexes were prepared via ligand exchange between the (phosphine)MCl_2 complexes and Na_2(mnt)[21]. The preparation of the Pd title complex and the associated spectra are present in the chapter as a representative example. All other spectra may be found in the Appendix. (Figure 2.1)

*2:2.2a Synthesis of (dppe)Pd(mnt), **2**.*

Solid 0.5 g (0.87 mmol) (dppe)$PdCl_2$ was added to a solution of 1.16 g (0.87 mmol) Na_2(mnt) in cold acetone (50 mL, 0 °C) (Figure 2.2). The color of the resulting solution changed instantly from bright yellow to pale orange. The solution was allowed to stir overnight and warm to room temperature. A small amount of white precipitate formed which was removed by centrifugation and the resulting orange solution was taken to dryness on a rotary evaporator. The product was purified via column chromatography

---

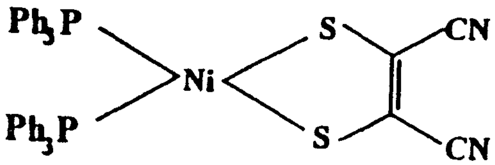

4

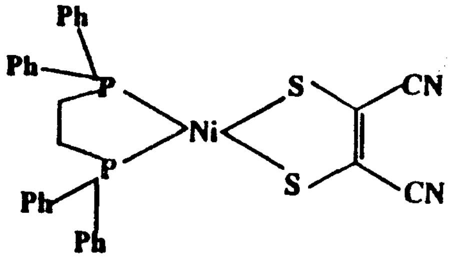

1

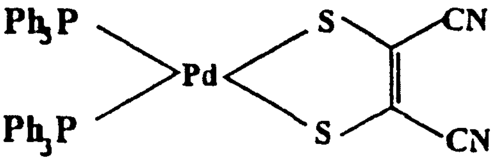

5

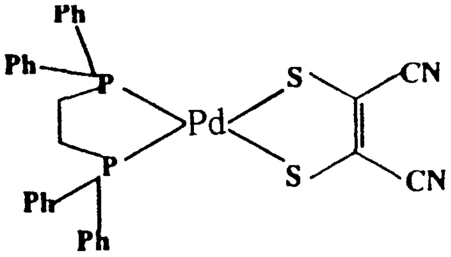

2

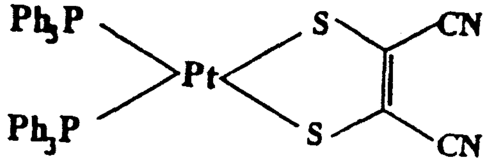

6

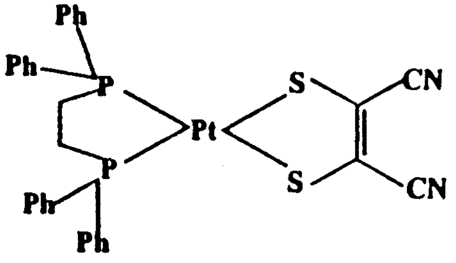

3

Figure 2.1: List of Compound Numbers.

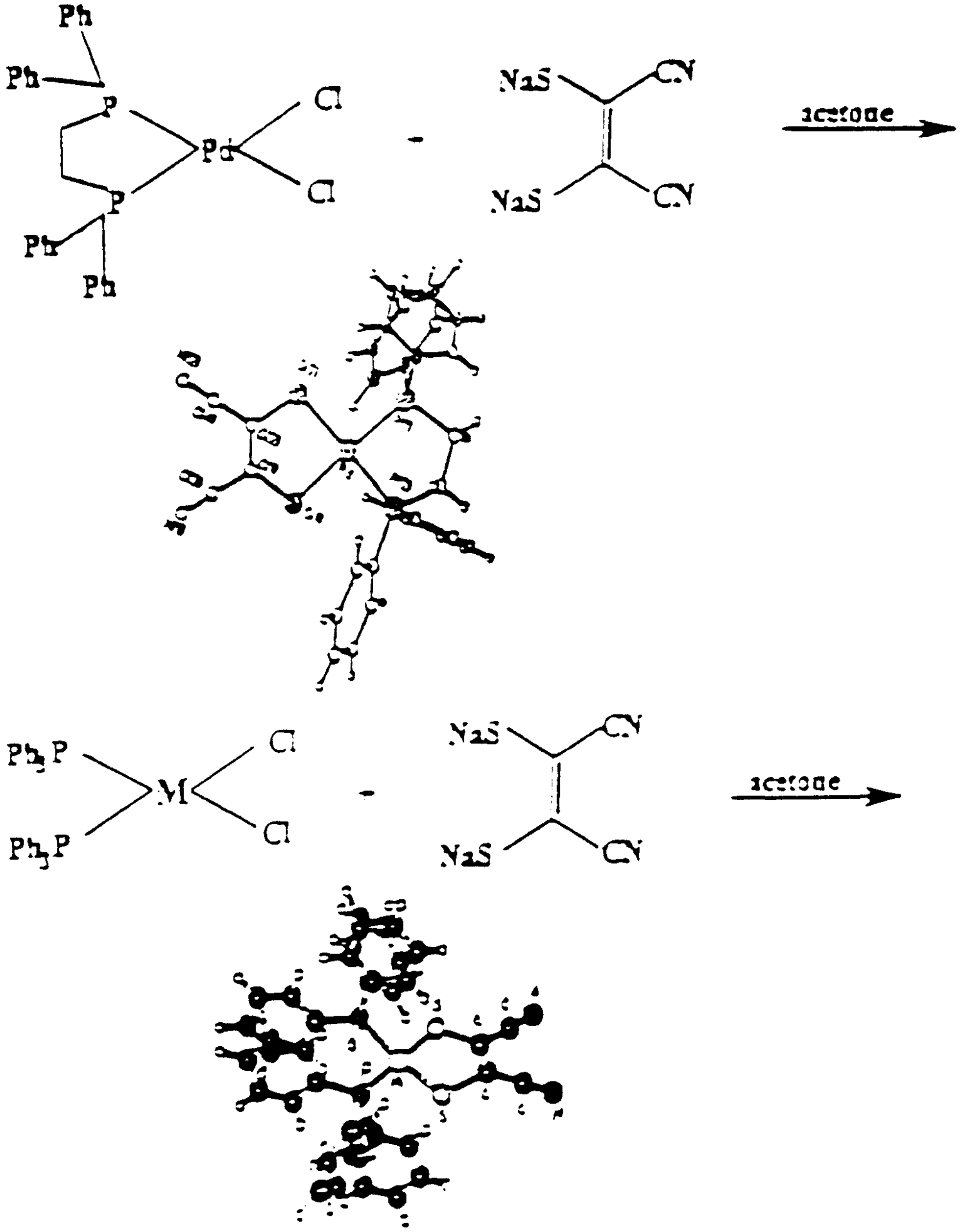
Ph
Ph
P
P
Pd
Cl
Cl
Ph
Ph
+
NaS
NaS
CN
CN
acetone
Ph3P
Ph3P
M
Cl
Cl
+
NaS
NaS
CN
CN
acetone

Figure 2.2: Synthesis of Intermediate Complexes.

on silica gel using chloroform as the eluent. Crystals of the desired compound, (dppe)Pd(mnt), **2**, were formed upon slow evaporation from chloroform in 95.4% yield (0.53 g, 0.83 mmol).

For $C_{30}H_{24}N_2PdP_2S_2$: ^{1}H NMR ($CDCl_3$): 7.8-7.5 (m, 20H, C_6H_5); 2.6 (s, 4H, P-CH_2-CH_2-P). ^{13}C NMR ($CDCl_3$): 133.58-129 (m, 24C, C_6H_5); 131.83 (s, 2C, C=C (mnt)); 116.72 (s, 2C, CN); 29.6 (m, 2C, P-CH_2-CH_2-P). ^{31}P ($CDCl_3$): -5.222 (t, 2P, P-Pt). UV-Visible ($CHCl_3$, λ_{max}, nm): =276, 246 and 364. IR ($CHCl_3$, cm^{-1}): 3058 (m, Ar-H), 2288 (w, CN), 1431 (w, Ar), 1412 (w, C-S), 1257 (s, Ar-P), 902 (w, C=C).

2:2.2b Synthesis of (dppe)Ni(mnt), 1 and (dppe)Pt(mnt), 3

These two complexes were prepared as described above yielding rusty red and pale yellow crystals for the Ni and Pt complexes, respectively. The compounds were produced in 92.4 and 94.5 % yields, respectively, for the Ni and Pt congeners.

For $C_{30}H_{24}N_2NiP_2S_2$: ^{1}H NMR ($CDCl_3$): 8.0-7.2 (m, 20H, C_6H_5); 2.48 (s, 4H, P-CH_2-CH_2-P). ^{13}C NMR ($CDCl_3$): 133.3 (m, 24C, C_6H_5); 130.8 (s, 2C, C=C (mnt)); 116.23 (s, 2C, CN); 27.6 (m, 2C, P-CH_2-CH_2-P). ^{31}P ($CDCl_3$): -0.398 (s, 2P, P-P). UV-Visible ($CHCl_3$, λ_{max}, nm): = 274 and 372. IR ($CHCl_3$, cm^{-1}): 3029 (m, Ar-H), 2290 (w, CN), 1827 (w, C-S), 1232 (s, Ar-P), 1034 (w, C=C).

For $C_{30}H_{24}N_2P_2PtS_2$: ^{1}H NMR ($CDCl_3$): 7.6-7.2 (m, 20H, C_6H_5); 3.683 (s, 4H, P-CH_2-CH_2-P). ^{13}C NMR ($CDCl_3$): 133.244 (m, 24C, C_6H_5); 131.8 (s, 2C, C=C (mnt)); 116.7 (s, 2C, CN); 53.4 (m, 2C, P-CH_2-CH_2-P). ^{31}P ($CDCl_3$): -15.156 (t, 2P, P-P). UV-Visible ($CHCl_3$, λ_{max}, nm): = 240 and 344. IR ($CHCl_3$, cm^{-1}): 3056 (m, Ar-H) 2230 (w, CN), 1431 (w, Ar), 1417 (w, C-S), 1289 (s, Ar-P), 902 (w, C=C).

*2:2.2c Synthesis of $(PPh_3)_2Ni(mnt)$, **4**, $(PPh_3)_2Pd(mnt)$, **5**, and $(PPh_3)_2Pt(mnt)$, **6**.*

These three complexes were prepared as described above except that the $(PPh_3)_2MCl_2$ complexes were used as the starting materials. Brownish-green, tangerine, and pale yellow crystals of the desired complexes were obtained in 87, 95, and 94 % yields, respectively, for the Ni, Pd, and Pt congeners.

For $C_{40}H_{30}N_2P_2NiS_2$: ^1H NMR ($CDCl_3$): 7.5-7.2 (m, 30H, C_6H_5). ^{13}C NMR ($CDCl_3$): 137.5-127 (m, 36C, C_6H_5); 132 (s, 2C, C=C (mnt); 117.5 (s, 2C, CN). ^{31}P ($CDCl_3$): -4.688 (s, 2P, P-P). UV-Visible ($CHCl_3$, λ_{max}, nm): = 268 . IR ($CHCl_3$, cm^{-1}): 3085 (m, Ar-H) 2403 (w, CN), 1523 (w, Ar), 1443 (w, C-S), 1219 (s, Ar-P), 969 (w, C=C).

For $C_{40}H_{30}N_2P_2PdS_2$: ^1H NMR ($CDCl_3$): 7.6-7.2 (m, 30H, C_6H_5). ^{13}C NMR ($CDCl_3$): 137-127 (m, 36C, C_6H_5); 132 (s, 2C, C=C (mnt); 117 (s, 2C, CN). ^{31}P ($CDCl_3$): -34.33 (t, 2P, P-P). UV-Visible ($CHCl_3$, λ_{max}, nm): = 296 and 248. IR ($CHCl_3$, cm^{-1}): 3056 (m, Ar-H) 2305 (w, CN), 1523 (w, Ar), 1431 (w, C-S), 1271 (s, Ar-P), 902 (w, C=C).

For $C_{40}H_{30}N_2P_2PtS_2$: ^1H NMR ($CDCl_3$): 7.5-7.2 (m, 30H, C_6H_5). ^{13}C NMR ($CDCl_3$): 134.7-127.95 (m, 36C, C_6H_5); 129.69 (s, 2C, C=C (mnt); 116.82 (s, 2C, CN). ^{31}P (methylene chloride-d_2): -17.08 (t, 2P, P-P). UV-Visible ($CHCl_3$, λ_{max}, nm): = 348 and 245. IR ($CHCl_3$, cm^{-1}): 3025 (m, Ar-H), 2302 (w, CN), 1523 (w, Ar), 1431 (w, C-S), 1271 (s, Ar-P), 902 (w, C=C).

2:2.3 Synthesis and Characterization of Maleonitriledithiolate Complexes of C_{60}.

Two synthetic approaches were attempted to construct a maleonitriledithiolate containing -C_{60} complex. Initially, it was believed that a transition metal would act as a bridge to form a C_{60}-metal-mnt complex. The (dppe)M(mnt) intermediate complexes were refluxed in benzene under argon for varying amounts of time with C_{60}. No appreciable amount of product was ever recovered despite numerous attempts and a variety of reaction conditions. The formation of this complex proved to be difficult and eventually, a new synthetic approach was implemented in an effort to obtain a higher yield and a product that could be easily isolated (Figure 2.3).

The second approach involved synthesizing Fagan and Calabrese's mono-substituted $(PPh_3)_2$-platinum-C_{60} complex and then oxidizing the platinum atom, while attached to C_{60} and reacting that with sodium maleonitriledithiolate to form the metal-bridged C_{60} complex (Figure 2.4). Tetrakis(triphenylphosphine) platinum(0) and C_{60} were reacted in deoxygenated benzene for two hours in a glovebox and the solution turned from purple to dark green. The dark green solid precipitate was filtered and dried under vacuum. The mono-substituted triphenylphosphine platinum-C_{60} complex was then dissolved in deoxygenated THF. Iodine and a large excess of sodium maleonitriledithiolate were added to the THF solution and allowed to stir overnight at room temperature. Within a sixteen hour period, the reaction mixture changed from a dark green to a rusty red color and a brown platelet-like precipitate formed. The precipitate was filtered, washed with 10 ml of THF and allowed to dry in the glovebox. Solubility tests showed the product to be insoluble in all common organic solvents. This

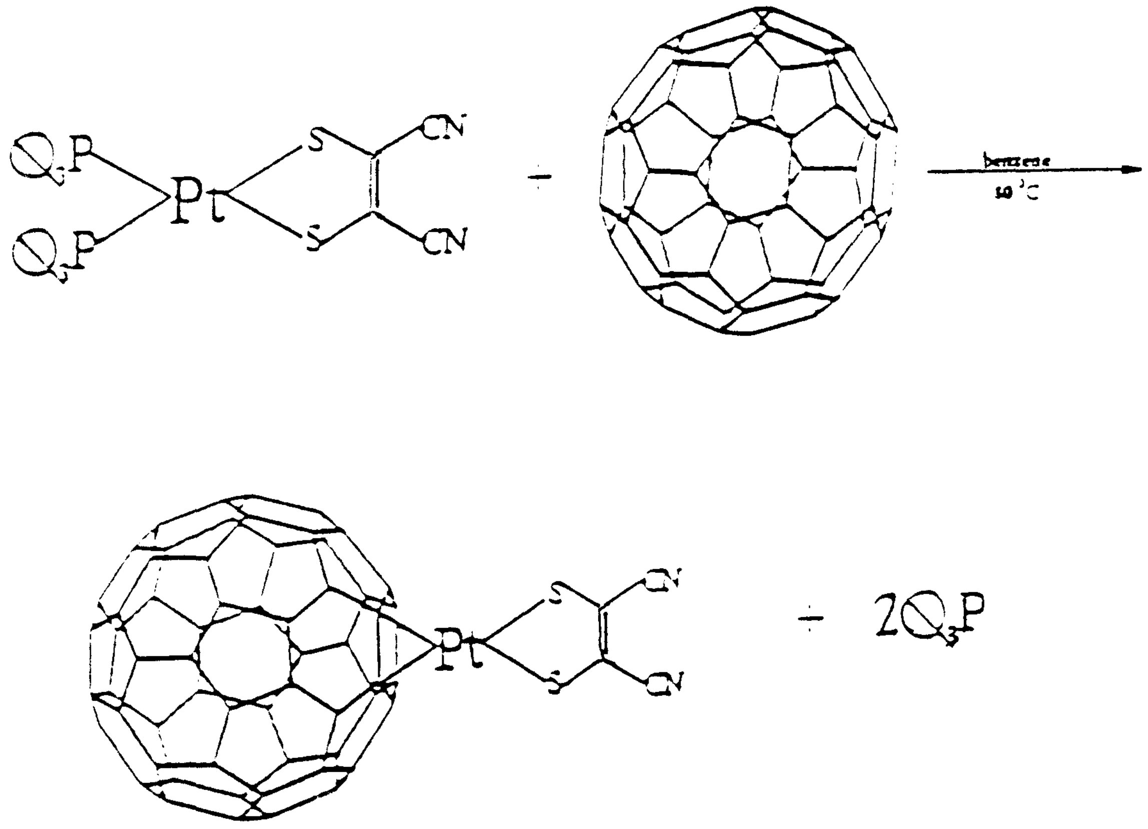
Φ3P
Φ3P
Pt
S
S
CN
CN
+
benzene
50 °C
Pt
S
S
CN
CN
+ 2Φ3P

Figure 2.3: Synthesis of C60-metal-mnt.

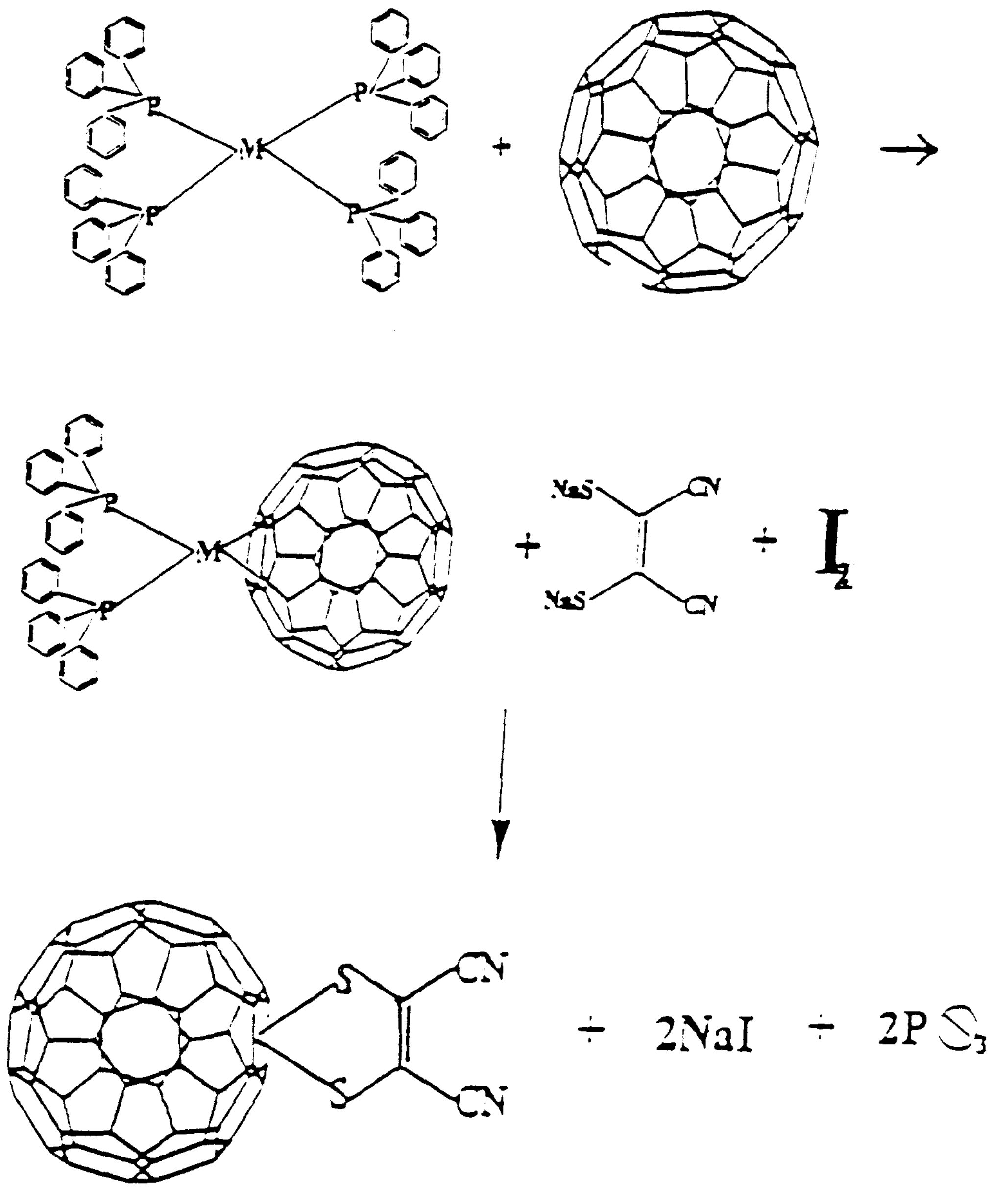
P
M
+
→
NaS
CN
I2
S
+ 2NaI + 2PS3

Figure 2.4: Synthesis of C60-mnt.

crude product was characterized via UV-Vis and IR spectroscopy, TGA, DSC, mass spectrometry and elemental analysis.

2:3 X-ray Diffraction Analysis

2:3.1 X-Ray Diffraction Analysis of the Title Compounds.

Single crystals of the (dppe)M(mnt) complexes were grown via slow evaporation from chloroform solutions of the respective complexes. Several well formed crystals were selected by optical microscopy and mounted on a glass fiber using epoxy glue. Each crystal was optically centered in the X-ray beam of a Siemens P4 automated diffractometer. Rotation photographs and peak profiles of representative reflections were used to choose the best crystal, which was then used in subsequent data collection. Data collection and structure solution parameters are summarized in the Appendix. X-ray quality single crystals of the $(Ph_3P)_2M(mnt)$ complexes proved to be very difficult to prepare. Other methods of isolating such materials are currently being pursued.

Data was collected with the XSCANS package from Siemens[22]. A preliminary unit cell was obtained by centering reflections chosen from the rotation photograph. After inspection of axial photographs and a fractional search, a thin shell search was used to obtain and center additional reflections for a total of 79, 100, and 100 reflections for determining the final unit cell parameters of complexes **1**, **2**, and **3**, respectively. Bravais lattice and Laue symmetry determinations were performed. Three of the strong and nearly orthogonal reflections from the thin shell list were chosen as standards and were recollected after each 97 data reflections. Doug Powell's program Chi90[2] [23] was used to choose the reflections for which Ψ scans were then carried out.

Structure solution was carried out using the SHELXTL package for DOS from Siemens[24] on Gateway2000 Pentium and/or Pentium Pro computers. Data was corrected for Lorenz and polarization effects and also for absorption using the empirical Ψ-scan data. The refinements were carried out on F^2 for all data[24]. Structure solution proceeded in a routine fashion for all three compounds utilizing the SHELXS-86 and SHELXL-93 structure solution packages included in SHELXTL[24]. All atomic scattering factors were taken by SHELXTL from the International Tables, Volume C. The initial solution was obtained from Direct Methods in SHELXTL-XS[24]. All non-hydrogen atoms were located from electron density difference maps and were refined first with isotropic displacement parameters and then with anisotropic displacement parameters. All hydrogen atoms were also located from electron density difference maps and were then refined isotropically. Extinction was refined in later refinement cycles and the weighting scheme used was that suggested by SHELXTL-XL[24]. Molecular graphics and tabular data were generated with SHELXTL-XP and SHELXTL-XCIF, respectively[24].

Final fractional atomic coordinates and equivalent isotropic displacement parameters are listed in the appendix, as well the selected bond lengths and angles.

2:4 **Results and Discussion**

2:4.1 Synthesis and characterization of the (phosphine)M(mnt) complexes

---

[2] Chi90 in a program for choosing optimum reflections for empirical Ψ scans [23].

The desired metal phosphine maleonitriledithiolate complexes were prepared by metathesis reactions, i.e.,

$$(\mathrm{dppe})\mathrm{MCl_2} + \mathrm{Na_2(mnt)} \rightarrow (\mathrm{dppe})\mathrm{M(mnt)} + 2\,\mathrm{NaCl} \tag{1}$$

$$(\mathrm{PPh_3})_2\mathrm{MCl_2} + \mathrm{Na_2(mnt)} \rightarrow (\mathrm{PPh_3})_2\mathrm{M(mnt)} + 2\,\mathrm{NaCl} \tag{2}$$

(where dppe = $Ph_2PCH_2CH_2PPh_2$ and M = Ni, Pd, and Pt). These reactions proceeded smoothly in greater than 85 % isolated yields to give rusty red to pale yellow crystals of the desired products. These d^8 diamagnetic materials are air and moisture stable in the solid state. They are very soluble in polar organic solvents, such as acetone, but are insoluble in non-polar solvents such as hexane. They are best recrystallized from moderately polar solvents such as chloroform.

The complexes were initially identified by their characteristic spectroscopic properties. All of this data is consistent with the proposed structures of the mnt complexes. In particular, the low resolution mass spectroscopic data established their molecular formulae (Figure 2.10), while the IR, UV-Vis, and ^1H, ^{13}C, and ^{31}P NMR (Figures 2.5, 2.6, 2.7, 2.8 and 2.9, respectively and Tables 2.1, 2.2, 2.3, 2.4 and 2.5, respectively) data unambiguously indicated that the phosphorous atoms were attached *cis* to one another and that the mnt ligand was coordinated to the metal center. In addition, the Pd and Pt complexes exhibited the characteristic "triplet" which is the result of the coupling of the ^{31}P nuclear spin to the spin ½ of the metal isotopes. For two strong field ligands like phosphines and mnt it was not surprising that this data was consistent with

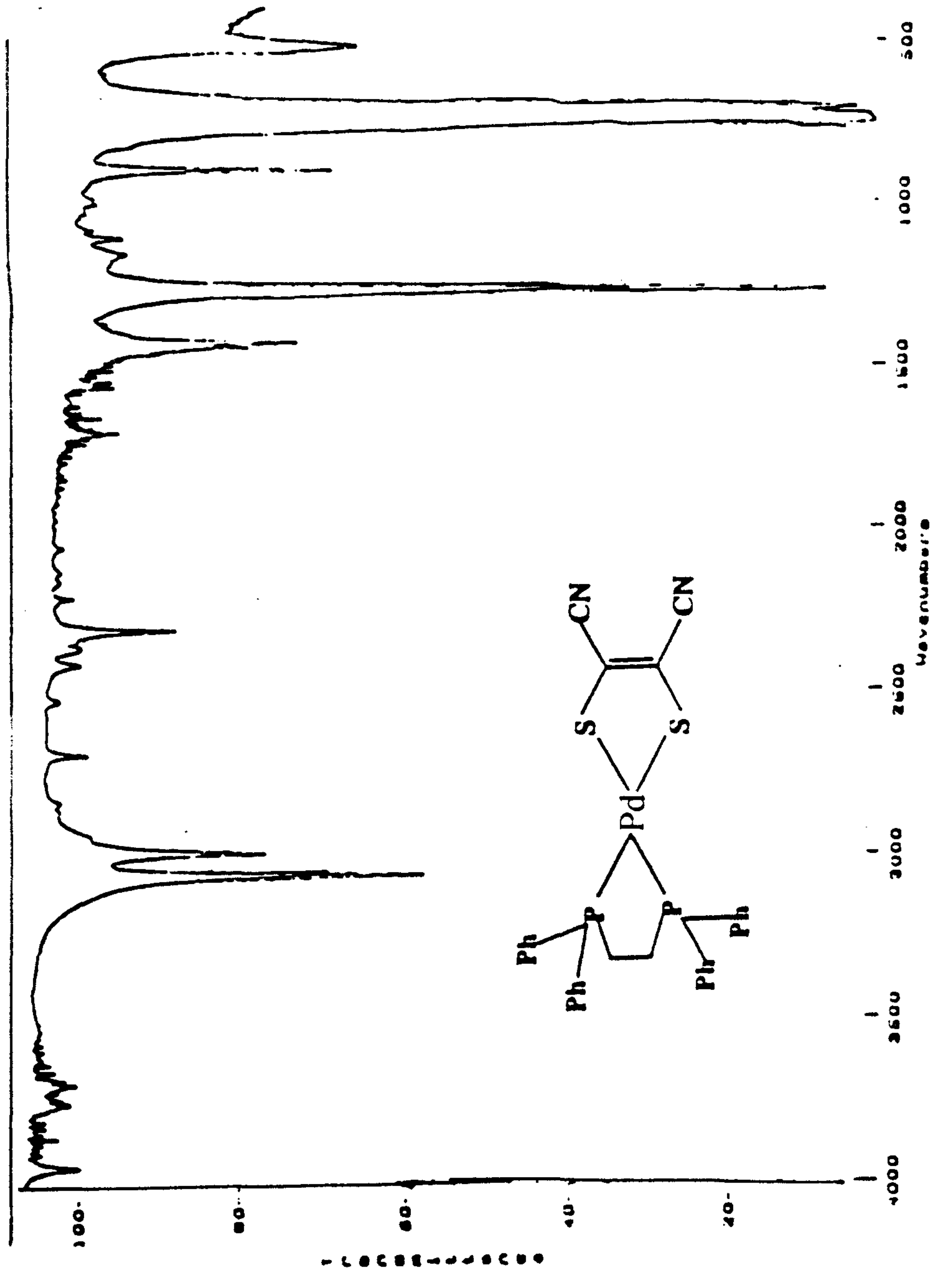

Figure 2.5: IR of (dppe)Pd(mnt).

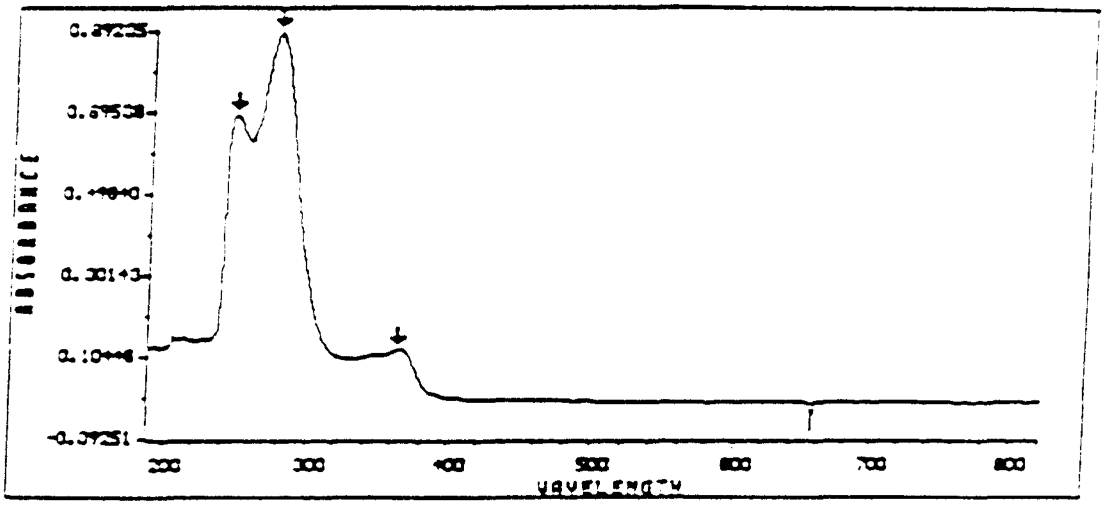

```
Marked Wavelengths
  Reg B: L 246 =  0.69296
  Reg B: L 276 =  0.89235
  Reg B: L 364 =  0.12424
```

Figure 2.6: UV-Vis of (dppe)Pd(mnt).

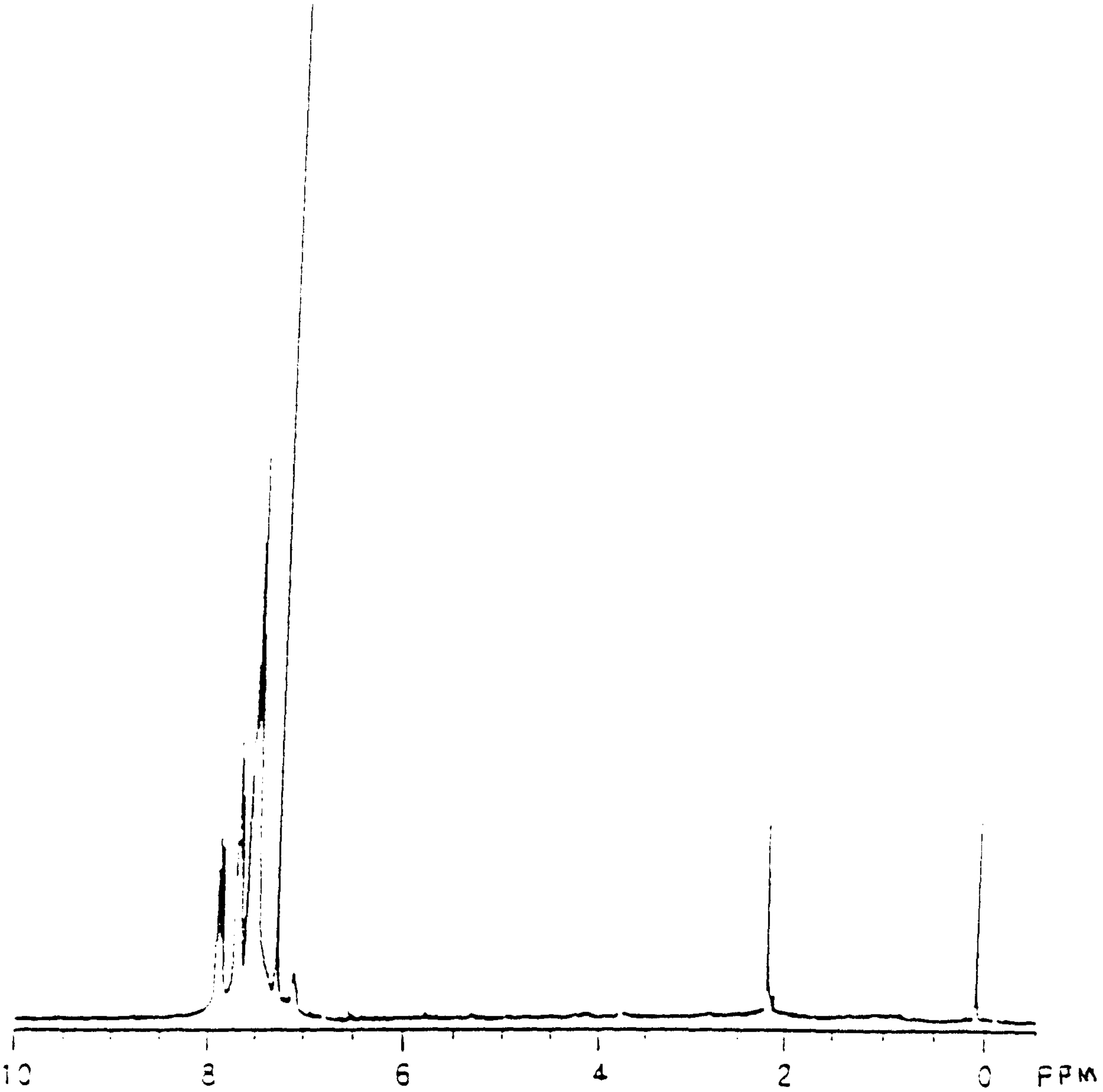

Figure 2.7: ^{1}H NMR of (dppe)Pd(mnt).

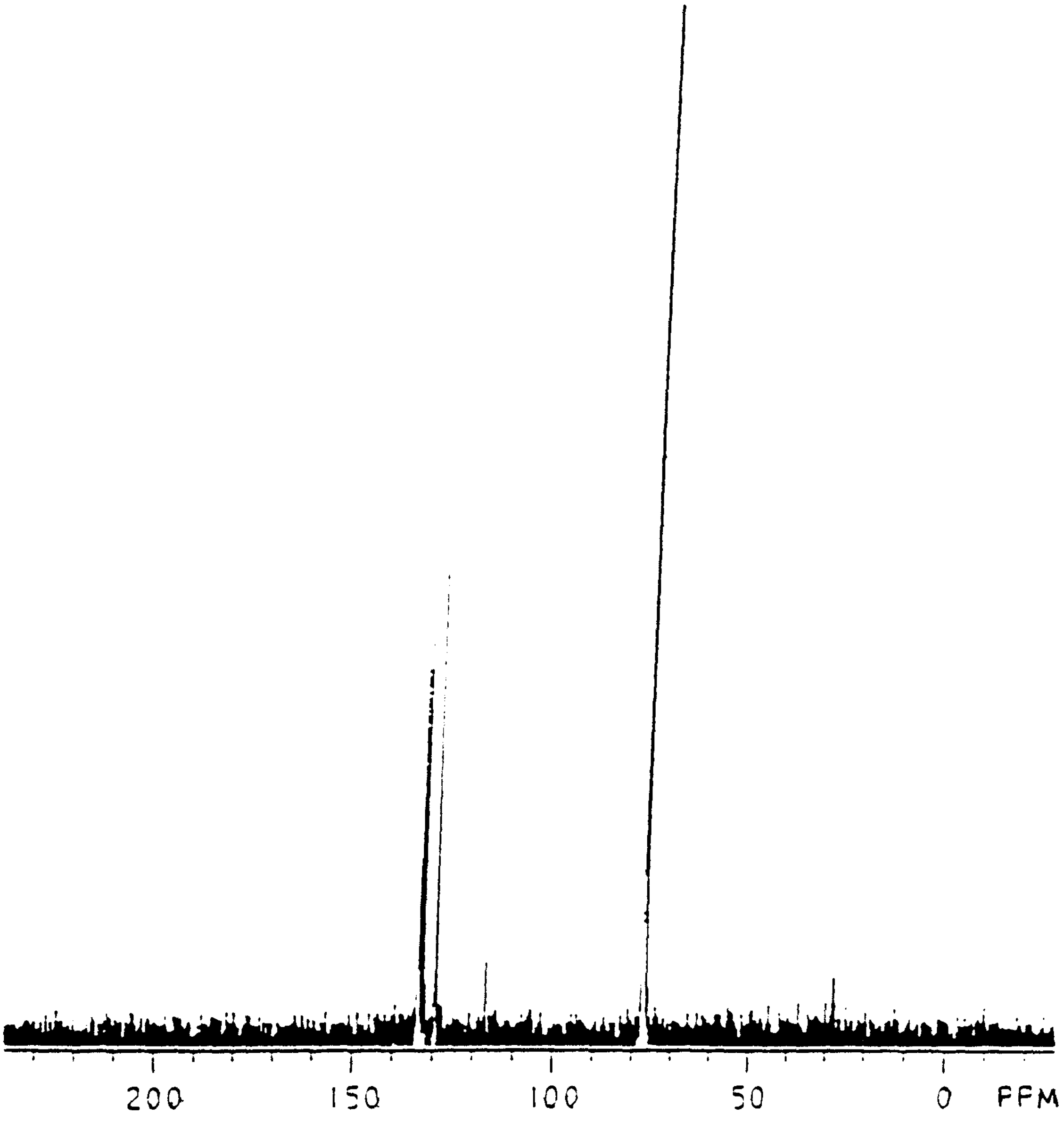

Figure 2.8: ^{13}C NMR of 9dppe)Pd(mnt).

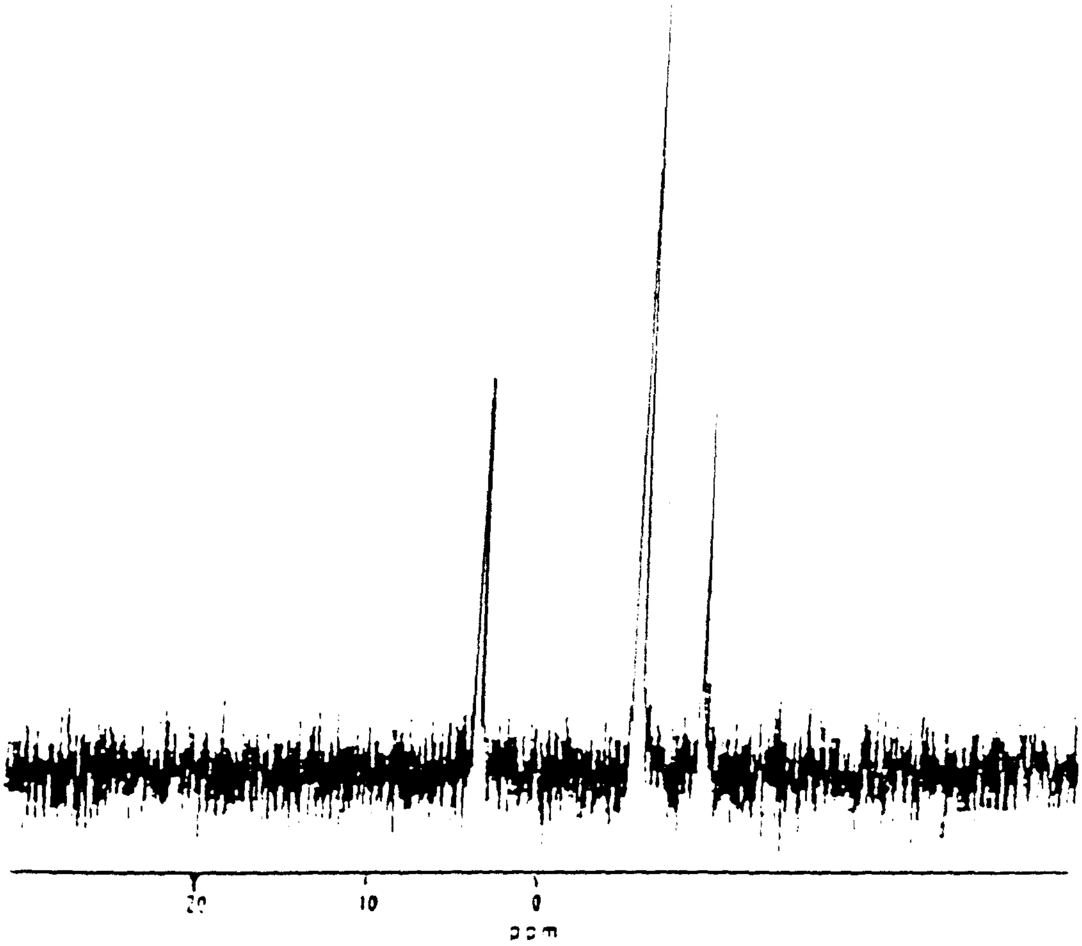

Figure 2.9: ^{31}P NMR of (dppe)Pd(mnt).

IR Data* for DPPE and TPP M-mnt Complexes

	C-S	C=C	Ar-H	Ar-P	Ar	CN	M.S.
DPPE Ni-Cl	---	---	3056	1258	1443	---	743
DPPE Ni-mnt	1827	1034	3029	1234	1470	2407	763
DPPE Pd-Cl	---	---	3058	1247	1431	---	743
DPPE Pd-mnt	1412	902	3058	1257	1431	2288	751
DPPE Pt-Cl	---	---	3055	1280	1430	---	752
DPP Pt-mnt	1417	902	3056	1289	1431	2288	757
TPP Ni-Cl	---	---	3024	1217	1557	---	772
TPP Ni-mnt	1443	969	3028	1219	1523	2403	766
TPP Pd-Cl	---	---	2950	1100	1431	---	740
TPP Pd-mnt	1431	902	3056	1271	1523	2302	743
TPP Pt-Cl	---	---	3024	1219	1569	---	769
TPP Pt-mnt	1433	931	3025	1221	1521	2363	766

* All numerical data in this table is expressed in cm^{-1}

Table 2.1: IR data for Starting Materials and Intermediates.

UV-vis Data

	λ_{max} (nm)
DPPE Ni-Cl	282
DPPE Ni-mnt	274
DPPE Pd-Cl	262
DPPE Pd-mnt	276
DPPE Pt-Cl	260
DPPE Pt-mnt	240
TPP Ni-Cl	247
TPP Ni-mnt	268
TPP Pd-Cl	341
TPP Pd-mnt	296
TPP Pt-Cl	242
TPP Pt-mnt	348

Table 2.2: UV-Vis data for Starting Materials and Intermediates.

^1H NMR Spectroscopic data

	Ph-H δ (ppm)	CH_2-P δ (ppm)
DPPE Ni-Cl	7.6 (m)	2.7 (s)
DPPE Ni-mnt	7.5 (m)	3.7 (s)
DPPE Pd-Cl	7.7 (m)	2.7 (s)
DPPE Pd-mnt	7.5 (m)	2.6 (s)
DPPE Pt-Cl	7.5 (m)	2.2 (s)
DPPE Pt-mnt	7.5 (m)	2.5 (s)
TPP Ni-Cl	7.5 (m)	---
TPP Ni-mnt	7.5 (m)	---
TPP Pd-Cl	7.3 (m)	---
TPP Pd-mnt	7.3 (m)	---
TPP Pt-Cl	7.3 (m)	---
TPP Pt-mnt	7.5 (m)	---

Table 2.3: ^1H NMR data for Starting Materials and Intermediates.

^{13}C NMR Spectroscopic data

	Ph δ (ppm)	C=C-S δ (ppm)	CN δ (ppm)
DPPE Ni-Cl	132 (m)	---	---
DPPE Ni-mnt	132 (m)	131 (s)	116 (s)
DPPE Pd-Cl	133 (m)	---	---
DPPE Pd-mnt	133 (m)	132 (s)	116 (s)
DPPE Pt-Cl	132 (m)	---	---
DPPE Pt-mnt	132 (m)	131 (s)	116 (s)
TPP Ni-Cl	137 (m)	---	---
TPP Ni-mnt	137 (m)	132 (s)	117 (s)
TPP Pd-Cl	137 (m)	---	---
TPP Pd-mnt	137 (m)	132 (s)	117 (s)
TPP Pt-Cl	134 (m)	---	---
TPP Pt-mnt	134 (m)	129 (s)	116 (s)

Table 2.4: ^{13}C NMR data of Starting Material and Intermediates.

^{31}P NMR Spectroscopic data

	P-P δ (ppm)	P-M δ (ppm)
DPPE Ni-Cl	-2.906 (s)	---
DPPE Ni-mnt	-0.398 (s)	---
DPPE Pd-Cl	6.524 (s)	---
DPPE Pd-mnt	-5.20 (s)	---
DPPE Pt-Cl	-15.15 (s)	-27.8, -9.9 (d)
DPPE Pt-mnt	-18.96 (s)	-22.1, -8.2 (d)
TPP Ni-Cl	-4.370 (s)	---
TPP Ni-mnt	25.913 (s)	---
TPP Pd-Cl	-36.81 (s)	---
TPP Pd-mnt	-34.33(s)	---
TPP Pt-Cl	-45.79 (s)	---
TPP Pt-mnt	17.08 (s)	24.3, 9.87 (d)

Table 2.5: ^{31}P NMR data for Starting Materials and Intermediates.

square planar coordination for the d^8 Pd and Pt centers. However, the coordination geometry about the Ni center was less certain. (Figure 2.10)

The spectroscopic results are in excellent correlation with values of related mnt complexes. Also, the dppe complexes correlate very well with the PPh_3 complexes for each individual metal. The structures proposed for the title complexes have been confirmed by single crystal X-ray diffraction analyses.

2:4.2 *X-ray crystallographic characterization of the (phosphine)M(mnt) title complexes*

The title complexes readily form excellent crystals upon slow evaporation of their chloroform solutions. These were used in the single crystal X-ray diffraction analyses which proceeded routinely for all of the complexes. (Table 2.6) Interestingly, all three of the title complexes are isomorphous, crystallizing in the monoclinic crystal system and the $P2_1/n$ space group. The unit cells were remarkably similar. Indeed, the fractional positions and displacement parameters of the atoms are sufficiently correspondent that the fractional coordinates and displacement parameters of all of the atoms of one of the congeners can be used to start the least squares refinement of the others. Indeed, even the hydrogen atoms are well behaved and the solution converges within a few refinement cycles.

The M-P, C-C, C-H and P-C bonds in and to the dppe ligand are unexceptional[25,26] and no significant intermolecular contacts are observed. More interestingly, all of these complexes show essentially square planar metal centers with approximately 90 and 180° bond angles around the metals. The maximum deviation from the least squares planes defined by Ni, Pd, or Pt and S1, S2, P1, and P2 is 0.171 Å

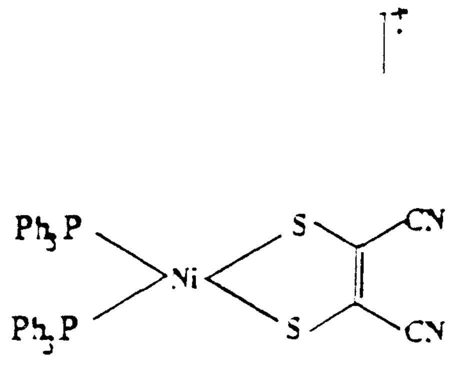
Ph$_3$P
Ph$_3$P
Ni
S
S
CN
CN

MW = 724

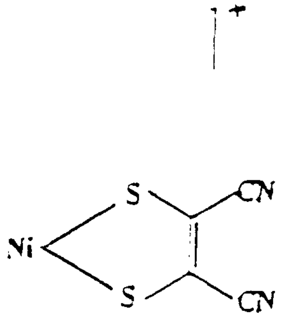

MW = 200

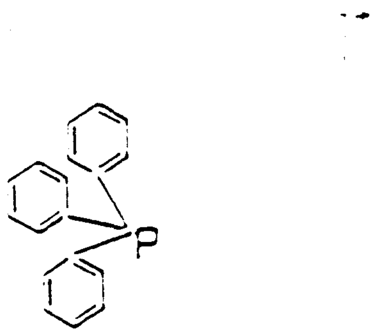

MW = 262

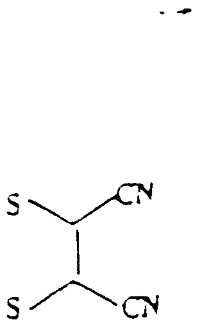

MW = 140

Figure 2.10: Mass Spectrum fragments of (dppe)Pd(mnt).

Table 2.6: Crystal Data Tables for (dppe)M(mnt).

Crystal data and structure refinement

Complex	(dppe)Ni(mnt) (1)	(dppe)Pd(mnt) (2)	(dppe)Pt(mnt) (3)
Empirical formula	$C_{30}H_{24}N_2NiP_2S_2$	$C_{30}H_{24}N_2P_2PdS_2$	$C_{30}H_{24}N_2P_2PtS_2$
Formula weight	597.28	644.97	733.66
Temperature (K)	293(2)	293(2)	293(2)
Radiation, wavelength (Å)	Cu Kα, 1.54178	Mo Kα, 0.71073	Mo Kα, 0.71073
Crystal system	monoclinic	monoclinic	monoclinic
Space group	$P2_1/n$	$P2_1/n$	$P2_1/n$
a (Å)	11.2359(13)	11.5170(12)	11.4853(8)
b (Å)	12.655(2)	12.636(6)	12.4617(6)
c (Å)	19.711(2)	19.796(2)	19.8013(13)
β (°)	91.270(9)	91.237(8)	91.346(5)
Volume (Å^3)	2802.1(6)	2880(2)	2833.3(3)
Z	4	4	4
D_{calc} (Mg m^{-3})	1.416	1.487	1.720
Absorption coefficient (mm^{-1})	3.643	0.923	5.235
$F(000)$	1232	1304	1432
Crystal size (mm)	0.18 × 0.16 × 0.10	0.40 × 0.20 × 0.10	0.40 × 0.30 × 0.12
θ Range data collection (°)	4.15–56.15	2.03–30.04	1.93–30.00
Limiting indices	$-12 \leq h \leq 12$	$-16 \leq h \leq 16$	$-1 \leq h \leq 16$
	$-13 \leq k \leq 13$	$-17 \leq k \leq 17$	$-1 \leq k \leq 17$
	$-21 \leq l \leq 21$	$0 \leq l \leq 27$	$-27 \leq l \leq 27$
Reflections collected	7479	9866	10379
Independent reflections	3651 ($R_{int} = 0.0327$)	8182 ($R_{int} = 0.0419$)	8259 ($R_{int} = 0.0392$)
Observed reflections (criterion)	2614 ($I > 2\sigma(I)$)	5251 ($I > 2\sigma(I)$)	5692 ($I > 2\sigma(I)$)
Max., min. transmission	0.123, 0.0439	0.9201, 0.4763	0.0641, 0.0253
Data/restraints/parameters	3651/0/431	8150/0/431	8258/0/431
Goodness-of-fit on F^2	1.041	1.026	1.006
Final R indices ($I > 2\sigma(I)$)			
$R1$	0.0412	0.0600	0.0404
$wR2$	0.0990	0.1413	0.0825
R indices (all data) [a]			
$R1$	0.0592	0.1069	0.0730
$wR2$	0.1184	0.2030	0.0960
Extinction coefficient	0.00000(9)	0.0010(4)	0.00332(14)
Final difference map, largest peak, hole (e Å^{-3})	0.61, −0.35	1.18, −2.33	0.68, −0.89

---

[a] As noted in Ref. [24]: Refinement on F^2 for all reflections. Weighted R-factors, $wR2$ and all goodnesses-of-fit, S, are based on F^2. Conventional R-factors, $R1$, are based on F, with F set to zero for negative F^2. The observed criterion of $F^2 > 2\sigma(F^2)$ is used only for calculating R-factors, etc., and is not relevant to the choice of reflections for refinement. R-factors based on F^2 are statistically about twice as large as those based on F, and R-factors based on all data will be even larger.

for the nickel complex. This geometry is typical for d^8 transition metal complexes of second and third row transition elements, but is somewhat surprising for the nickel complex.

The maleonitriledithiolate portion of the complex is also planar. The maximum deviation from the least squares plane of the mnt ligand is 0.1029 Å for the platinum complex. This is typical of mnt containing transition metal complexes. The plane of the ligand is tilted slightly at an angle of 8.2, 8.1, and 7.9 ° with respect to the metal square planes in the Ni, Pd, and Pt complexes, respectively. The bond lengths observed within the mnt ligand are more consistent with a structure dominated with the α,β-dithiolate resonance form than the α,β-dithione resonance form, i.e.

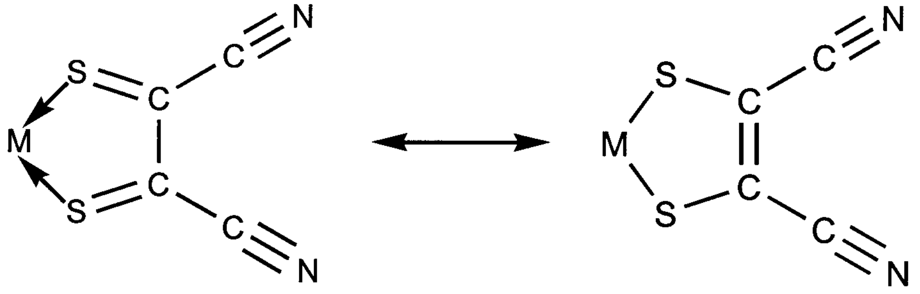

α,β-dithione α,β-dithiolate

Thus, the observed metal-mnt structural fragments are similar to those reported previously for other Ni and Pt dithiolate complexes[26]. Namely, a largely dithiolate structure with a small dithione component. Thus, the observed S1-C2/S2-C3 and C1-C2/C3-C4 distances are consistent with formal single S-C and C-C bonds (i.e. 1.75 Å for S-C(sp^2) bonds and 1.43 Å, C(sp)-C(sp^2) bonds, respectively) while the observed N1-C1/N2-C4 and C2-C3 distances are consistent with formal triple and double bonds (i.e.

1.14 Å for N(sp)-C(sp) bonds and 1.32 Å for C(sp^2)-C(sp^2) bonds, respectively)[25]. This is presumably due to the preference for the metal centers to retain a formal +2 oxidation state in these complexes and delocalization of electron density from the filled d orbitals on the metals to the vacant π*-antibonding orbitals on the mnt ligand. This bonding description is consistent with the IR and UV-Visible spectroscopic evidence presented above (Figures 2.11, 2.10, 2.12 and 2.14).

2:2.3 Synthesis of C_{60}-(mnt)$_2$.

The mass spectrum of this complex displays a parent ion peak at approximately 1002 m/z and major fragmentation peaks at 925, 860, 846, 783, 750 and 718 m/z. No isotopic distribution appropriate for a heavy metal such as platinum was detected. The peak at 1002 m/z corresponds to a C_{60} that is disubstituted with mnt and the peak that appears at 915 m/z correlates with a mono-substituted C_{60}-mnt. The peak a 718 m/z indicates the presence of C_{60} (Figure 2.15).

These complexes are primarily organic in nature and elemental analysis revealed that they contain only carbon, nitrogen, sulfur and sodium. Thermal gravimetric analysis showed that the crude product experienced a sharp decrease in mass at 430 °C which indicated that the C_{60}-(mnt)$_2$ complex was stable to up to that point (Figure 2.16). C_{60} itself is thermally stable to approximately 560 °C. This suggests that C_{60} has undergone some type of addition reaction and the product is less stable than C_{60} itself. The data from the DSC is in agreement with this finding. Analysis of the data reveals a sharp exotherm at approximately 315 °C, which is characteristic of substituted C_{60} complexes.

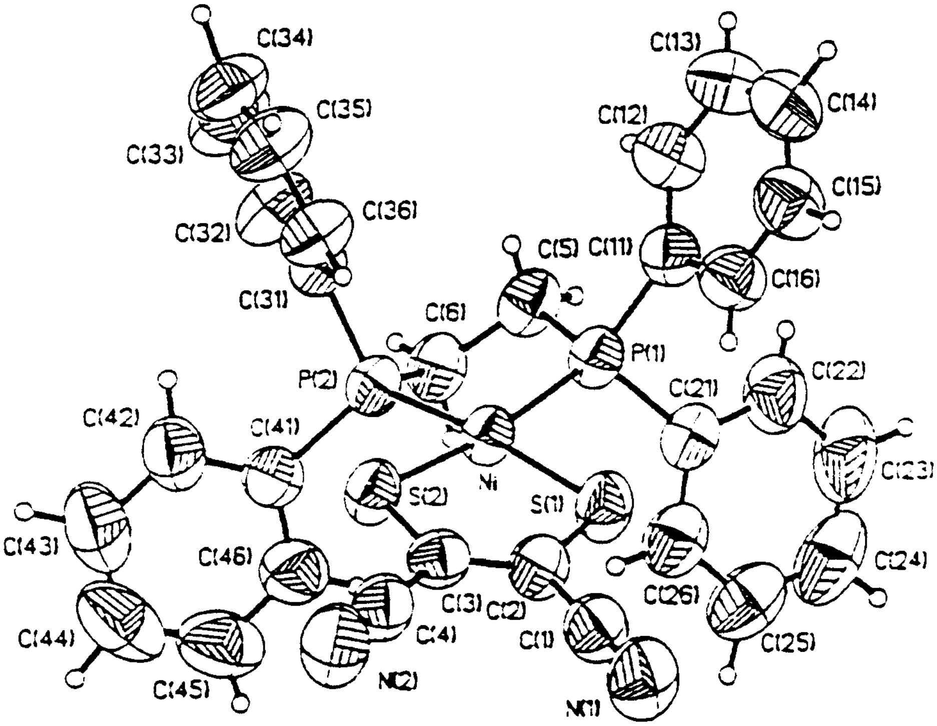
C(34)
C(13)
C(14)
C(35)
C(12)
C(33)
C(15)
C(36)
C(32)
C(5)
C(11)
C(16)
C(31)
C(6)
P(1)
P(2)
C(21)
C(22)
C(42)
C(41)
Ni
C(23)
S(2)
S(1)
C(43)
C(46)
C(24)
C(3)
C(2)
C(26)
C(4)
C(44)
C(1)
C(25)
C(45)
N(2)
N(1)

Figure 2.11: ORTEP Plot for (dppe)Ni(mnt), 50% ellipsoids, perspective view.

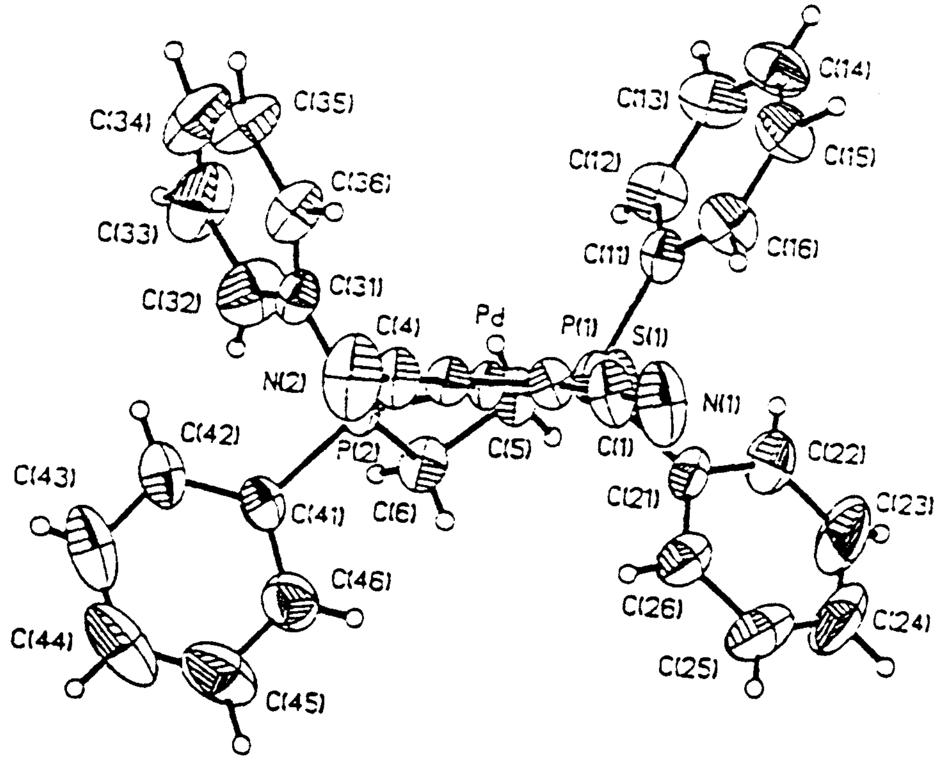
C(34)
C(35)
C(36)
C(33)
C(32)
C(31)
C(4)
Pd
P(1)
S(1)
C(11)
C(12)
C(13)
C(14)
C(15)
C(16)
N(2)
N(1)
C(42)
P(2)
C(5)
C(1)
C(22)
C(43)
C(41)
C(6)
C(21)
C(23)
C(46)
C(26)
C(44)
C(45)
C(25)
C(24)

Figure 2.12: ORTEP Plot for (dppe)Pd(mnt), 50% ellipsoids, view in the square plane.

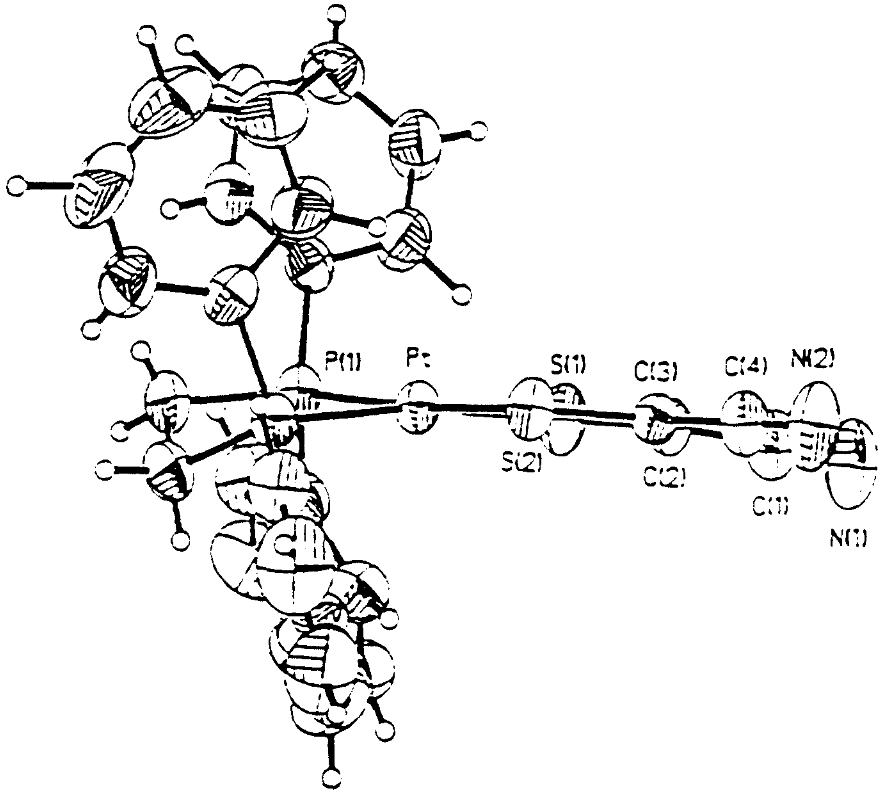
P(1)
Pt
S(1)
C(3)
C(4)
N(2)
S(2)
C(2)
C(1)
N(1)

Figure 2.13: ORTEP Plot for (dppe)Pt(mnt), 50% ellipsoids, view in the square plane.

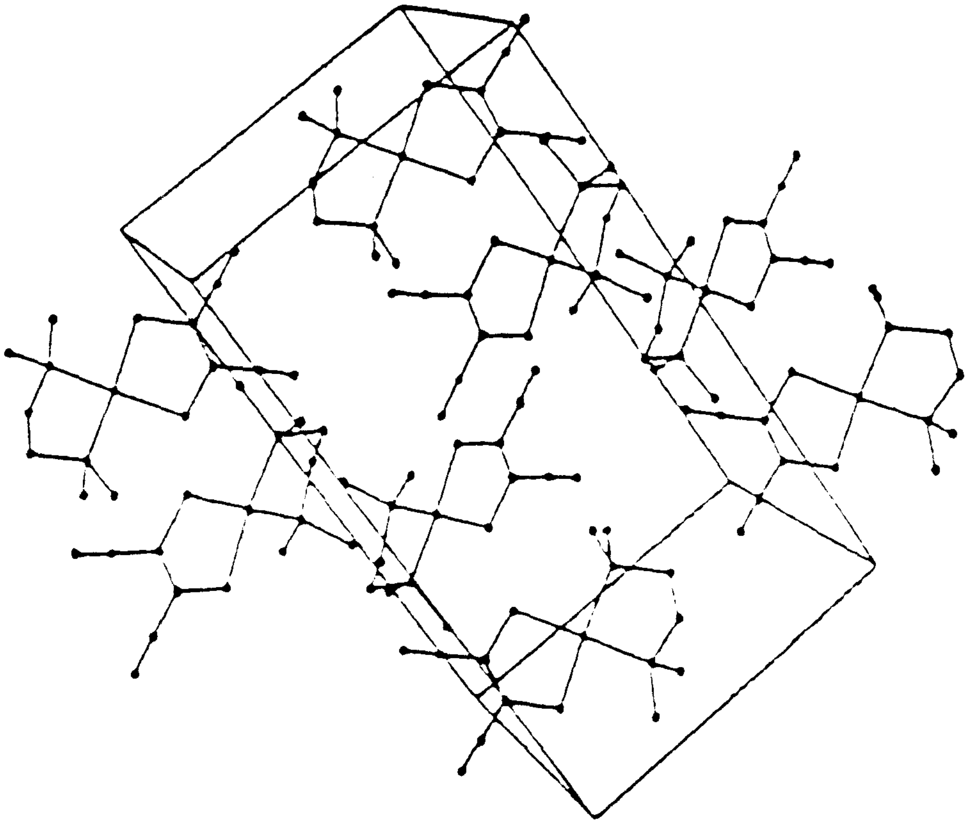

Figure 2.14: Unit Cell of (dppe)Pd(mnt).

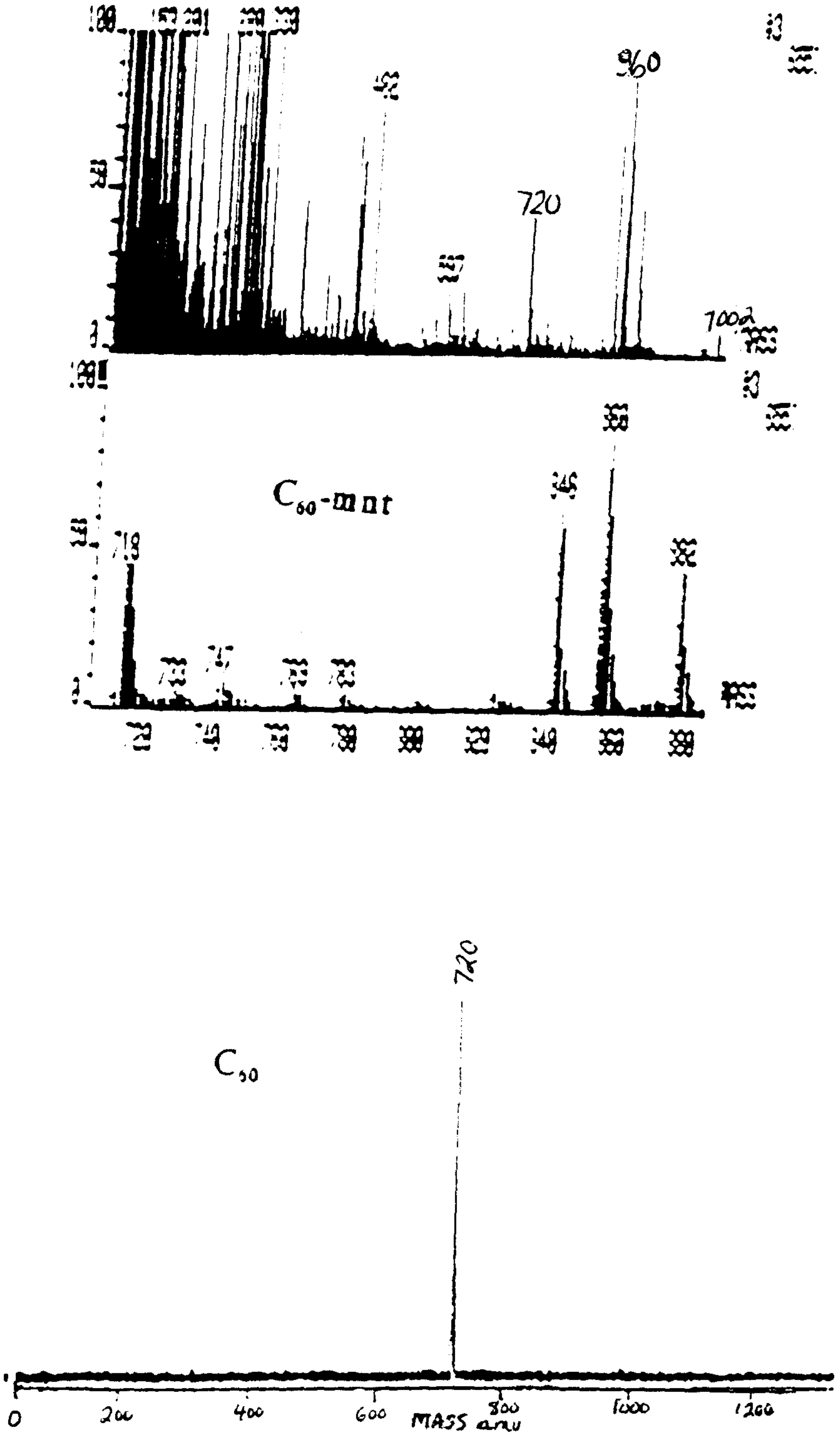

Figure 2.15: Mass Spectrum of C_{60}-mnt.

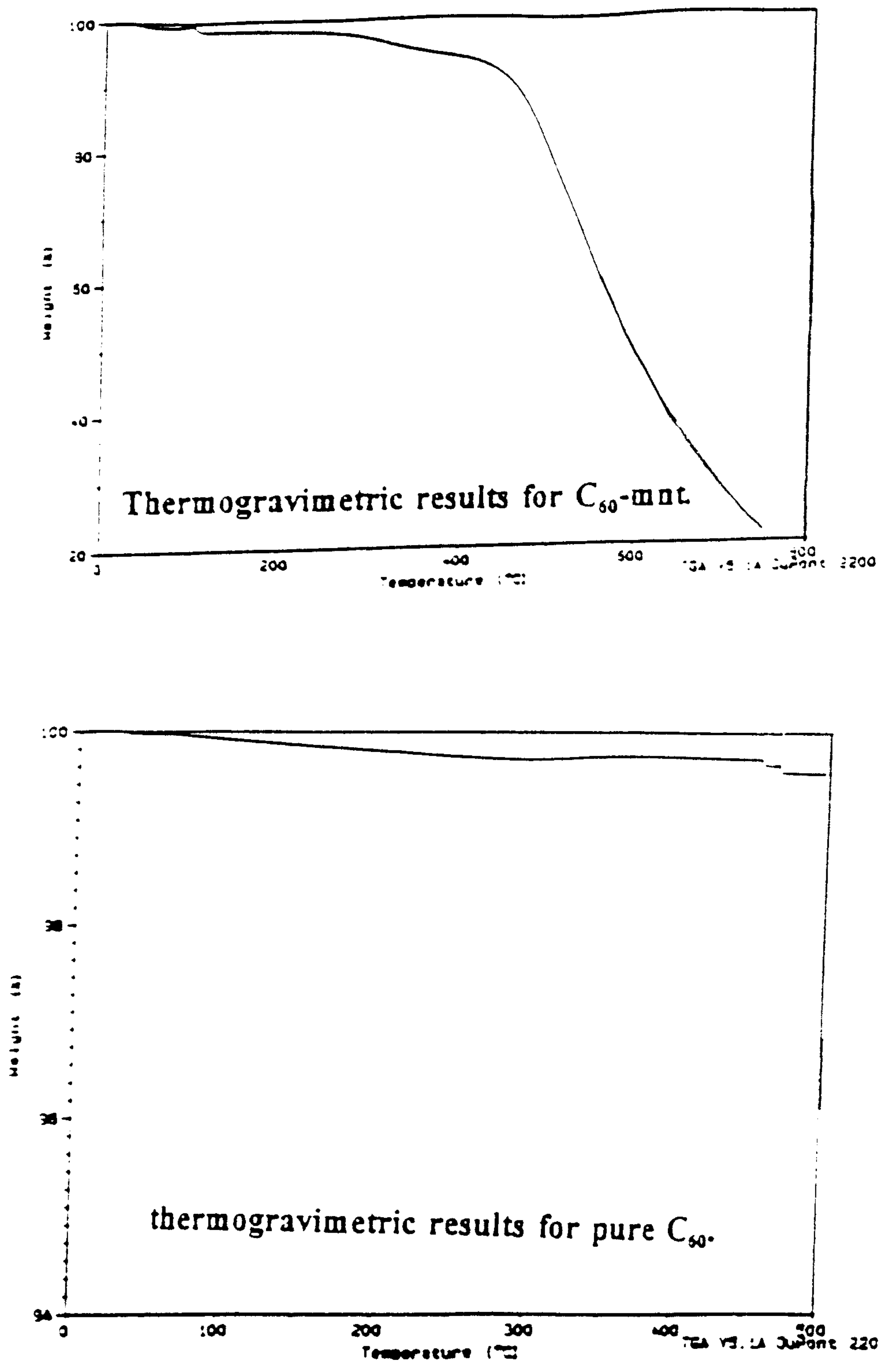

Figure 2.16: Thermal Gravimetric Analysis of C_{60}-mnt.

The UV-Vis spectra (Figure 2.17) were unremarkable, except for the absence of a band at 608 nm, which may correspond to a ligand to metal charge transfer band. Fagan and Calabrese observed a similair phenomenon in their complexes. The IR spectra (Figure 2.18) is weak, but the presence of a nitrile group is easily detected. Further attempts to isolate the products contained in the mixture and a full characterization of these complexes are still being pursued.

2:5 Conclusions

The synthesis and characterization of a series of (phosphine)M(mnt) complexes of the group X metals is reported. These materials could not be converted into the desired fullerene mnt complexes via ligand displacement of the phosphine(s). However, they should serve as interesting models for the structure and electrochemistry of exohedrally substituted fullerene complexes. Maleonitriledithiolate was chosen as this ligand because it was believed that it could be attached via a transition metal bridge. One of the problems with using the mnt ligand for this project is that the nickel, palladium or platinum atoms that act as the transition metal bridge would have to remain in the +2 oxidation state. The +2 oxidation state implies that the transition metal is electron deficient. The reactivity of C_{60} is most similiar to that of an electron deficient arene. Therefore, it is unlikely that a transition metal that is in an oxidation state of +2 would be able to bond to the C_{60} cage. The results of this chapter agree with this hypothesis.

The intermediates were fully characterized through single crystal X-ray diffraction and various spectroscopic techniques. The data obtained via single crystal X-ray diffraction analysis unequivocally shows that the title complexes have been successfully

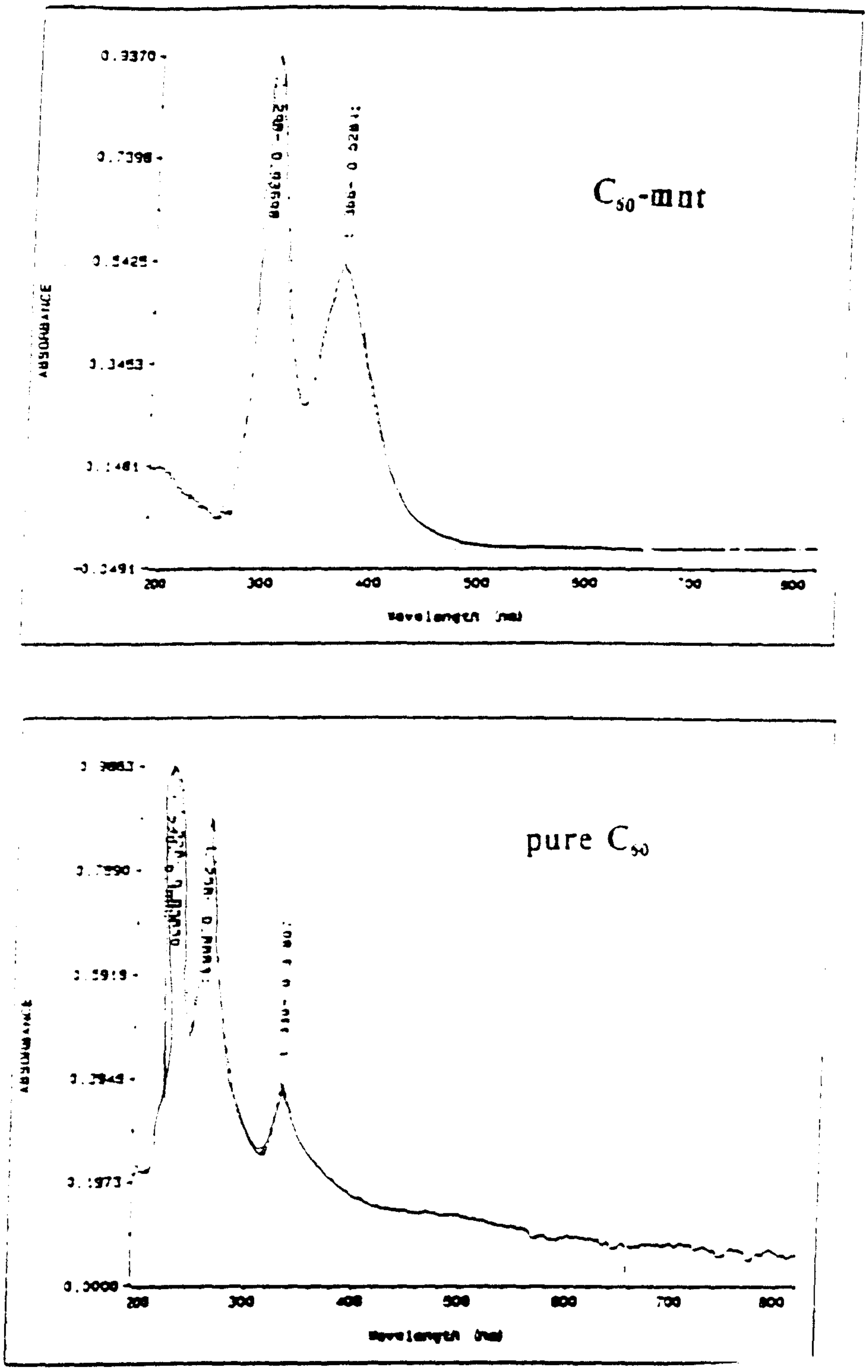

Figure 2.17: UV-Vis of C_{60}-mnt.

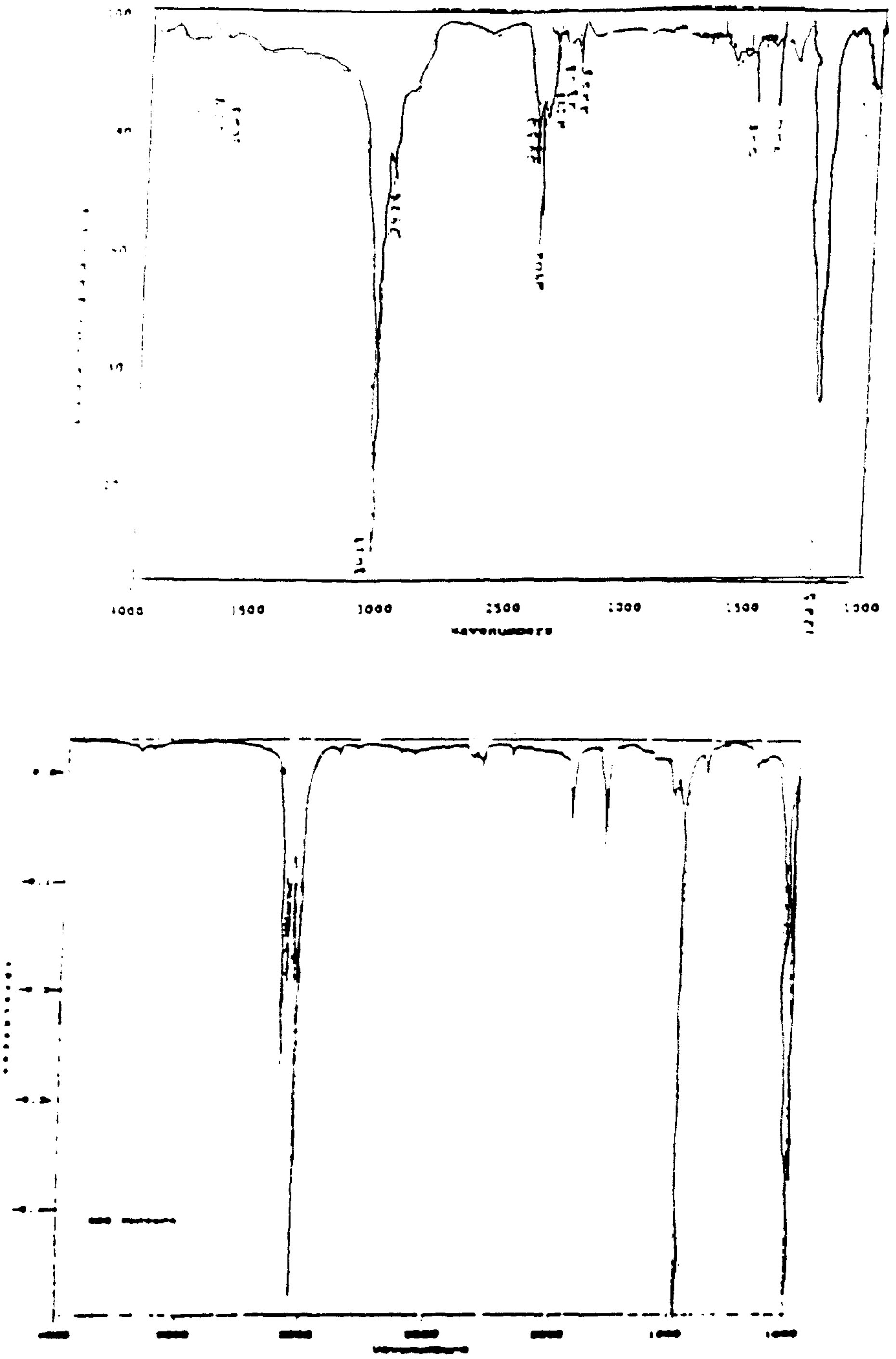

Figure 2.18: IR of C_{60}-mnt.

synthesized and that all are essentially square planar about the metal center. The NMR data demonstrates the phosphorus coordination with transition metal center and the IR data reveals the presence of nitrile stretching. The combination of the structural and spectroscopic data also suggests substantial delocalization of electron density to the mnt ligand in these complexes.

References Cited:

(1) Kroto, H. W.; Heath, J.R.; O'Brian, S. C.; Curl, R. F.; and Smalley, R. E., *Nature*, **1985**, *318*, 162-163.

(2) Heath, J. R., *J. Am. Chem. Soc.*, **1985**, *107*., 7779-7780.

(3) Kroto, H. W., *Nature*, **1987**, *329*, 529-531.

(4) Holczer, K., *Science*, **1991**, *252*, 1154.

(5) Chen, F., Doctoral Dissertation, Temple University, **1993**.

(6) Fagan, P. J.; Calabrese, J.C.; Malone, B. J., *Science*, **1991**, *252*, 1160-1161.

(7) Fagan, P. J.; Calabrese, J.C.; Malone, B. J., *J. Am. Chem. Soc.*, **1991**, *113*, 9408-9409.

(8) Fagan, P. J.; Ward, M.D.; Calabrese, J. C., *J. Am. Chem. Soc.*, **1989**, 111, 1698.

(9) Landis, M., Master's Thesis, Temple University, **1996**.

(10) Hunter, A. D.; Mozol, V.; and Tsai, S. D. *Organometallics,* **1992,***11,* 2251-2262.

(11) Tsai, S. D.; Ph.D. Thesis entitled "Long-Range Electron Transfer", **1995**, Department of Chemistry, University of Alberta, Edmonton, Alberta, Canada.

(12) Cai (Tsai), S. D.; and Hunter, A. D., 203rd ACS National Meeting, San Francisco, C.A., April **1992**, INOR 413.

(13) Eisenberg, R.; Ibers, J. A.; Clark, R. J.; and Gray, H. B., *J. Am. Chem. Soc.*, **1964**, *96*, 113-115.

(14) Williams, R.; Billig, E.; Waters, J. H.; and Gray, H. B., *J. Am. Chem. Soc.*, **1996**, *88*(1), 43-50.

(15) Best, S. P.; Clark, J. H.; McQueen, R. C.; and Watson, R. J., Inorg. Chem., **1988,** *27*, 884-890.

(16) Filler, F. L., Master's Thesis, Temple University, **1996**.

(17) Richter-Addo, G. B.; and Hunter, A. D. *Inorg. Chem.,* **1989,** *28,* 4063-4065.

(18) Hunter, A. D.; and Szigety, A. B. *Organometallics,* **1989,** *8*, 2670-2679.

(19) Shriver, D. F.; and Drezdzon, M. A. *The Manipulation of Air-Sensitive Compounds*, Wiley, New York, 2nd edn., **1986**.

(20) Perrin, D. D.; Armarego, W. L. F.; and Perrin, D. R. *The Purification of Laboratory Chemicals*, Pergamon, New York, 2nd edn., **1980**.

(21) Muetterties, E. L., ed., Inorganic Syntheses, Vol. 10, McGraw-Hill Book Co., New York, N. Y., **1967**, 11-13.

(22) XSCANS Version 2.1 and 2.2, Siemens Industrial Automation, Inc., Analytical X-Ray Instruments, 6300 Enterprise Lane, Madison, WI, USA, 53719-1173.

(23) Powell, D. Chi-90 Prrogram for selecting psi scans, Department of Chemistry, University of Wisconsin - Madison, Madison, Wisconsin, 53706.

(24) SHELXTL Version 5.03, 9/1/94 release, Siemens Industrial Automation, Inc., Analytical X-Ray Instruments, 6300 Enterprise Lane, Madison, WI, USA, 53719-1173.

(25) Allen, F. H.; Kennard, O.; Wilson, D. G.; Brammer, L.; Orpen, A. G.; Taylor, R. "Typical Interatomic Distances: Organic Compounds." in *International Tables for Cystallography, Volume C. Mathematical, Physical and Chemical Tables*, Wilson, A. J. C., ed., Kluwer Academic Publishers: Boston, **1995**; 685-706.

(26) Orpen, A. G.; Brammer, L.; Allen, F. H.; Kennard, O.; Wilson, D. G.; Taylor, R. . "Typical Interatomic Distances: Organometallic Compounds and Coordination Complexes of the d- and f- Block Metals." in *International Tables for Cystallography, Volume C. Mathematical, Physical and Chemical Tables*, Wilson, A. J. C., ed., Kluwer Academic Publishers: Boston, **1995**; 707-791.

Chapter 3

The Synthesis, Characterization and Electrochemistry of 1,1,-*Bis*(diphenylphosphino)ferrocene Metal Fullerene Complexes.

3.1 Introduction

The focus of this project is to quantify the extent of communication between C_{60} and the metal diphosphine ligands; most notably the effects of the phosphorus ligand upon such communications. As stated in Chapter 1, extensive research has been performed on the electron transfer properties of metal-C_{60} complexes. The extent of electronic communication between C_{60}, the metal (i.e. Pt), and the phosphorus ligands, however, is complicated and remains largely unexplored.[1] Consequently, the extent of interaction between C_{60} and the phoshorus ligands remains unknown.

The long-term goal of the project outlined in Chapter 2 of this thesis was to place an electroactive ligand in close proximity to the C_{60} cage.[3] Fortunately, the overall goals are not inclusive to maleonitrilediolates and the strategy of this project may be extended to other electroactive ligands that would enable the transition metal to remain in the zero-valent state.

1,1'- (diphenylphosphino)ferrocene (dppf) is an excellent alternative (Figure 3.1) to mnt because it is active in the UV-Vis region of the electromagnetic spectrum, with a reasonably high molar absorptivity. The electrochemistry of ferrocene is well documented in the literature and appears in the anodic region of the voltammogram,

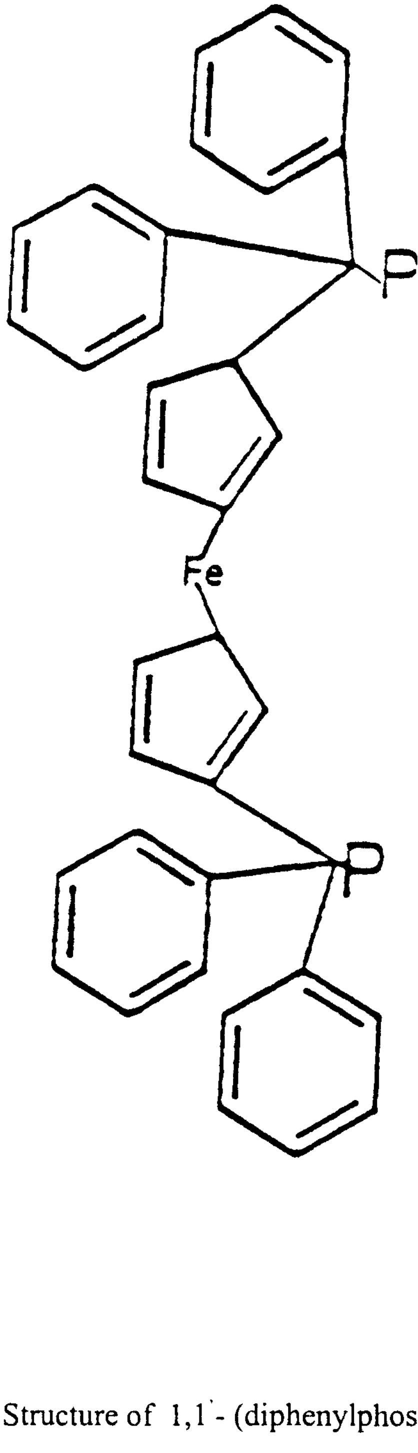

Figure 3.1: Structure of 1,1'- (diphenylphosphino)ferrocene (dppf).

whereas, the C_{60}-metal electrochemistry occurs in the cathodic region. This results in a simplified voltammogram in which the electrochemistry of the dppf ligand is readily isolated from that of the metal-C_{60} fragment. Thus, electrochemical interferences from the ligands are minimized.

This chapter establishes a viable synthetic route to C_{60}-metal-dppf complexes (Figure 3.2). The complexes were characterized via multinuclear NMR, Infrared and UV-Vis spectroscopy to establish the structure of products. Cyclic voltammetry was performed to quantify the reversibility of the electrochemical processes and to determine the extent of electronic communication in the complexes. The project's immediate goals include establishing a quick and relatively easy synthetic route for synthesizing the C_{60}-metal-dppf complexes in reasonably high yields and characterizing these complexes using NMR and electrochemistry as well as a variety of other supporting techniques. The long term goals of this project include spectroelectrochemical studies in the UV-Vis region and establishment of electron transfer pathways and kinetics between the metal containing ligands and the fullerene cage.

3.2 Experimental Section

3.2.1 General experimental procedures

The general procedures used in the lab have been described previously in great detail.[4] Unless otherwise noted, all reactions and any subsequent manipulations were conducted at ambient temperatures using conventional techniques for the manipulation of inorganic compounds.[5] When required, anaerobic and anhydrous conditions were maintained by using a prepurified argon atmosphere and a combination of vacuum-line

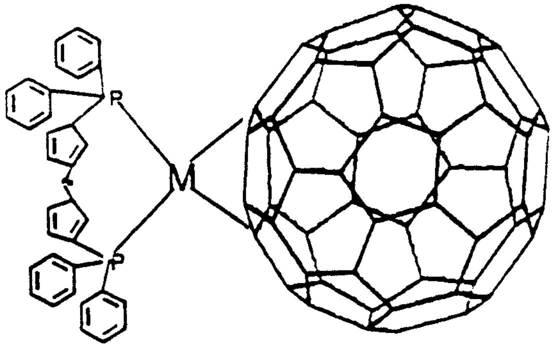

DPPF-Metal-C_{60} complex

Figure 3.2: Structure of $(C_{60})M(dppf)$.

and inert atmosphere glove box techniques. Chemicals were purchased from the Aldrich or Fisher Chemical Companies or were prepared by published procedures and were of reagent grade or comparable purity. Where necessary, reagents were purified before use. Dinitrogen and argon were of 99.9999% purity and were not further purified. Solvents were dried and deaerated by standard procedures and stored under dinitrogen or argon.

IR spectra were recorded on a Perkin-Elmer 1600 FT-IR spectrometer. ^{1}H NMR, ^{13}C NMR and ^{31}P NMR were recorded on a Varian Gemini-2000 400 MHz NMR spectrometer with a reference to the deuterium signal of the solvent employed. Chemical shifts are reported in parts per million down field from tetramethylsilane. Electronic spectra were recorded on a Hewlett Packard 8452A diode array UV-Visible spectrophotometer with wavelengths reported in nm.

Electrochemical data was recorded on a BioAnalytical Systems 100B potentiostat/galvanostat without iR compensation. The working electrode was a 1 mm platinum disk electrode provided by BAS and the counter electrode was a platinum wire. The non-aqueous reference electrode was silver / silver nitrate in a 1 molar solution of tetra-*n*-butylammonium perchlorate in THF. The electrochemical cell used was a one compartment cell provided by BAS. Freshly distilled, deoxygenated THF was the solvent used for all of the voltammetry in this Chapter.

3.2.2 Synthesis of the 1,1′-(diphenylphosphino)ferrocene metal dichlorides

All of the dppf metal dichlorides were purchased from Aldrich chemical company or were synthesized from metal tetrachlorides via ligand exchange between two chlorines and one dppf ligand. The preparation of the Pt complex is given as a representative example (Figure 3.3 and Figure 3.4).

3.2.2.1 Synthesis of (dppf)PtCl$_2$, 3.

0.50 g (1.20 mmol) K_2PtCl_4 was dissolved in 75 ml in deionized water. 0.50 g (0.9 mmol) dppf was dissolved in 50 ml of methylene chloride and was added to the K_2PtCl_4 solution with vigorous stirring to insure thorough mixing of the two solutions. The color of the methylene chloride layer turned from bright yellow-orange to rusty red. The solution was allowed to stir overnight and was heated until the methylene chloride evaporated. This slurry was extracted twice using methylene chloride and DI H_2O. The organic layer was rotovapped to dryness and dissolved in a minimal amount of methylene chloride. The product was purified via column chromatography on silica gel using methylene chloride as the eluent. A bright orange solid was formed upon slow evaporation from methylene chloride in 94.4 % yield (0.693 g, 0.850 mmol).

For $C_{34}H_{30}Cl_2FeP_2Pt$: ^{13}C NMR ($CDCl_3$): 145-143 ppm (m, 5C, C_5,H_4), 133-129 ppm (m, 6C, C_6H_5); ^{31}P NMR ($CDCl_3$): 14.102 ppm (s, 2P, P-P) 25.775 and 2.422 ppm (d, 2P, P-M-P); UV-Visible (CH_2Cl_2, λ_{max}, nm): 302, 350 and 430; IR (CH_2Cl_2, cm^{-1}): 3010, 1171 and 1371.

3.2.2.2 Synthesis of (dppf)NiCl$_2$, 1 and (dppf)PdCl$_2$, 2.

These two complexes were prepared as described above yielding dark green and rusty red crystals for the Ni and Pd complexes, respectively. The compounds were produced in 88.2 % and 95.1 % yields, respectively for the Ni and Pd complexes.

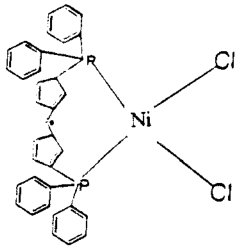

1

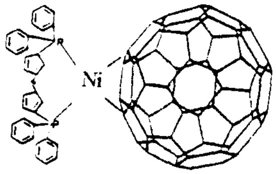

4

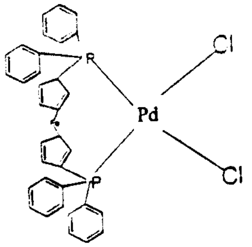

2

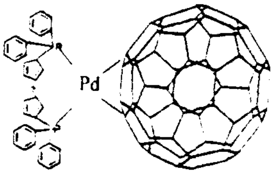

5

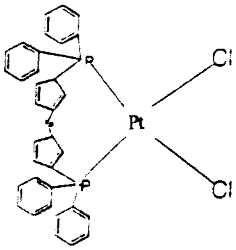

3

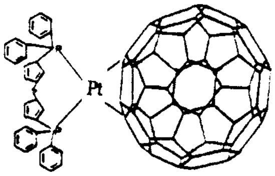

6

Figure 3.3: List of Compound Numbers.

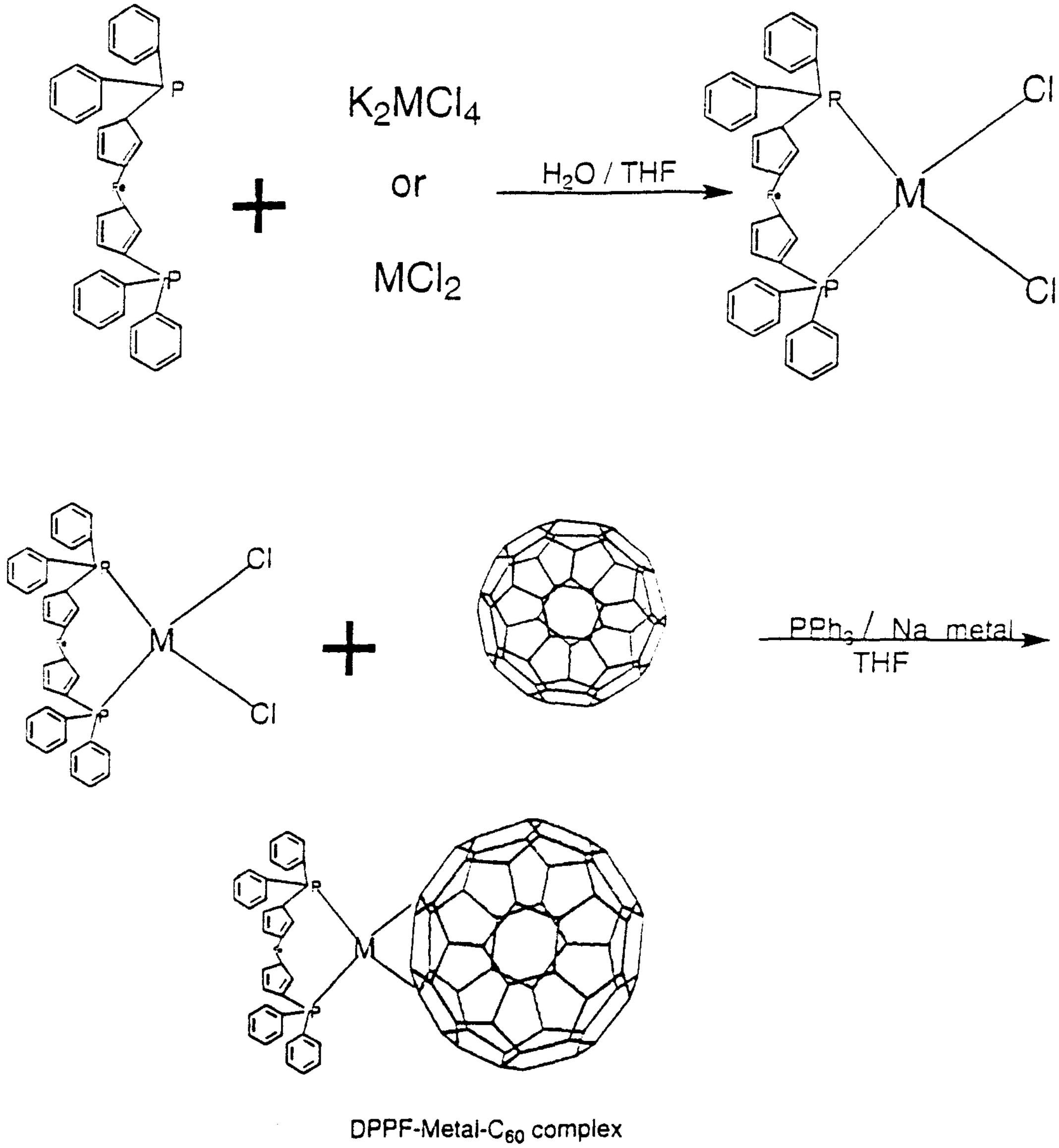
P
Fe
P
K2MCl4
or
MCl2
H2O / THF
M
Cl
Cl
PPh3 / Na metal
THF
DPPF-Metal-C60 complex

Figure 3.4: Synthesis of (dppf)MCl_2 and (dppf)M(C_{60}).

For $C_{34}H_{30}Cl_2FeNiP_2$: ^{13}C NMR ($CDCl_3$): 146-143 ppm (m, 5C, C_5,H_4), 133-130 ppm (m, 6C, C_6H_5); ^{31}P NMR ($CDCl_3$): 25.835 ppm (s, 2P, P-P); UV-Visible (CH_2Cl_2, λ_{max}, nm): 300 and 404; IR (CH_2Cl_2, cm^{-1}): 3022, 1170 and 1388.

For $C_{34}H_{30}Cl_2FeP_2Pd$: ^{13}C NMR ($CDCl_3$): 145-144 ppm (m, 5C, C_5,H_4), 133-130 ppm (m, 6C, C_6H_5); ^{31}P NMR ($CDCl_3$): 27.272 ppm (s, 2P, P-P) 30.254 and 25.835 ppm (d, 2P, P-M-P); UV-Visible (CH_2Cl_2, λ_{max}, nm): 300, 344 and 476; IR (CH_2Cl_2, cm^{-1}): 3012, 1171 and 1371.

3.2.3 Synthesis of (dppf)Pt(C_{60}), ***6****:*

0.500 g (0.0069 mol) of C_{60}, 0.491 g (0.00060 mol) of dppf(Pt)Cl_2 and 0.0520 g (0.00020 mol) of triphenylphosphine were dissolved in freshly distilled THF and allowed to stir at ambient temperature for 10 - 15 minutes under argon (Figure 3.4). Four to six pieces of Na metal shots were rinsed with hexane, pressed into a sheet and then added to the C_{60} mixture. The solution was allowed to reflux for 30 minutes and then allowed to cool to room temperature. The dark green solution was then rotovapped to dryness. The resulting dark green solid was dissolved in a minimum amount of methylene chloride and purified via column chromatography on silica gel using methylene chloride as the eluent. Dark green crystals were formed upon slow evaporation from methylene chloride in 88.6 % yield (0.782 g, 0.000532 mol).

For $C_{94}H_{30}Cl_2FeP_2Pt$: ^{13}C NMR ($CDCl_3$): 146-143 ppm (m, 5C, C_5,H_4), 135-129 ppm (m, 6C, C_6H_5); ^{31}P NMR ($CDCl_3$): 25.775 ppm (s, 2P, P-P) 29.303 and 24.319 ppm (d, 2P, P-M-P); UV-Visible (CH_2Cl_2, λ_{max}, nm): 302, 330 and 434; IR (CH_2Cl_2, cm^{-1}): 1181, 1365, 2997, 2850, 3047, 1181 and 1335.

3.2.3.1 Synthesis of (dppf)Ni(C_{60}),4 and (dppf)Pd(C_{60}), 5.

These two complexes were prepared as described above yielding dark green and rusty red crystals for the Ni and Pd complexes, respectively. The compounds were produced in 81.6 % and 87.5 % yields, respectively for the Ni and Pd complexes.

For $C_{94}H_{30}Cl_2FeNiP_2$: ^{13}C NMR ($CDCl_3$): 144-140 ppm (m, 5C, C_5,H_4), 135-129 ppm (m, 6C, C_6H_5); ^{31}P NMR ($CDCl_3$): 35.079 ppm (s, 2P, P-P); UV-Visible (CH_2Cl_2, λ_{max}, nm): 302, 330 and 438; IR (CH_2Cl_2, cm^{-1}): 1181, 1365, 2996, 2857, 3048, 1058 and 1336.

For $C_{94}H_{30}Cl_2FeP_2Pd$: ^{13}C NMR ($CDCl_3$): 145-142 ppm (m, 5C, C_5,H_4), 137-133 ppm (m, 6C, C_6H_5); ^{31}P NMR ($CDCl_3$): 26.121 ppm (s, 2P, P-P) 27.298 and 24.659 ppm (d, 2P, P-M-P); UV-Visible (CH_2Cl_2, λ_{max}, nm): 302, 330 and 438; IR (CH_2Cl_2, cm^{-1}): 1203, 1436, 2981, 2870, 3073, 1181, and 1361.

3.3 Results and Discussion

3.3.1 Synthesis and characterization of the (dppf)M(C_{60}) complexes

The desired (dppf)M(C_{60}) complexes were prepared by metathesis reactions, i.e.,

$$\text{(dppf)MCl}_2 + \text{C}_{60} + 2\ \text{Na}_{(\text{metal})} \rightarrow \text{(dppf)M(C}_{60}) + 2\ \text{NaCl} + \text{Na}_{(\text{metal})} \quad (\mathit{1})$$

These reactions proceeded smoothly to greater than 80 % isolated yields of the desired products as dark green to rusty red crystals. These materials are air and moisture stable in the solid state for over a week. This increase in stability is surprising because

Fagan and Calabrese's complexes were not stable in air at all and were handled only in a glovebox. We speculate that the ferrocene group is stabilizing the metal-C_{60} bond through some unknown mechanism. Experiments designed to elucidate this phenomenon are currently being pursued. Sodium metal was added to the reaction mixture to cause the *in-situ* reduction of the metals to the zero-valent state, allowing them to bond to the 6-6' bonding site of the C_{60}. Triphenylphosphine acted as a stabilizing agent after the reduction had taken place. The complexes are very soluble in polar organic solvents, such as acetone, but are insoluble in non-polar solvents such as hexane. They can be easily recrystallized from moderately polar solvents such as chloroform.

3.3.2 Spectroscopic data

The complexes were identified by their characteristic spectroscopic properties. All of the spectroscopic data are consistent with the proposed structures of these complexes and correlate very well with Fagan and Calabrese related complexes.[6] Representative spectra for (dppf)Pd(C_{60}) are shown. All other spectra may be found in the Appendix. The molecular weights of all of the complexes exceed the m/z limit of the GC/MS available at YSU. It was not possible, therefore, to determine the parent ions of the compounds. Evaluation of the parent ions will be performed via MALDI-MS at Louisiana State University in collaboration with Professor Robin L. McCarley.

The ^{31}P NMR data (Figure 3.5) displays a enormous shift from -16 ppm in the dppf starting material to approximately 25 ppm in the metal coordinated species. The nickel complex is shifted 43 ppm, the palladium complex is shifted 42 ppm and the

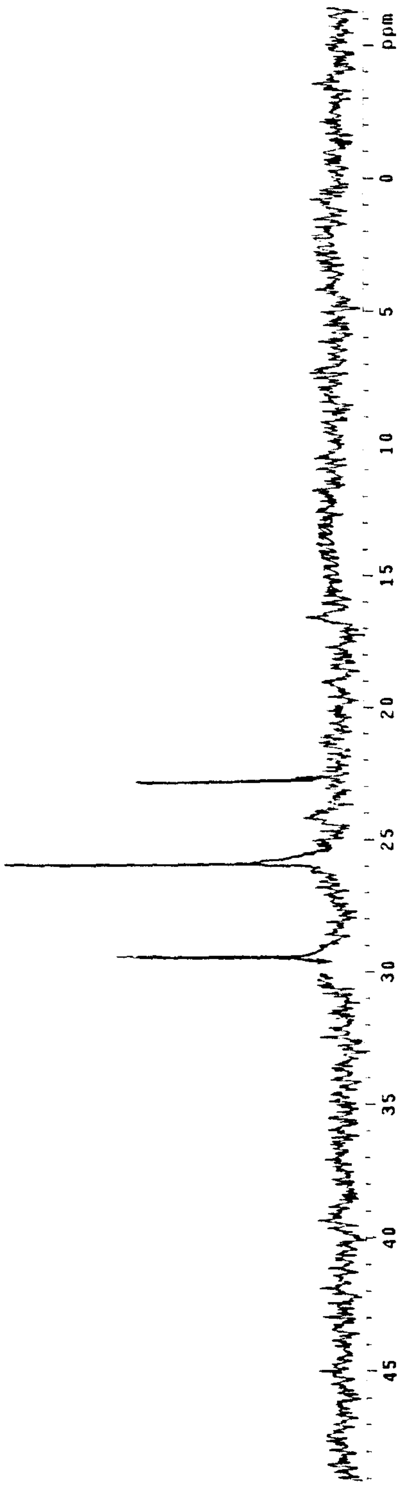

Figure 3.5: ^{31}P NMR of (dppf)Pd(C$_{60}$).

platinum complex is shifted 41 ppm with respect to dppf. This shift is repeatable and therefore significant despite the fact that there is only a small difference between the three. In addition, the (dppf)M(C_{60}) and (dppf)MCl_2 (M = Pd and Pt) complexes exhibited a characteristic false triplet which is the result of the coupling of the ^{31}P nuclear spin to the spin ½ of the metal isotopes. This result is consistent with triphenylphosphine complexes studied by Fagan.[7]

The ^{13}C NMR (Figure 3.6) was also integral in determining the presence of substituted C_{60}. Unsubstituted C_{60} displays a singlet which appears at 142 ppm. After the addition of a substituent, a complex multiplet appears and is upfield with respect to C_{60} by approximately 4-8 ppm. This appears in all three (dppf)M(C_{60}) complexes and unequivocally demonstrates that C_{60} is substituted. This is consistent with the complexes synthesized by Fagan and Calabrese. The presence of ferrocene and phenyl rings are also indicative of the dppf coordination to the transition metal and are easily detected on the ^{13}C NMR spectra. These signals are all in the appropriate area of the spectrum, but are shifted upfield with respect to dppf by approximately 3-5 ppm. The ^{13}C NMR data is in close agreement with the expected spectra and with what is already documented in the literature.

UV-Vis spectral data is shown in Figure 3.7 and is supportive of the NMR data. The principle band in the spectrum of C_{60} appears at 330 nm. The same band appears in all of the dppf-metal-C_{60} complexes and is unshifted with respect to C_{60} itself. λ_{max} in the spectra of dppf appears at 442 nm. This band is present in all of the dppf-containing

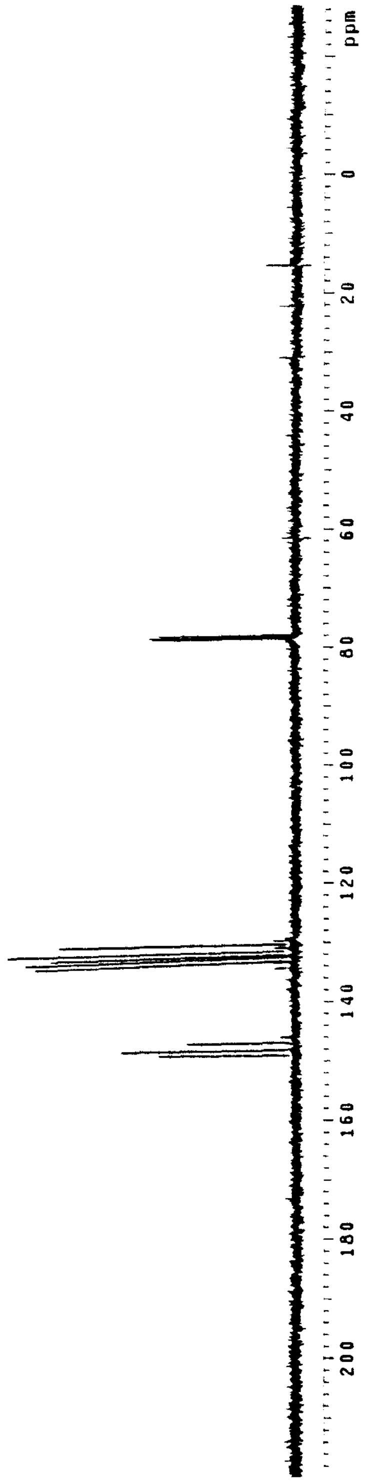

Figure 3.6: ^{13}C NMR of (dppf)Pt(C_{60}).

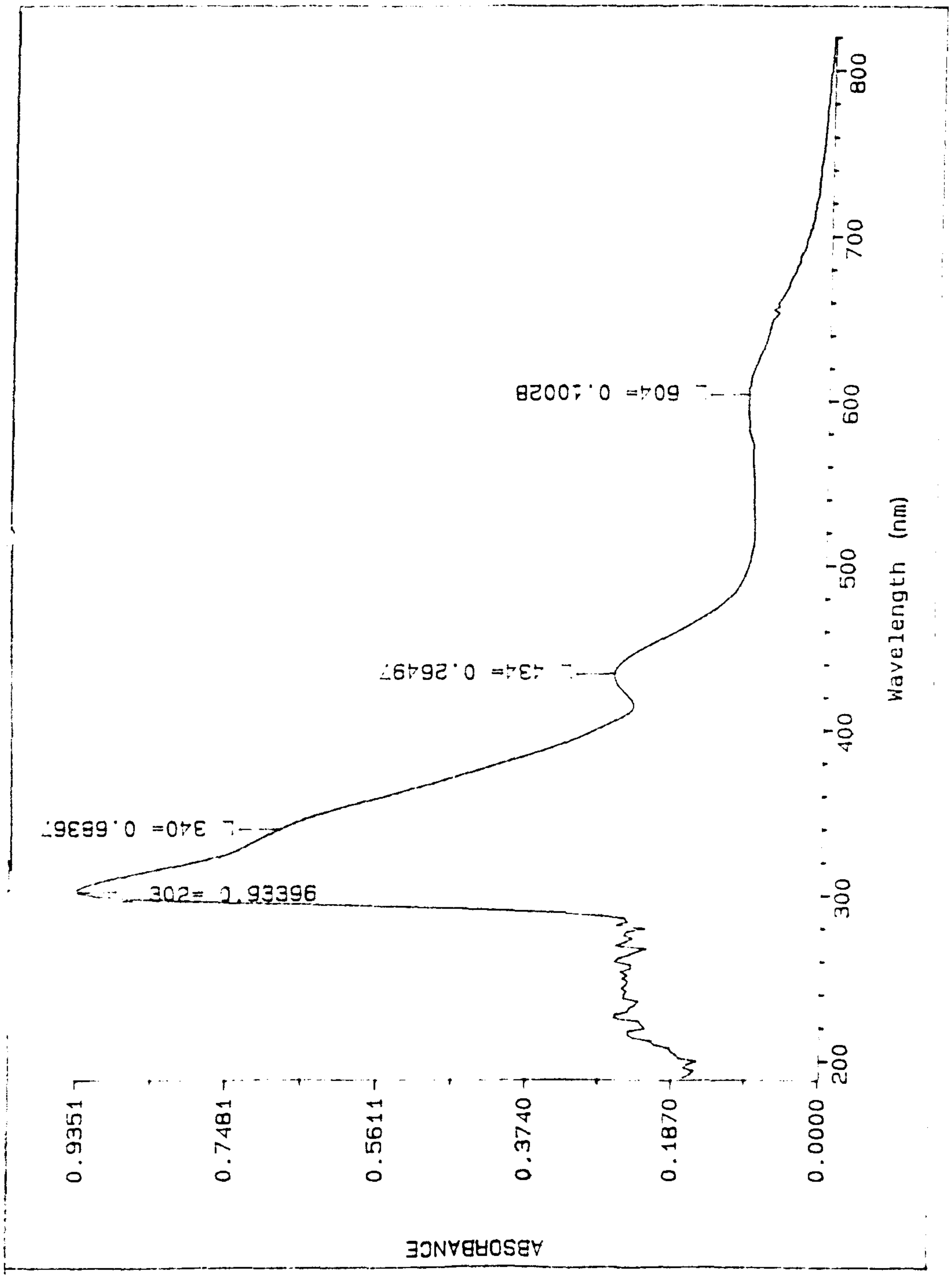

Figure 3.7: UV-Vis of (dppf)Pd(C_{60}).

materials and is blue shifted by 5 - 10 nm upon metal coordination. In addition, a ligand to metal charge transfer band appears at approximately 620 nm which is indicative of ligand attachment to the C_{60} cage. The appearance of the LMCT band is also evidence that the (dppf)Pt(C_{60}) complex was formed. The LMCT band does not appear in the UV-Vis spectrum of the nickel complex due to the periodic decrease in the absorptivites from the platinum to nickel.

The infrared spectra (Figure 3.8) of the starting materials and products is in agreement with the NMR and UV-Vis. The presence of all of the functional groups, such as C_{60} and aromatic rings, is detected. The band that appears at approximately 3030 cm^{-1} in all of the complexes corresponds to the aromatic rings present of the ligand. Due to the complexity of the fingerprint region, absolute identification of the metal-C_{60} bond was not achievable. However, the IR data is supportive of other spectroscopic and electrochemical data (see below).

3.3.3 Electrochemistry

Cyclic voltammetry was performed on the (dppf)metal(C_{60}) complexes. Preliminary data suggests that all of these complexes have one anodic wave and two cathodic waves. The anodic wave corresponds to the ferrocene in the dppf ligand and the cathodic waves result from the metal-C_{60} (Figure 3.9 and 3.10).

A number of obstacles were encountered that have made obtaining electrochemical data difficult. The principle problem was the narrow solvent window observed in the voltammetry. Several attempts were made to expand the solvent window,

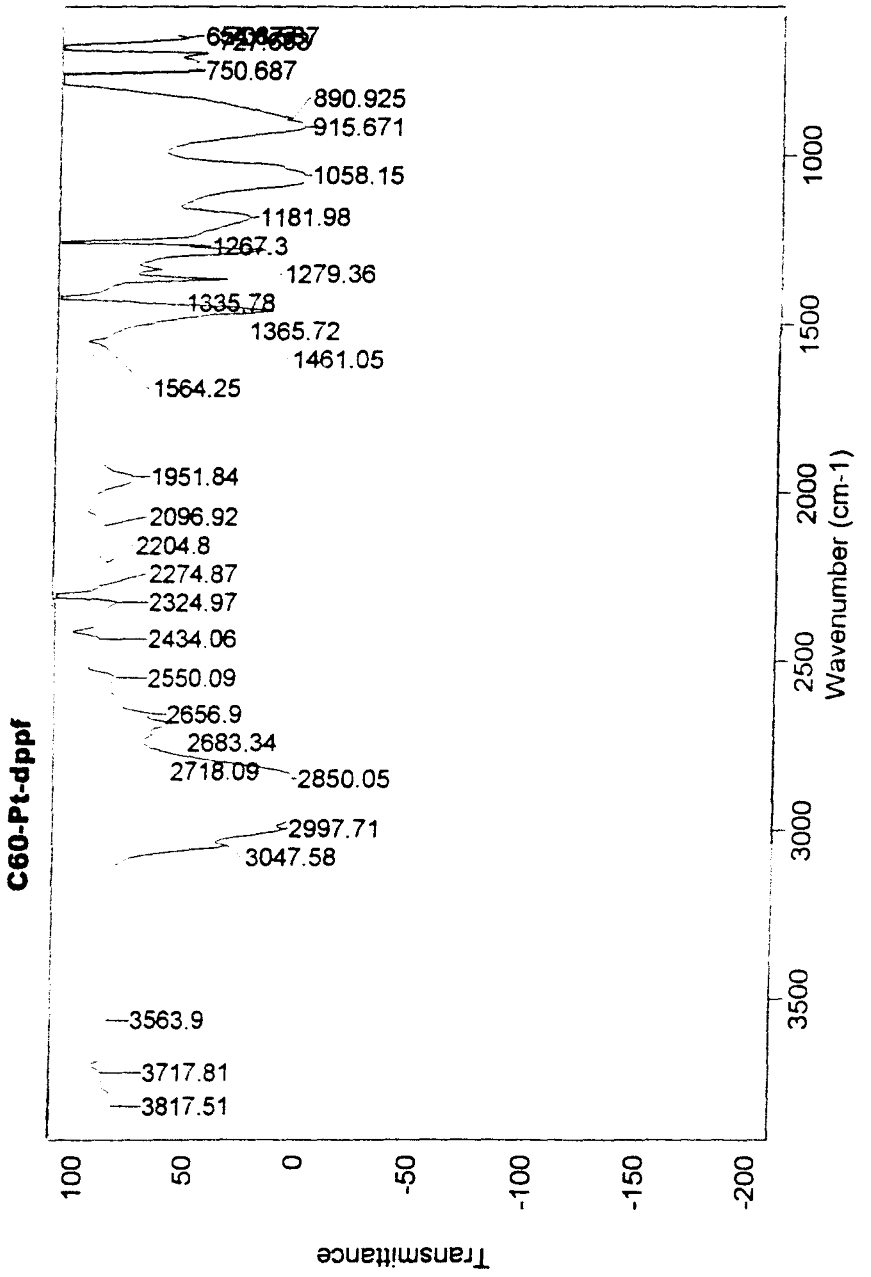

Figure 3.8: IR of (dppf)Pd(C_{60}).

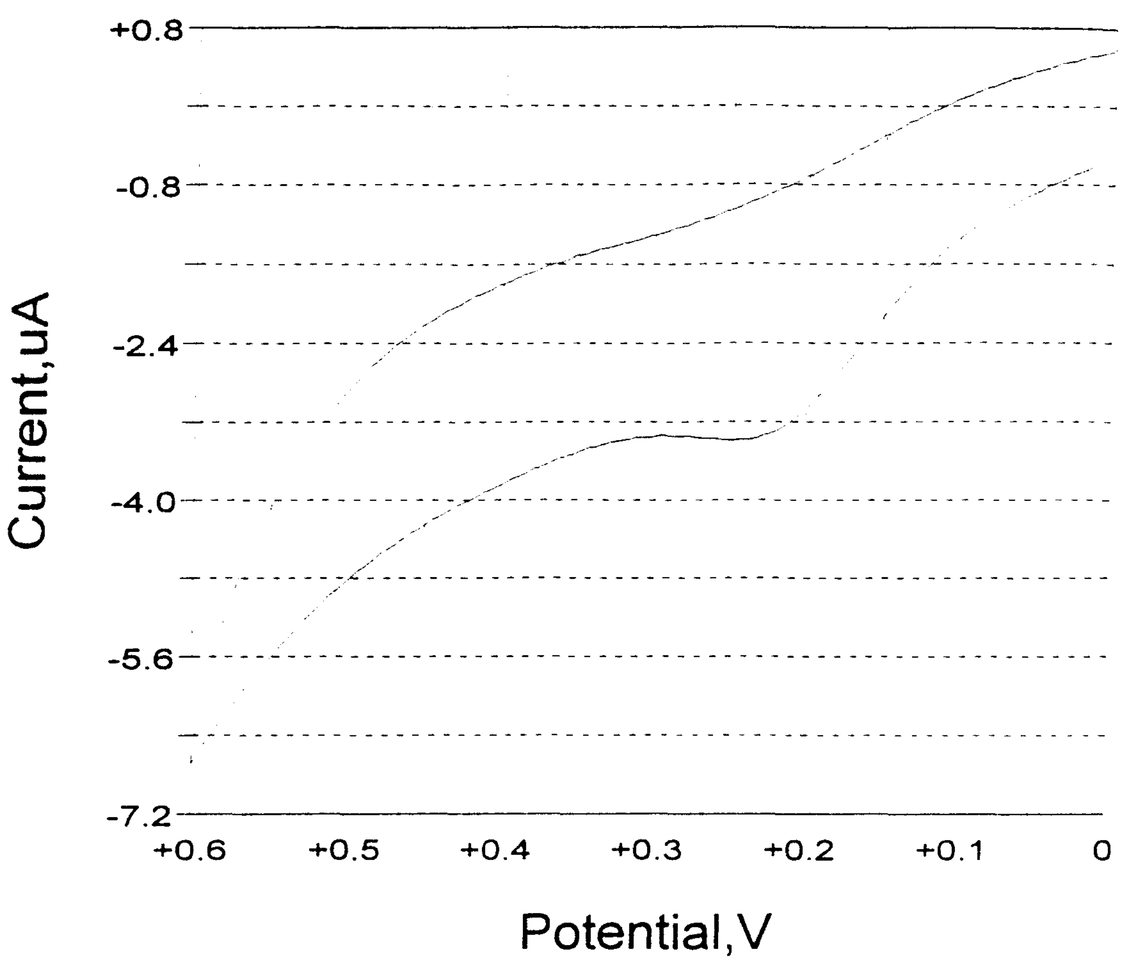

24-Jul-98
16:09:42
Mode: CV
RC1

Init E (mV) = 0
High E (mV) = 600
Low E (mV) = 0
Init P/N = P
V (mV/s) = 1003
Sweep Segments = 2
Smpl Int (mV) = 1
Quiet T (s) = 2
Sens (A/V) = 1E-6

Figure 3.9: Anodic Voltammetry of (dppf)Pd(C_{60}).

(Where the electrolyte (t-BAP) is 0.1M, the (dppf)Pd(C_{60}) is 10 mM, the scan rate = 500 mV/sec.)

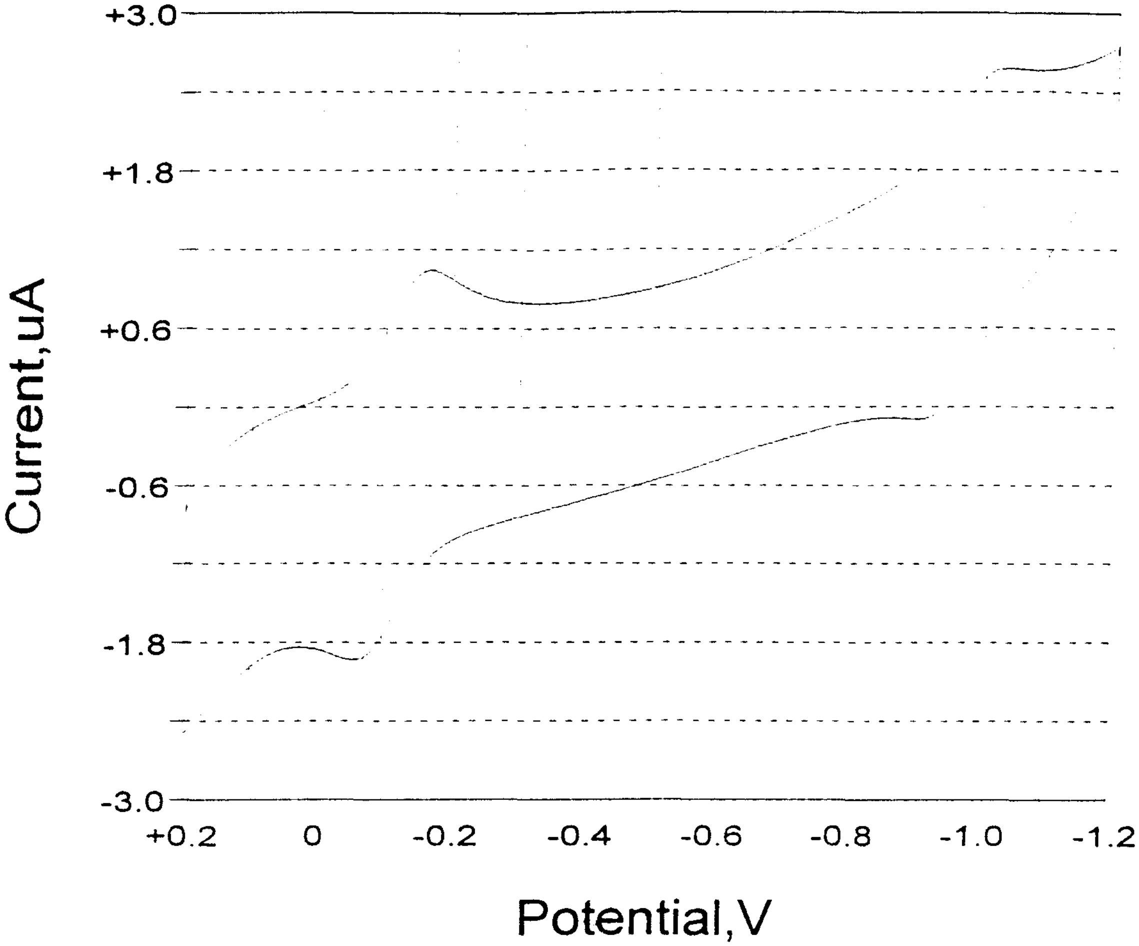

25-Jul-98
13:09:40
Mode: CV
RC1

Init E (mV) = 200
High E (mV) = 200
Low E (mV) = -1200
Init P/N = N
V (mV/s) = 500
Sweep Segments = 2
Smpl Int (mV) = 1
Quiet T (s) = 2
Sens (A/V) = 1E-6

Figure 3.10 Cathodic Voltammetry of (dppf)Pd(C_{60}).

(Where the electrolyte (t-BAP) is 0.1M, the (dppf)Pd(C_{60}) is 10 mM, the scan rate = 500 mV/sec.)

but all proved to be ineffective. Freshly distilled THF was used in combination with a variety of recrystallized electrolytes and working and reference electrodes. A small amount of activated alumina was also added at the bottom of the electrochemical cell to act as a water scavenger. The solutions were even cooled to 0 °C before examining the voltammetry. All of these attempts resulted in a slightly expanded solvent window, but no more than two cathodic processes could be observed in all of the voltammograms. Further attempts to expand the solvent window will involve performing the electrochemical experiments in an inert atmosphere dry box. Reproducibility from day to day was another problem that was frequently encountered. A possible reason for this is the varying humidity in the laboratory on a daily basis (experiments were performed on the bench top). As a result of these complications only preliminary electrochemical results are presented.

The anodic cyclic voltammetry of the (dppf)Pd(C_{60}) complex is displayed in Figure 3.11 at several scan rates. The absence of a return cathodic peak at all scan rates employed clearly demonstrates that the oxidation is chemically irreversible on the time scale of the voltammetric experiment (scan rates up to 3 V/s). This behavior was also observed in the case of the Pt containing complex but different results were obtained for the Ni complex. The return cathodic peak for oxidation of the Ni complex increased in magnitude over the same range of scan rates employed for the other metal derivatives and became reversible at a scan rate of 2 V/s. This indicates that the rate of the chemical reaction that occurs subsequent to oxidation is significantly slower in the Ni complex than it is in the Pd and Pt derivatives. The observation of a return cathodic peak of equal magnitude at 2 V/s for (dppf)Ni(C_{60}) indicates that the chemical reaction has become comparable to the time scale of the voltammetric experiment. A quantitative determination of the rate constant associated with the chemical reaction, however, is severely complicated by the fact that the anodic electron transfer is also electrochemically irreversible. Therefore, the only conclusion that can be obtained from this data is that the rate of the chemical step which follows the electron transfer is metal dependant and that the Ni derivative is slower than that for the other complexes.

Oxidation of the dppf fragment for all of the metal complexes is also electrochemically irreversible, as evidenced by the observation that E_p is shifted to increasingly anodic potentials with increasing scan rate. Surprisingly, the rate of the electron transfer is essentially the same for all of the metal derivatives, based upon analysis of how E_p increases with an increase in scan rate. The rate constant associated with the electron transfer is difficult to quantitatively determine because of the chemical reaction that occurs subsequent to the electron transfer, but the data clearly indicates that the electron transfer is electrochemically irreversible on the time scale of the experiments which were performed.

The cathodic electrochemistry for (dppf)Pd(C_{60}) is presented as preliminary data. The nickel and platinum derivatives have been difficult to visualize or reproduce at a concentration of 1 mM because the faradaic currents were not well resolved from the non-faradaic currents. The palladium derivative discussed here is in a higher concentration than the nickel and platinum derivatives. Raising the concentration may be a way of improving the resolution of the peaks on the voltammograms.

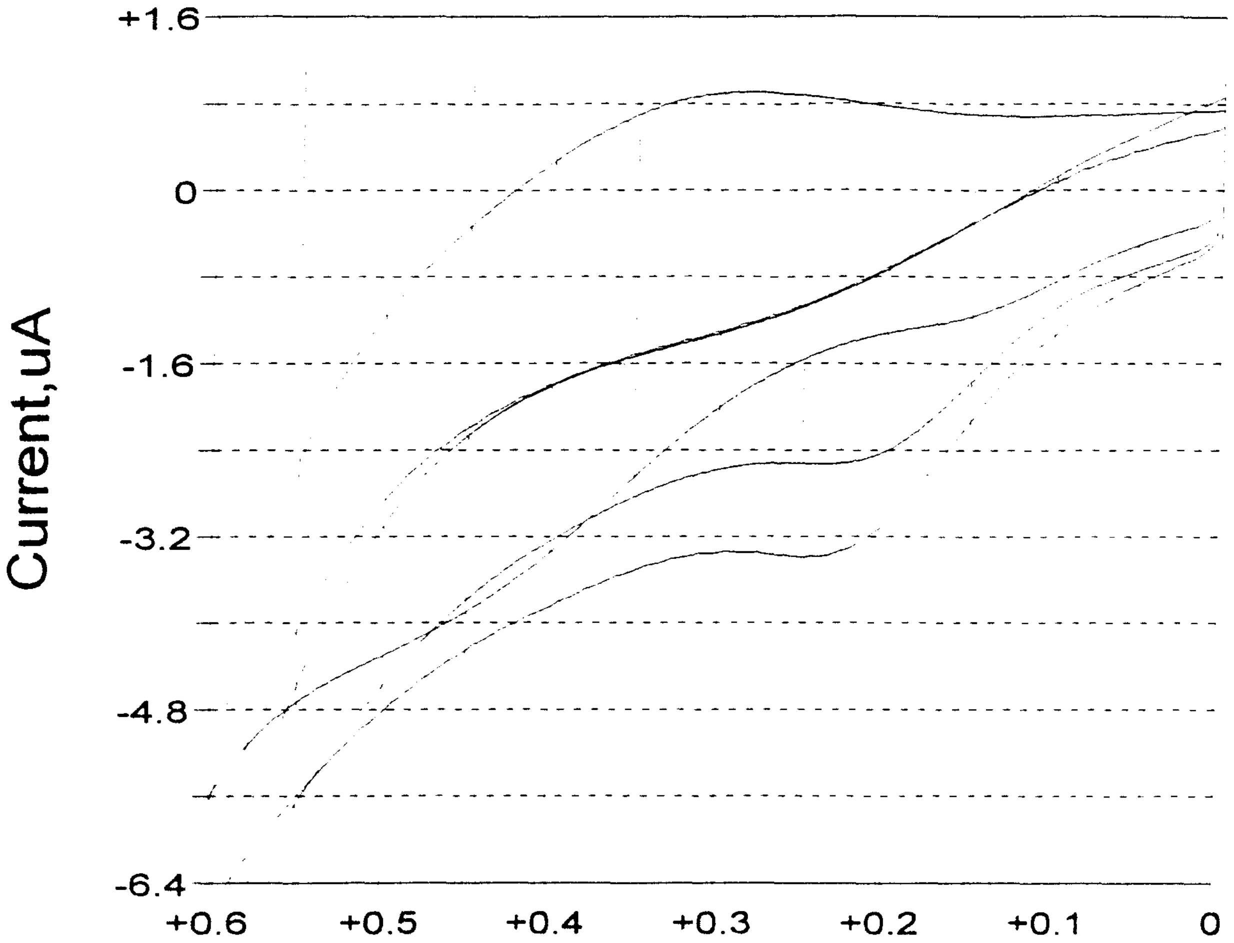

Figure 3.11: Multiple Scan Rates of Cathodic Voltammetry of (dppf)Pd(C_{60}).

(Where the electrolyte (t-BAP) is 0.1M, the (dppf)Pd(C_{60}) is 10 mM, the scan rate = 100, 500 and 1,000 mV/sec.)

The cathodic electrochemistry associated with the metal-C_{60} fragment supports the spectroscopic data presented above in that the (dppf)Pd(C_{60}) complex displays two C_{60} reductions which are shifted with respect to C_{60} itself in the cathodic direction. A shift in reduction potential was reported by Fagan and Calabrese upon substitution of C_{60} with $M(PPh_3)_2$ fragments. Both reduction waves were determined to be chemically reversible and electrochemically quasi-reversible.

3.4 Conclusions

All of the dppf metal dichlorides and dppf metal C_{60} complexes have been synthesized and characterized. ^{31}P, ^{13}C and the UV-Vis spectral data clearly demonstrates the presence of a (dppf) metal substituted C_{60} complex. This is further supported by the IR data.

Cyclic voltammetry was performed on the (dppf)M(C_{60}) complexes in order to support the spectroscopic data presented above and to determine the chemical and electrochemical reversibility of the newly prepared complexes. Preliminary data suggests that all of the complexes display one anodic and two cathodic waves. The anodic wave corresponds to the ferrocene in the dppf ligand and the cathodic waves result from the metal-C_{60} fragments. Peak currents for all of the waves are linearly related to $\nu^{1/2}$ indicating that the electrochemical response is diffusion controlled. This result is not unexpected for solution voltammetry under the experimental conditions employed in this study.

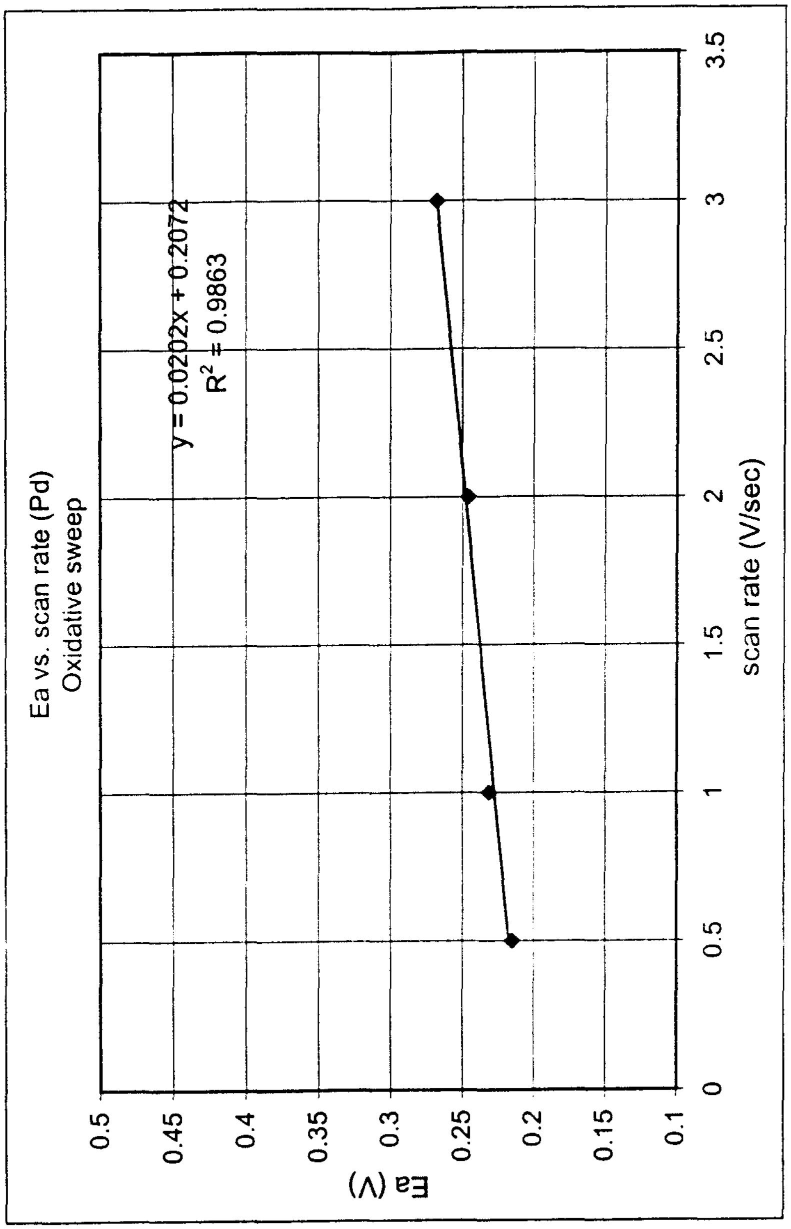

Figure 3.12: Electrochemical Irreversibility of (dppf)Pd(C_{60}).

one of the unique aspects in the synthetic approach which is presented in this thesis is that it is the only documented methods in which the transition metal is reduced *in situ* and attached to the C_{60} cage. This approach has many advantages. It is a relatively easy one-flask reaction that is quick, easy to reproduce, and has eliminated the difficult task of purifying C_{60} intermediates. This original synthetic strategy may potentially be applied to other transition metals for the purpose of attaching them to the C_{60} cage. This series of compounds are also remarkably more stable than Fagan and Calabrese's products. They have a shelf-life of approximately one to two weeks when exposed to the atmosphere. Fagan and Calabrese's complexes must be used in the glovebox only.

The (dppf)M(C_{60}) complexes have been found to be air and thermally stable for over a week, synthesized via a new synthetic approach and have significant spectroscopic characteristics. The preliminary electrochemical data obtained and presented in this thesis is interesting and may serve as a stepping stone for the future of this project.

References Cited:

(1) Lerke, S. A. *J. Am. Chem. Soc.*, **1992**, *114*, 7807 -7813.

(2) Filler, F. Master's Thesis, Temple University, **1996.**

(3) Personal Communication with Francesca Filler, **1996**.

(4) Landis, K. G.; Hunter, A. D.; Wagner, T. R.; Curtin, L. S.; Filler, F. L.; Jansen-Varnum, S. A. *Inorg. Chim. Acta*, **1998**, submitted for publication.

(5) Perrin, D. D.; Armarego, W. L. F.; and Perrin, D. R. *The Purification of Laboratory Chemicals*, Pergamon, New York, 2nd edn., **1980**.

(6) Fagan, P. J.; Calabrese, J.C.; Malone, B. J. *J. Am. Chem. Soc.*, **1991**, *113*, 9408-9409.

(7) Fagan, P. J.; Calabrese, J.C.; Malone, B. J. *Science*, **1991**, *252*, 1160-1161.

(8) Lerke, S. A. *J. Am. Chem. Soc.*, **1992**, *114*, 7807 -7813.

Bibliography

Allen, F. H.; Kennard, O.; Wilson, D. G.; Brammer, L.; Orpen, A. G.; Taylor, R. "Typical Interatomic Distances: Organic Compounds." in *International Tables for Cystallography, Volume C. Mathematical, Physical and Chemical Tables*, Wilson, A. J. C., ed., Kluwer Academic Publishers: Boston, **1995**; 685-706.

Bähr, G. and Schleitzer, G. N., *Chem. Ber.*, **1957,** *90*, 438.

Bard, A.J.; and Faulkner, L. R. *Electrochemical Methods*, 1980

Best, S. P.; Clark, J. H.; McQueen, R. C.; and Watson, R. J., Inorg. Chem., **1988,** *27*, 884-890.

Cai (Tsai), S. D.; and Hunter, A. D., 203rd ACS National Meeting, San Francisco, C.A., April **1992**, INOR 413.

Chen, F., Doctoral Dissertation, Temple University, **1993.**

Clark, R. J. and Turtle, P. C., *J. Am. Chem. Soc. Dalton Trans.*,**1977**, 2142 - 2148.

Dubois, D., *J. Am. Chem. Soc.*, **1991**, *113*, 7773.

Eisenberg, R.; Ibers, J. A.; Clark, R. J.; and Gray, H. B., *J. Am. Chem. Soc.*, **1964**, *96*, 113-115.

Fagan, P. J.; Ward, M. D.; Calabrese, J. C., *J. Am. Chem. Soc.*, **1989**, *111*, 1698.

Fagan, P. J.; Calabrese, J.C.; Malone, B. J., *J. Am. Chem. Soc.*, **1991**, *113*, 9408-9409.

Fagan, P. J.; Calabrese, J.C.; Malone, B. J., *Science*, **1991**, *252*, 1160-1161.

Filler, F., Master's Thesis, Temple University, **1996.**

Fowler, P. W. and Woolrich, *J., Chem. Phys. Lett.*, **1986**, *127*(1), 78 -83.

Haddon, R.C., *Chem. Phys. Lett.*, **1989**, *125*, 459.

Heath, J.R., *J. Am. Chem. Soc.*, **1985**, *107*, 7779-7780.

Holczer, K., *Science*, **1991**, *252*, 1154.

Hunter, A. D.; Mozol, V.; and Tsai, S. D. *Organometallics,* **1992,***11,* 2251-2262.

Hunter, A. D.; and Szigety, A. B. *Organometallics,* **1989,** *8*, 2670-2679.

Kroto, H. W., *Nature*, **1987**, *329*, 529-531.

Kroto, H.W.; Heath, J. R.; O'Brian, S.C.; Curl, R. F.; and Smally, R.E., *Nature*, **1985**, *318*, 162 - 163.

Landis, K. G.; Hunter, A. D.; Wagner, T. R.; Curtin, L. S.; Filler, F. L.; Jansen-Varnum, S. A. *Inorg. Chim. Acta*, **1998**, submitted for publication.

Landis, M. L., Master's Thesis, Temple University, **1996**.

Lerke, S. A., *J. Am. Chem. Soc.*, **1992**, *114*, 7807 -7813.

Muetterties, E. L., ed., Inorganic Syntheses, Vol. 10, McGraw-Hill Book Co., New York, N. Y., **1967**, 11-13.

Orpen, A. G.; Brammer, L.; Allen, F. H.; Kennard, O.; Wilson, D. G.; Taylor, R. . "Typical Interatomic Distances: Organometallic Compounds and Coordination Complexes of the d- and f- Block Metals." in *International Tables for Cystallography, Volume C. Mathematical, Physical and Chemical Tables*, Wilson, A. J. C., ed., Kluwer Academic Publishers: Boston, **1995**; 707-791.

Osawa, E. and Yoshida, Z., "Aromaticity", Kegaku-Dojin, Kyoto, **1971**.

Pearson, R. G. and Sweigart, D. A., *Inorg. Chem.*, **1970**, 9(5), 1167 - 1175.

Perrin, D. D.; Armarego, W. L. F.; and Perrin, D. R. *The Purification of Laboratory Chemicals*, Pergamon, New York, 2nd edn., **1980**.

Personal Communication with Francesca Filler, **1996**.

Powell, D. Chi-90 Prrogram for selecting psi scans, Department of Chemistry, University of Wisconsin - Madison, Madison, Wisconsin, 53706.

Richter-Addo, G. B.; and Hunter, A. D. *Inorg. Chem.,* **1989,** *28,* 4063-4065.

Rohlfing, E. A.; Cox, D. M.; and Kaldor, A., *J. Chem. Phys.*, **1984**, *81*(7), 3322 - 3330.

Schrauzer, G. N., *Accounts Chem. Res.*, **1969**, *2*, 72 - 80.

SHELXTL Version 5.03, 9/1/94 release, Siemens Industrial Automation, Inc., Analytical X-Ray Instruments, 6300 Enterprise Lane, Madison, WI, USA, 53719-1173.

Shriver, D. F.; and Drezdzon, M. A. *The Manipulation of Air-Sensitive Compounds*, Wiley, New York, 2nd edn., **1986**.

Tsai, S. D.; Ph.D. Thesis entitled "Long-Range Electron Transfer", **1995**, Department of Chemistry, University of Alberta, Edmonton, Alberta, Canada.

Williams, R.; Billig, E.; Waters, J. H.; and Gray, H. B., *J. Am. Chem. Soc.*, **1996**, 88(1), 43 -50.

Wilson, L. J.; Flanagan, S.; Chibante, L. P.; and Alford, J. M., *Buckminsterfullerenes*, **1993**, *11*, 285 - 289.

Wudl, F., *Acc. Chem. Res.*, **1992**, *25*, 157 - 161.

XSCANS Version 2.1 and 2.2, Siemens Industrial Automation, Inc., Analytical X-Ray Instruments, 6300 Enterprise Lane, Madison, WI, USA, 53719-1173.

Yang, S. H.; Pettiette, C. L.; Conceicao, J.; Cheshnovsky, O.; and Smally, R.E., *Chem. Phys. Lett.*, **1987**, *139*(3), 233 - 237.

Appendix

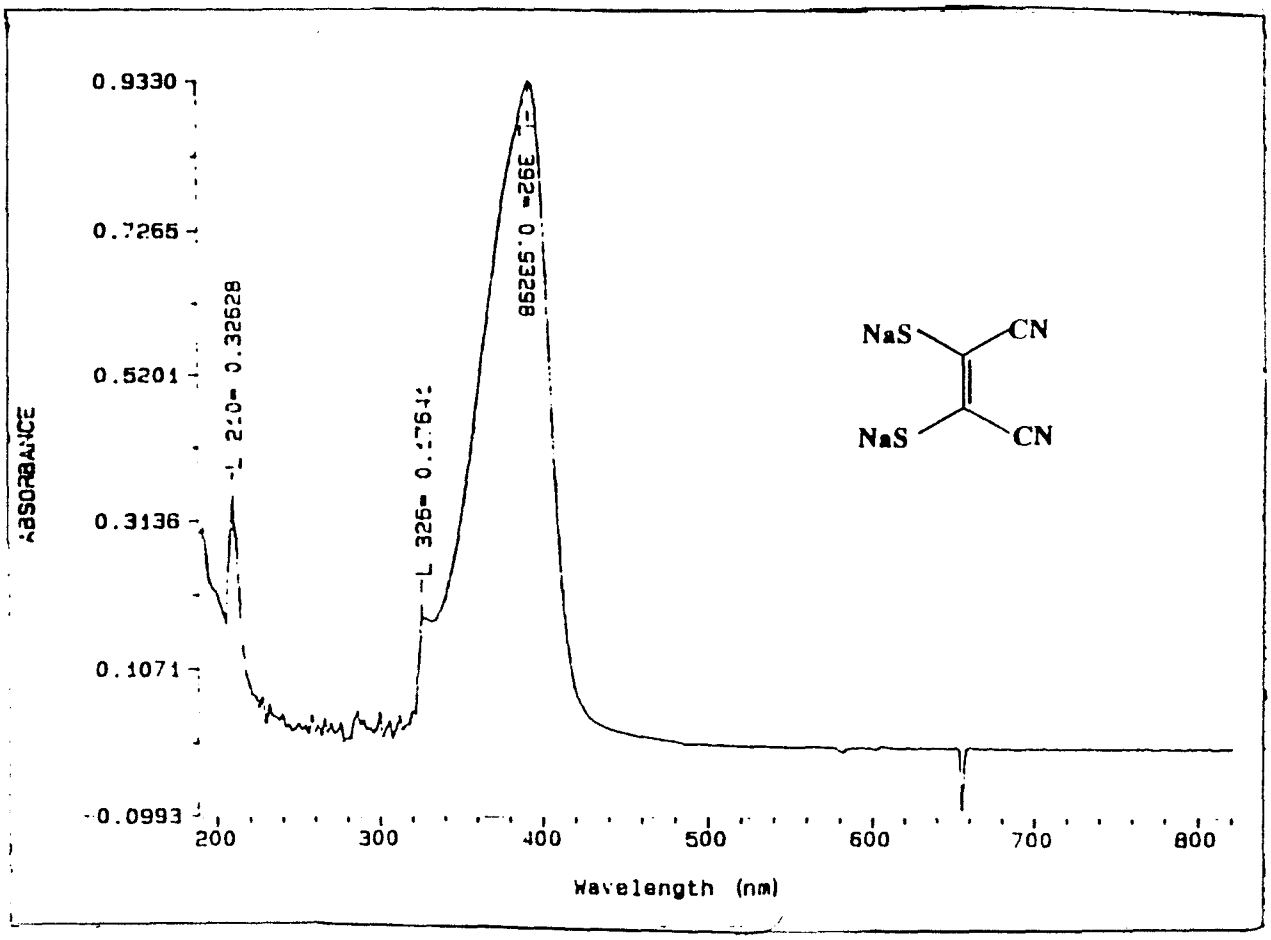
0.9330
0.7265
0.5201
0.3136
0.1071
-0.0993
ABSORBANCE
200
300
400
500
600
700
800
Wavelength (nm)
210= 0.32628
325= 0.17641
392= 0.93258
NaS
CN
NaS
CN

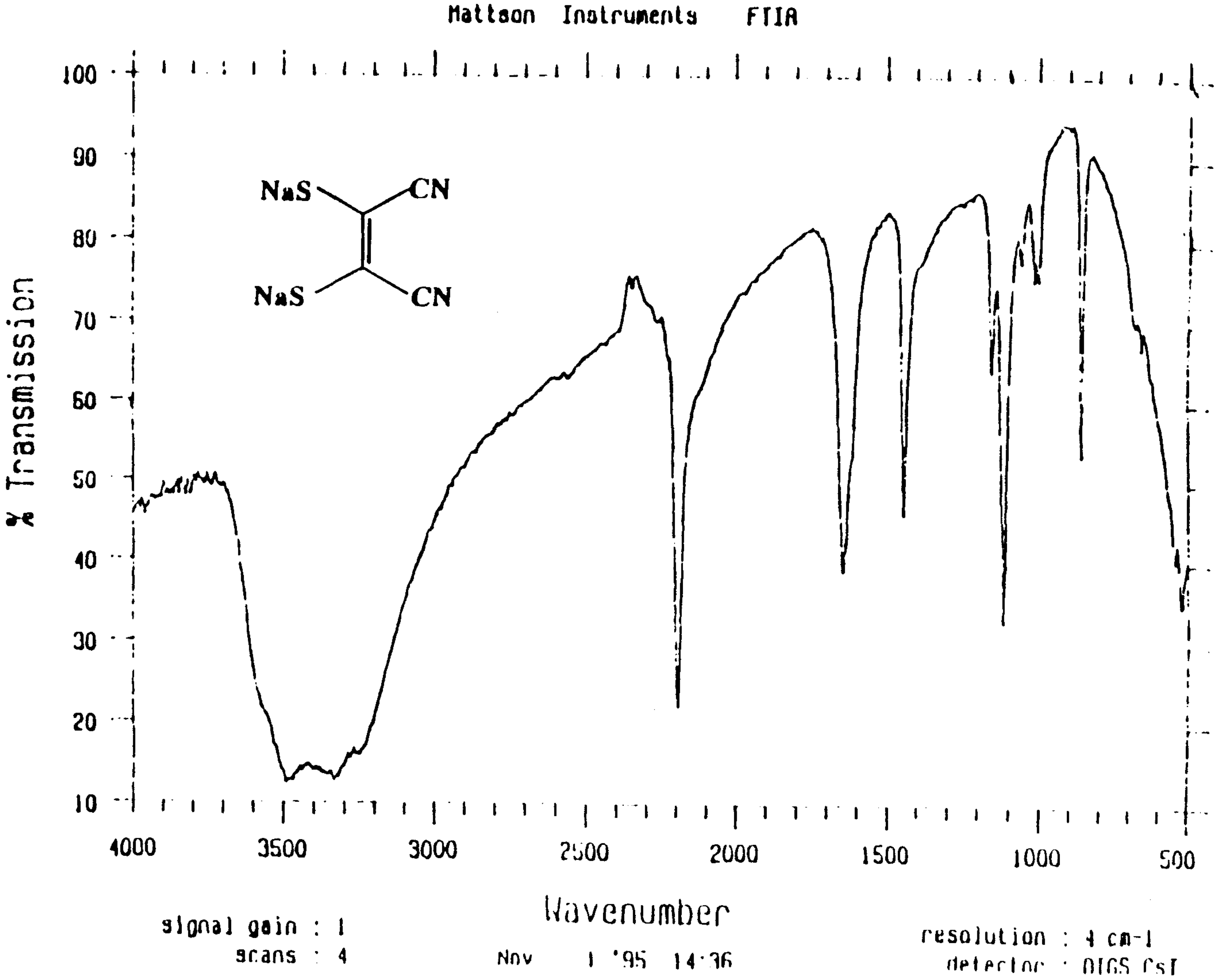
Mattson Instruments FTIR
NaS
CN
NaS
CN
% Transmission
100
90
80
70
60
50
40
30
20
10
4000
3500
3000
2500
2000
1500
1000
500
Wavenumber
signal gain : 1
scans : 4
Nov 1 '95 14:36
resolution : 4 cm-1
detector : DTGS CsI

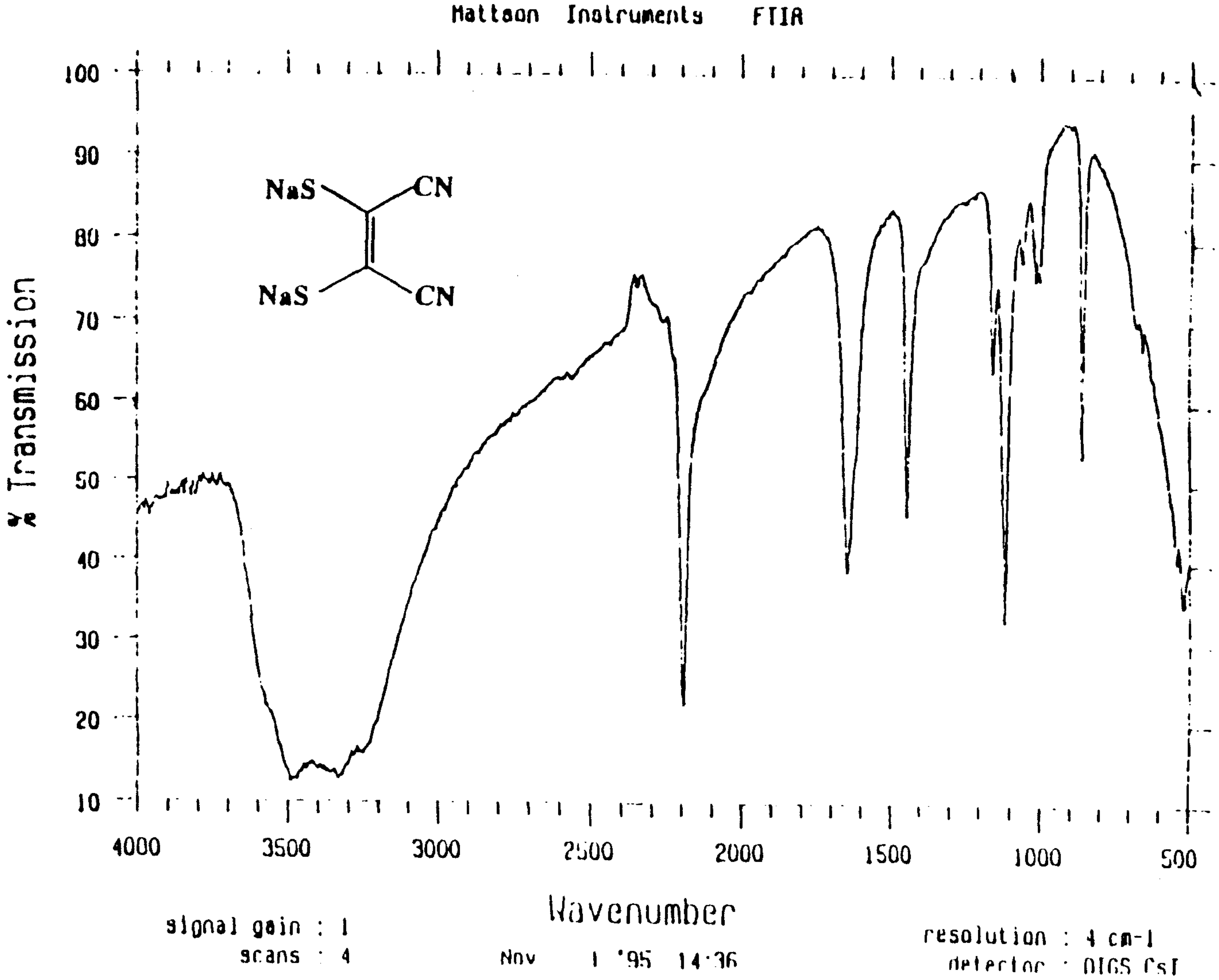
Mattson Instruments FTIR
NaS
CN
NaS
CN
100
90
80
70
60
50
40
30
20
10
% Transmission
4000
3500
3000
2500
2000
1500
1000
500
Wavenumber
signal gain : 1
scans : 4
Nov 1 '95 14:36
resolution : 4 cm-1
detector : DTGS CsI

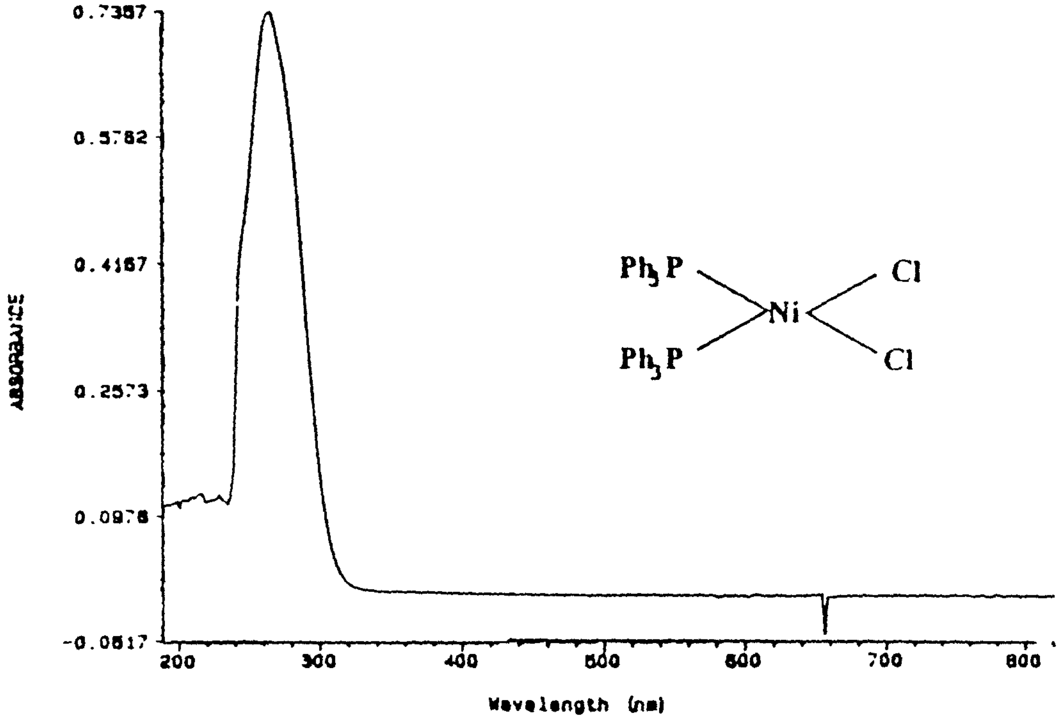
0.7387
0.5782
0.4167
0.2573
0.0978
-0.0617
ABSORBANCE
200
300
400
500
600
700
800
Wavelength (nm)
Ph3P
Ph3P
Ni
Cl
Cl

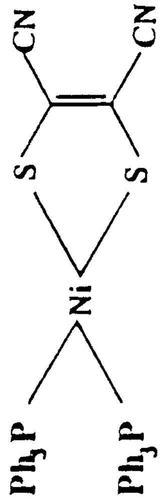
Ph$_3$P
Ph$_3$P
Ni
S
S
CN
CN

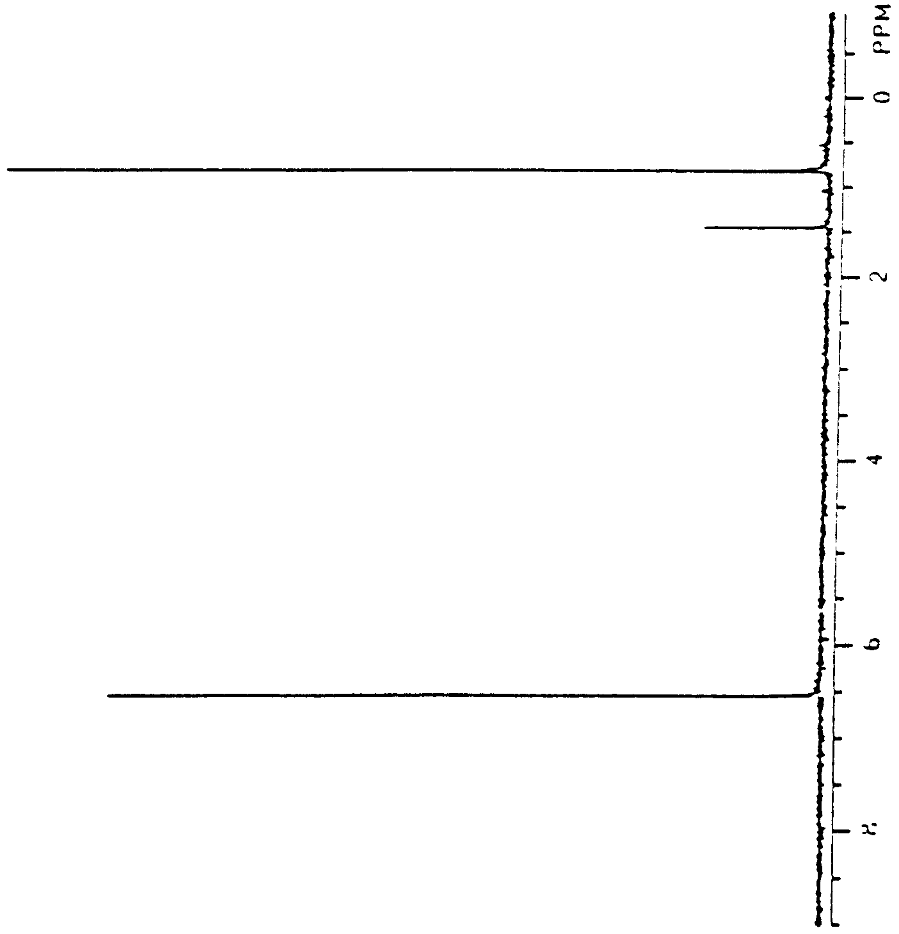
PPM
0
2
4
6
8

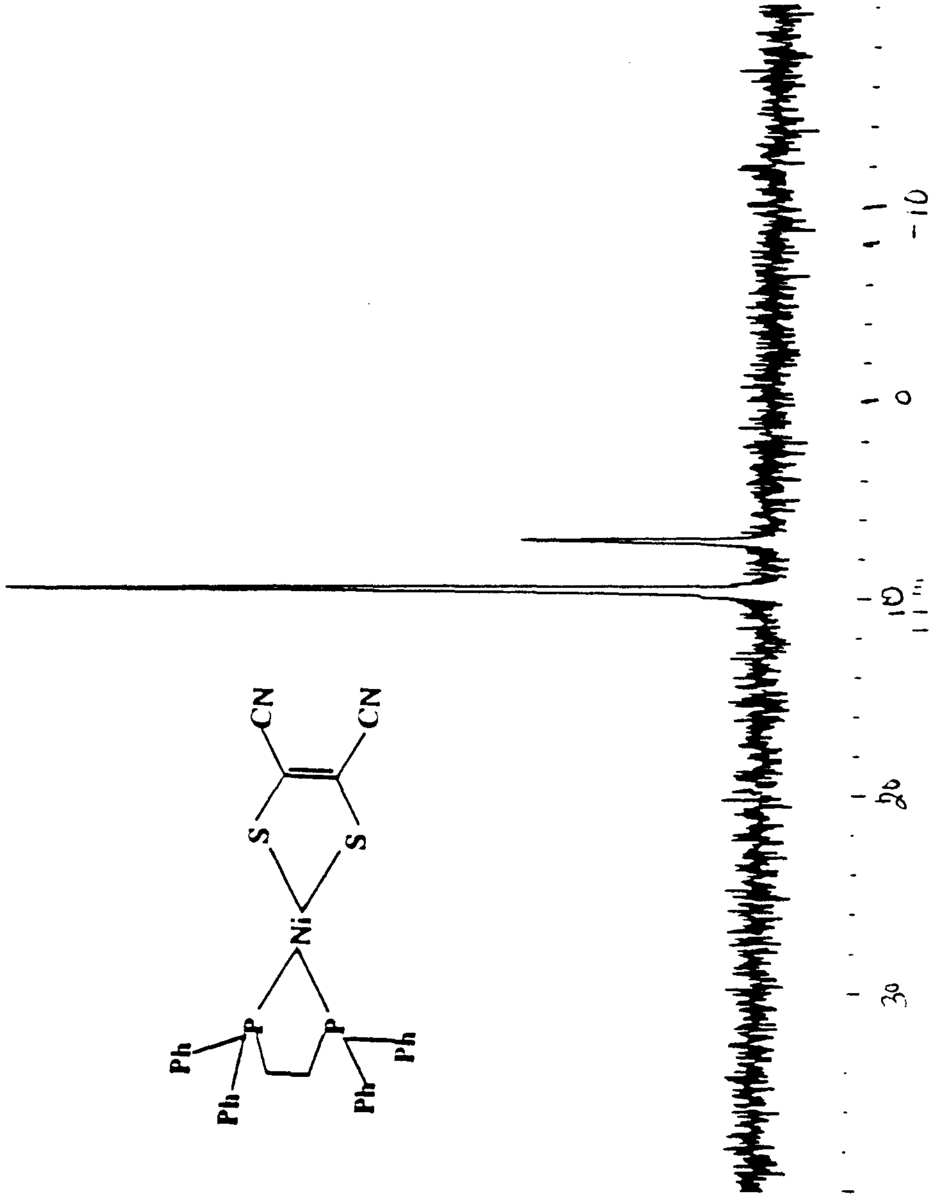
Ph
Ph
P
P
Ph
Ph
Ni
S
S
CN
CN
30
20
10
0
-10

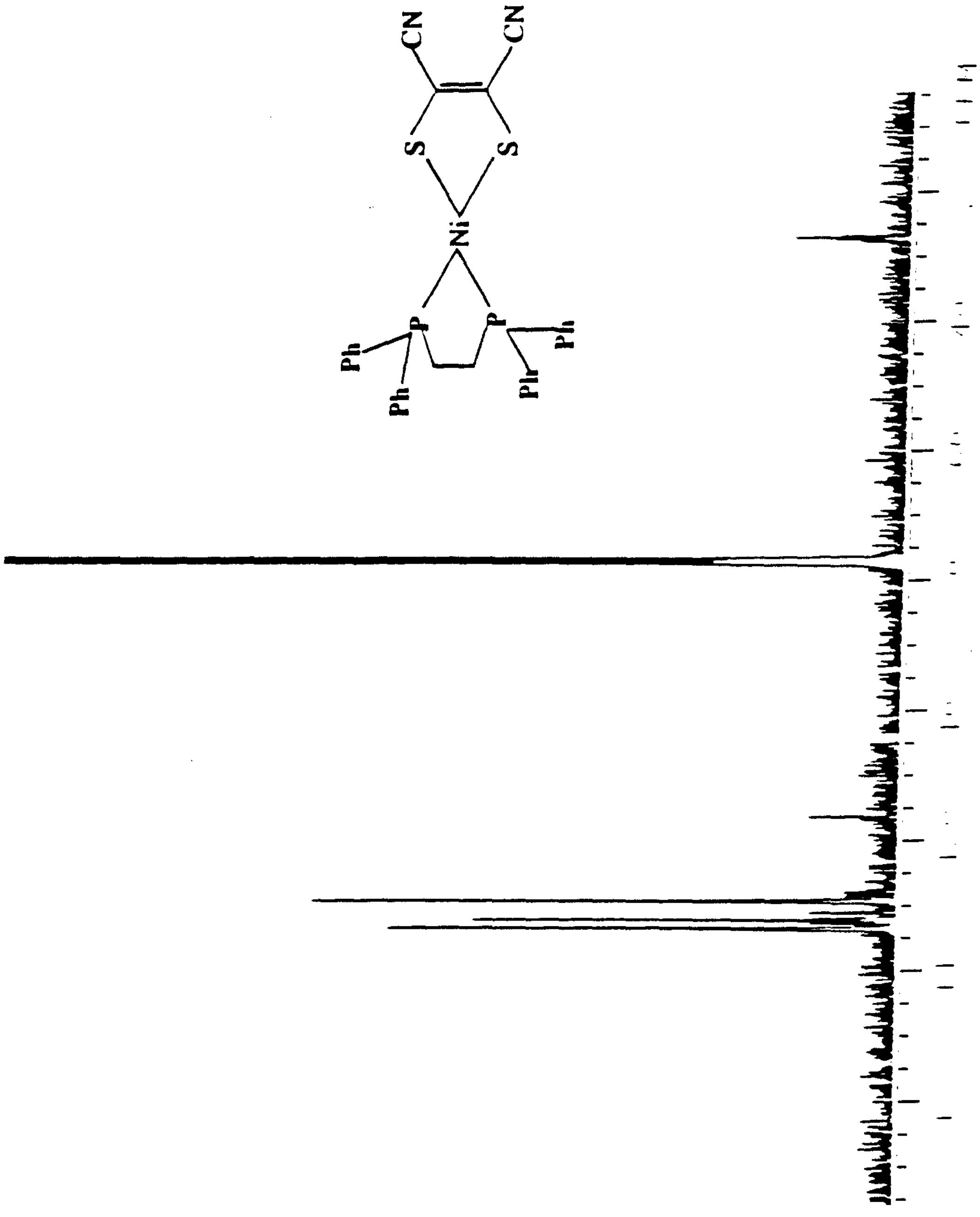
Ph
Ph
P
P
Ph
Ph
Ni
S
S
CN
CN

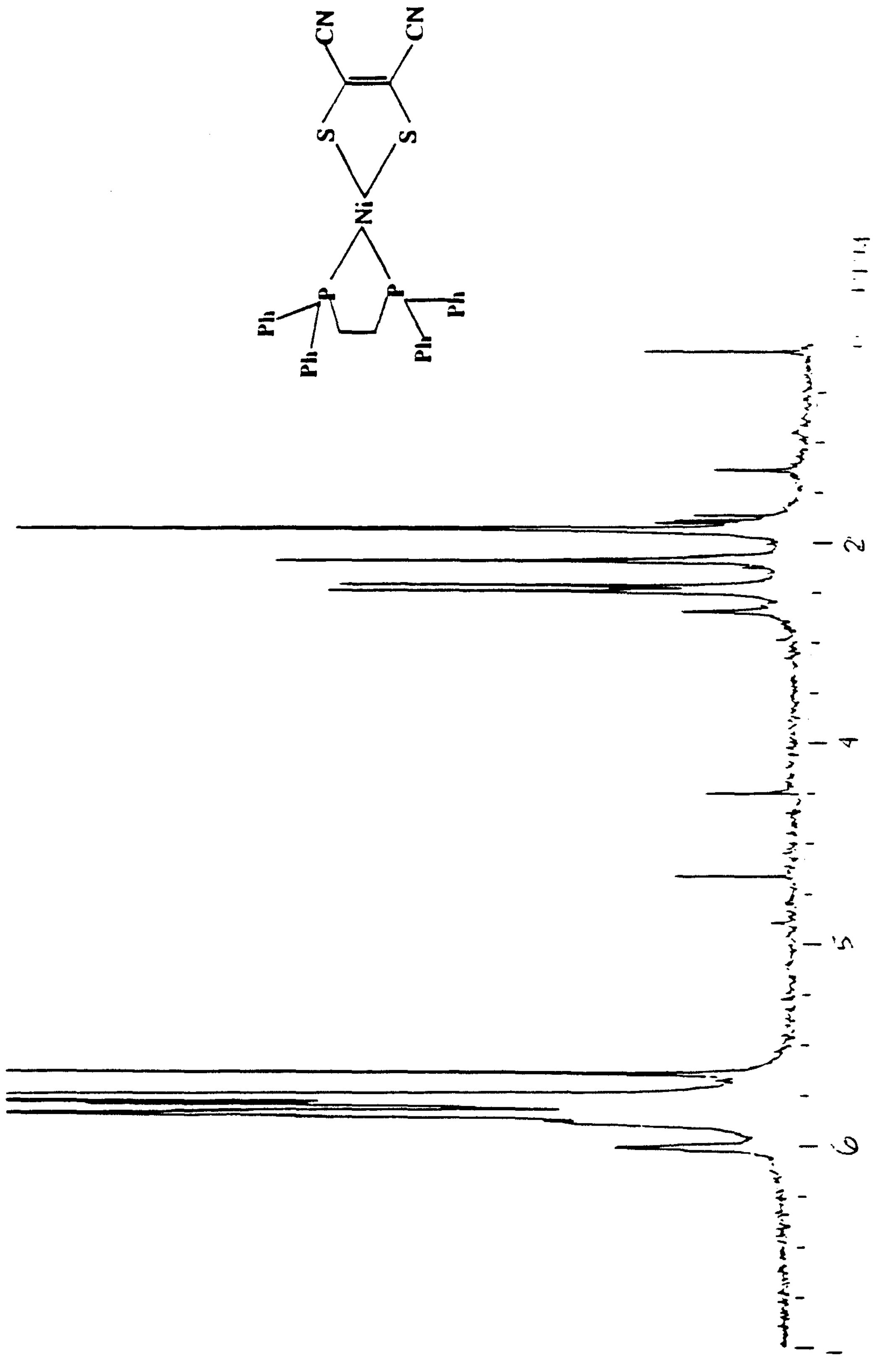

CN
CN
S
S
Ni
P
P
Ph
Ph
Ph
Ph
PPM
2
4
5
6

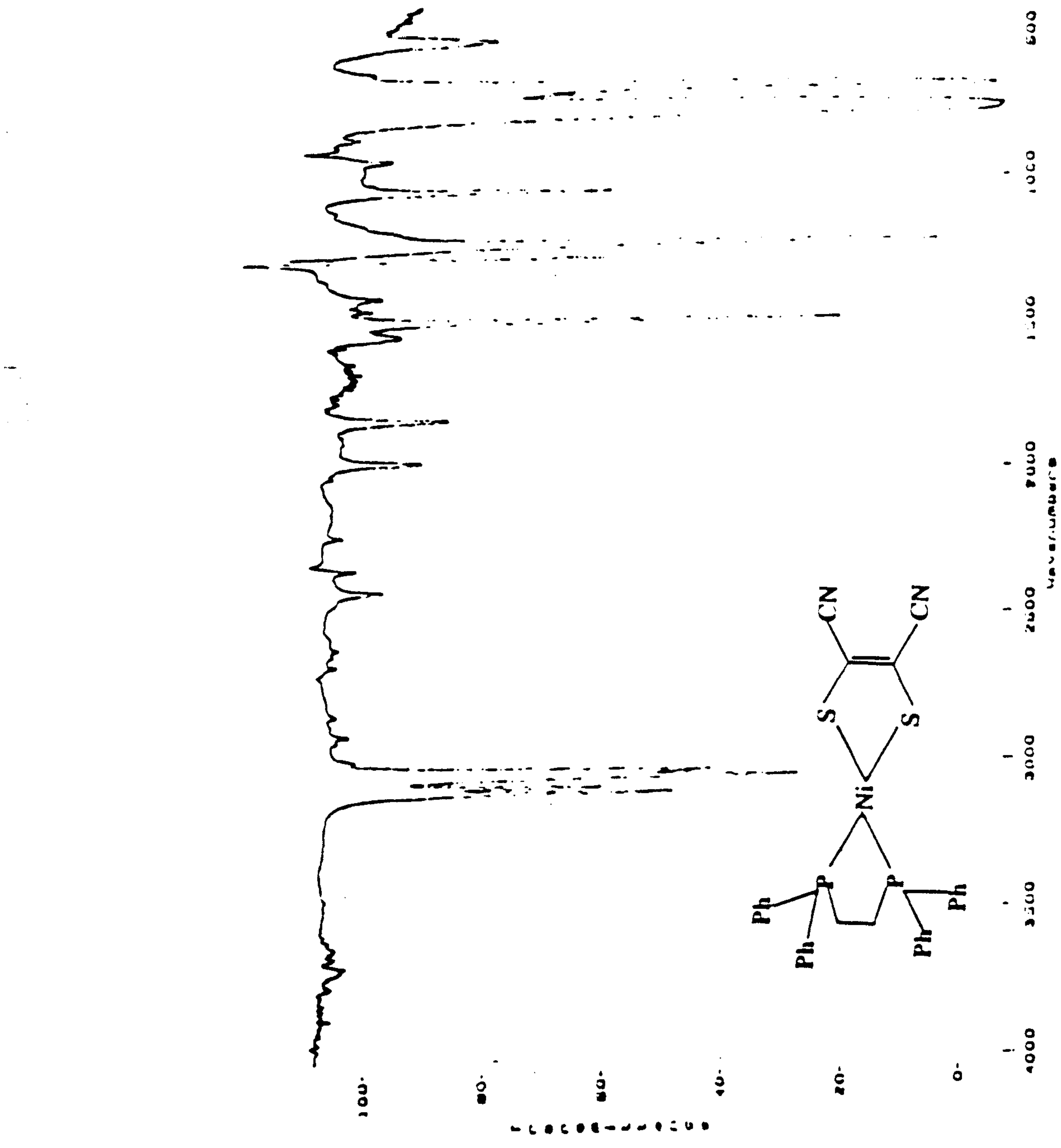
%Transmittance
100
80
60
40
20
0
4000
3500
3000
2500
2000
1500
1000
500
Wavenumbers
Ph
Ph
P
P
Ph
Ph
Ni
S
S
CN
CN

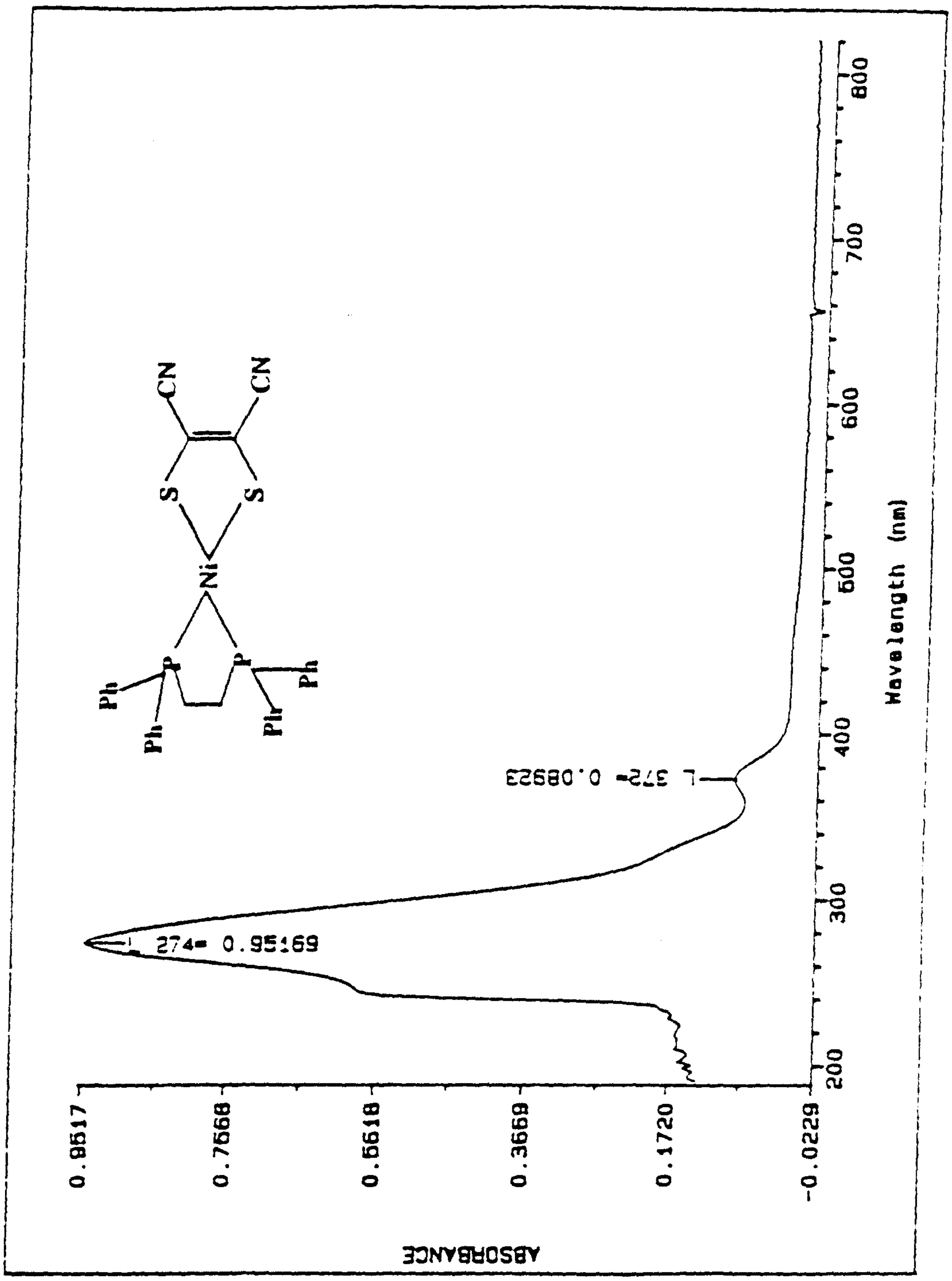
ABSORBANCE
0.9517
0.7568
0.5618
0.3669
0.1720
-0.0229
200
300
400
500
600
700
800
Wavelength (nm)
274= 0.95169
L 372= 0.08923
Ph
Ph
P
P
Ph
Ph
Ni
S
S
CN
CN

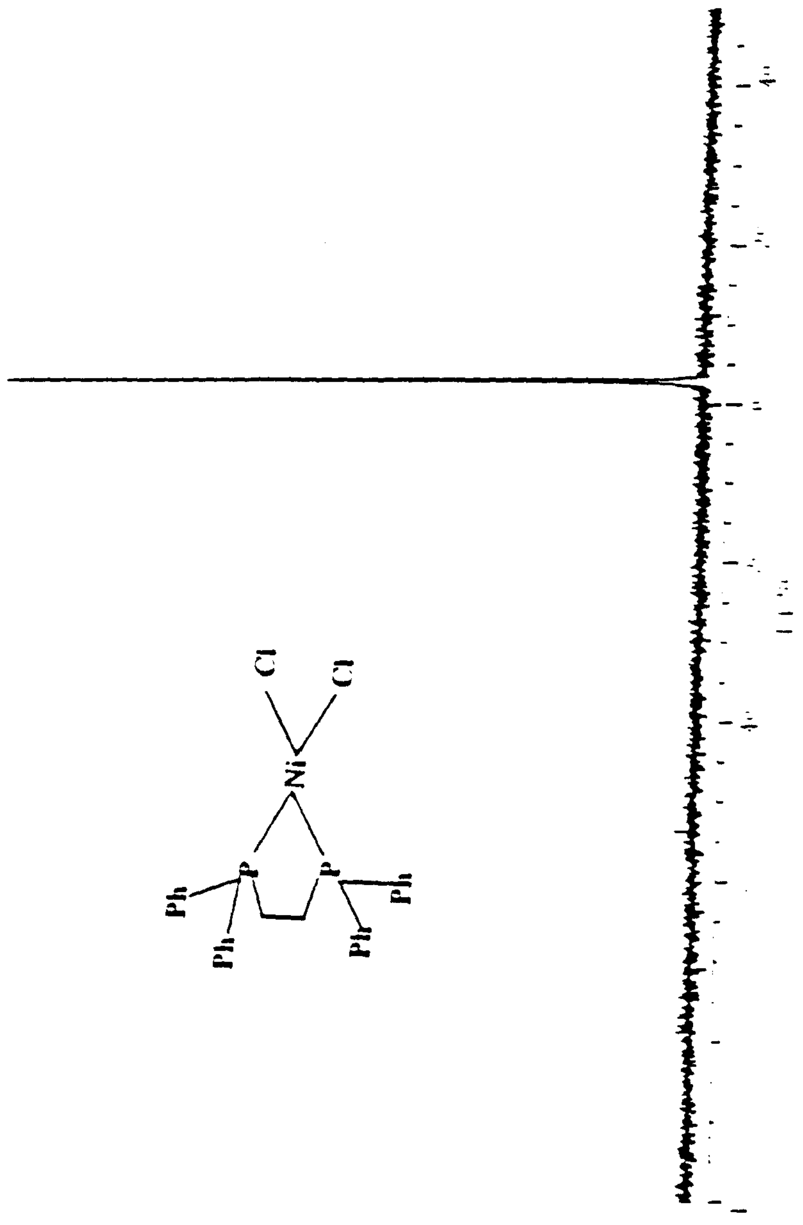
Cl
Cl
Ni
P
P
Ph
Ph
Ph
Ph

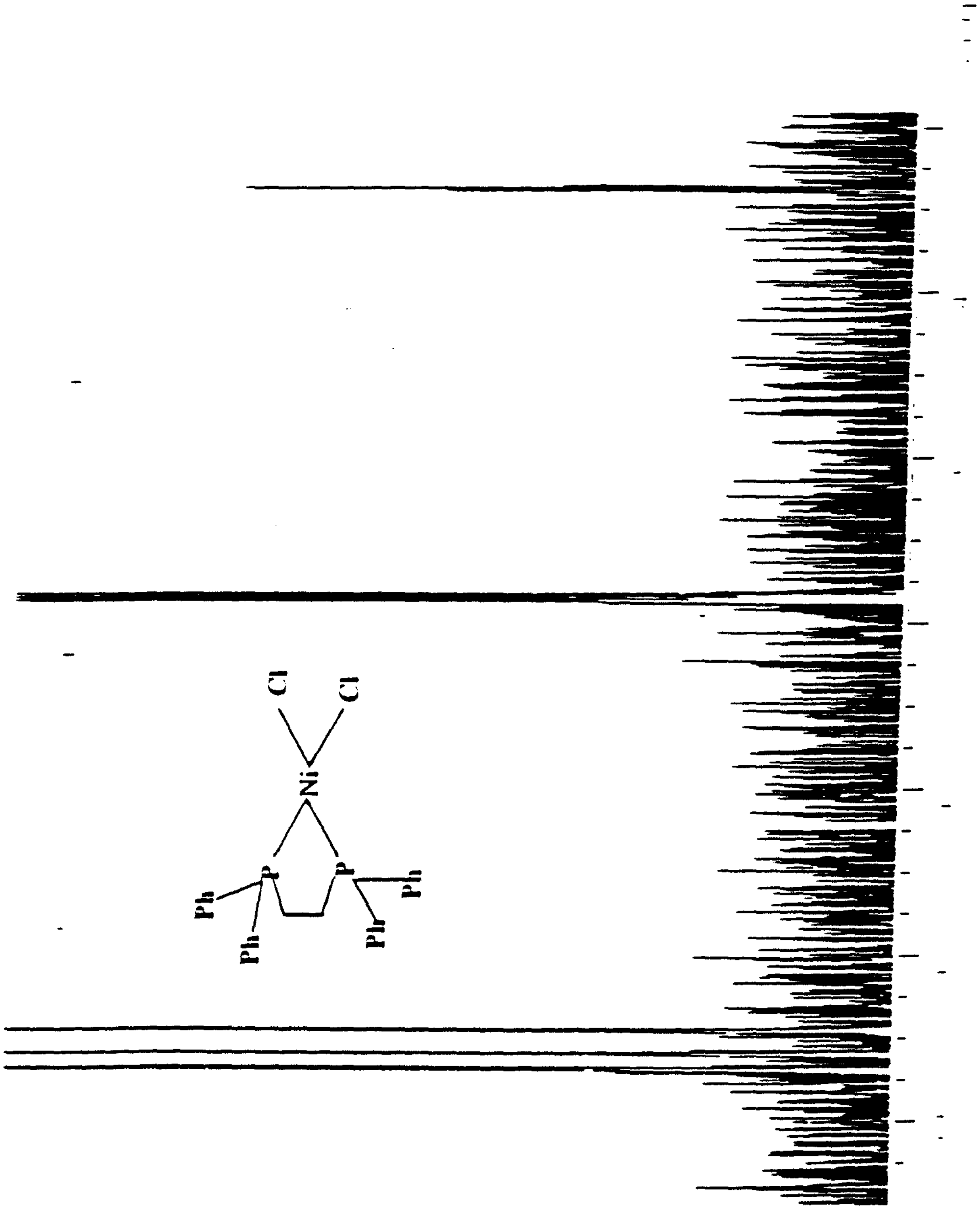
Cl
Cl
Ni
P
P
Ph
Ph
Ph
Ph

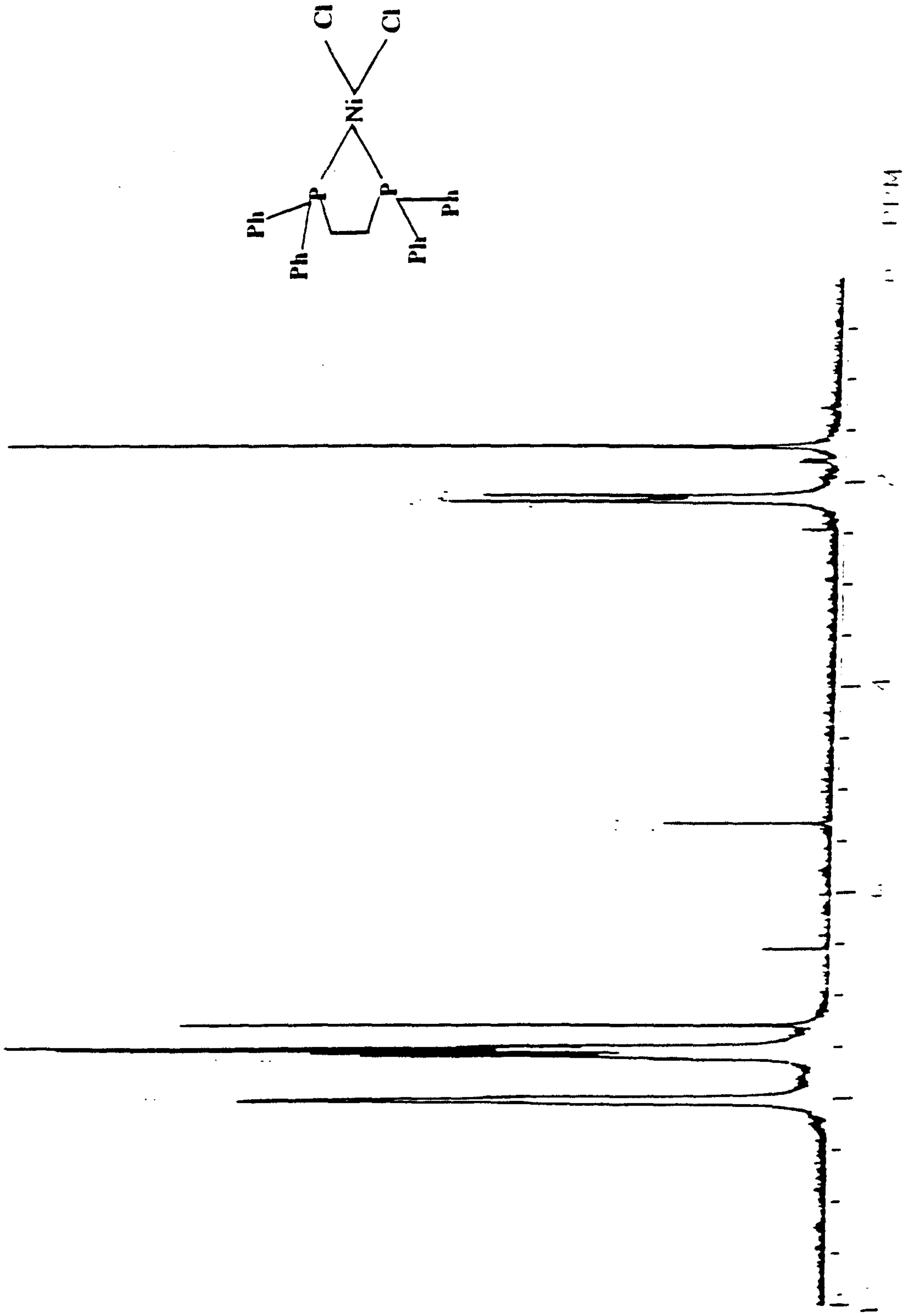
Cl
Cl
Ni
P
P
Ph
Ph
Ph
Ph
PPM

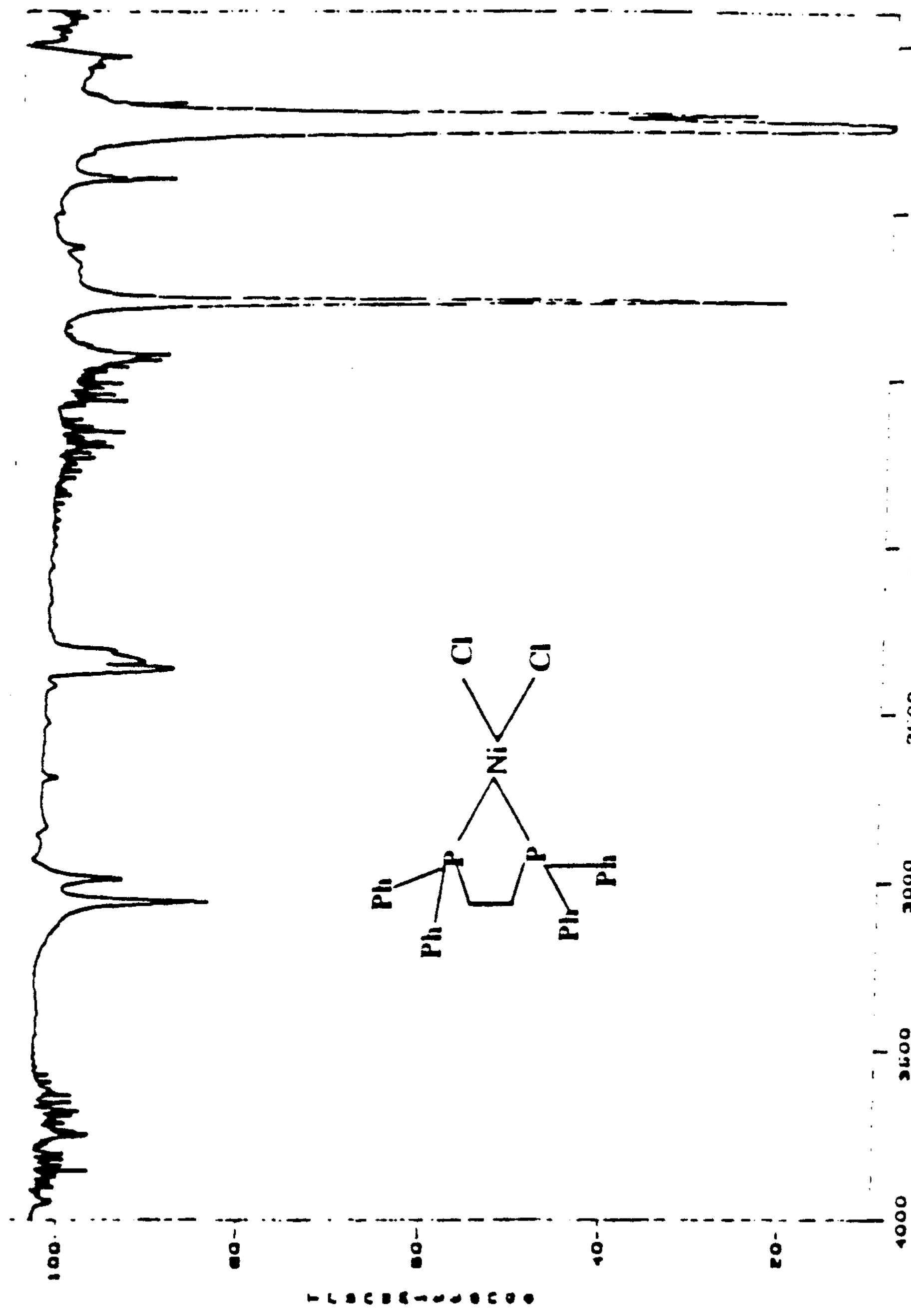

%Transmittance
Wavenumbers
100
80
60
40
20
4000
3500
3000
2500
2000
1500
1000
500
Cl
Cl
Ni
P
P
Ph
Ph
Ph
Ph

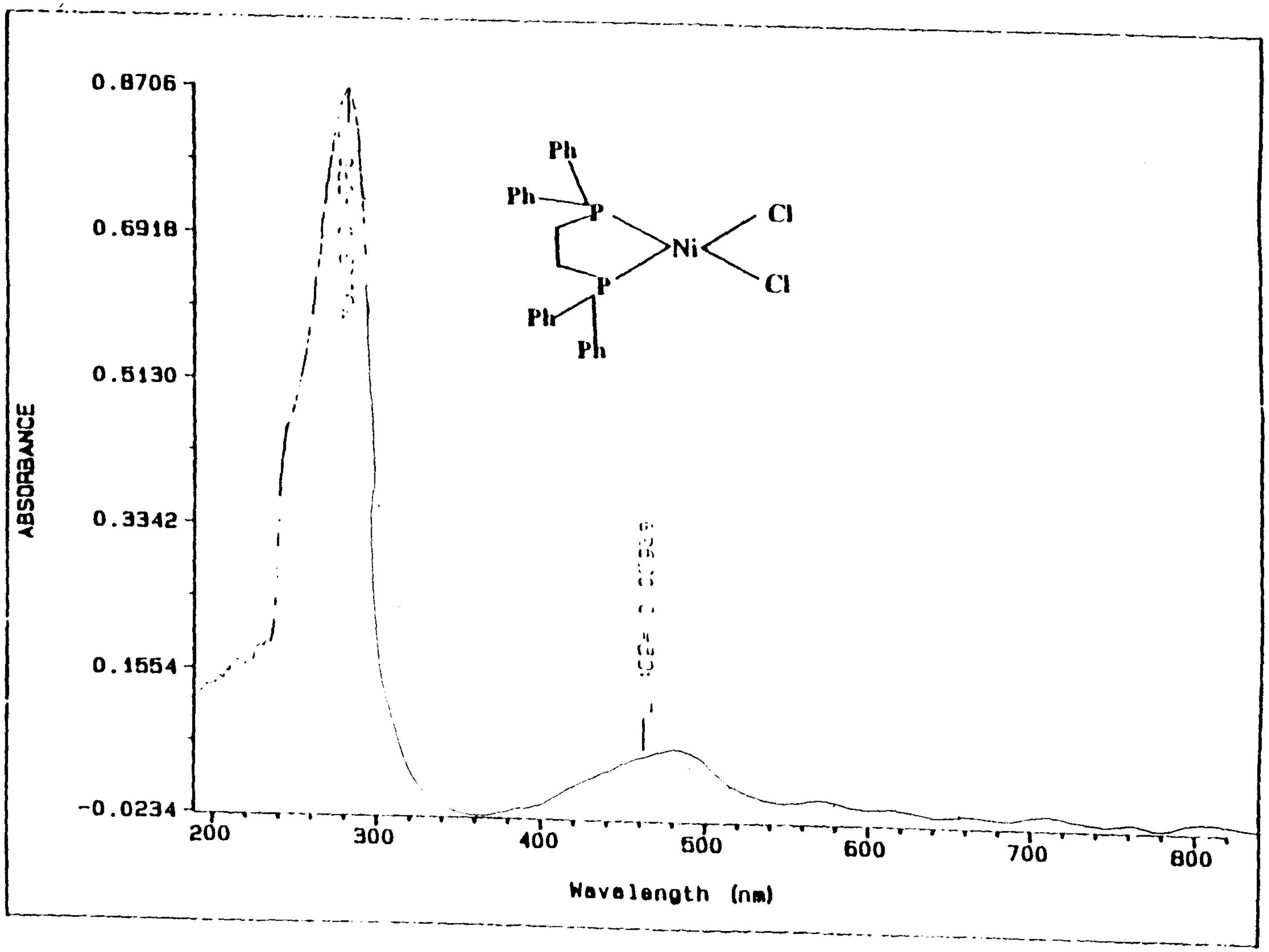
ABSORBANCE
0.8706
0.6918
0.5130
0.3342
0.1554
-0.0234
200
300
400
500
600
700
800
Wavelength (nm)
Ph
Ph
P
P
Ni
Cl
Cl
Ph
Ph

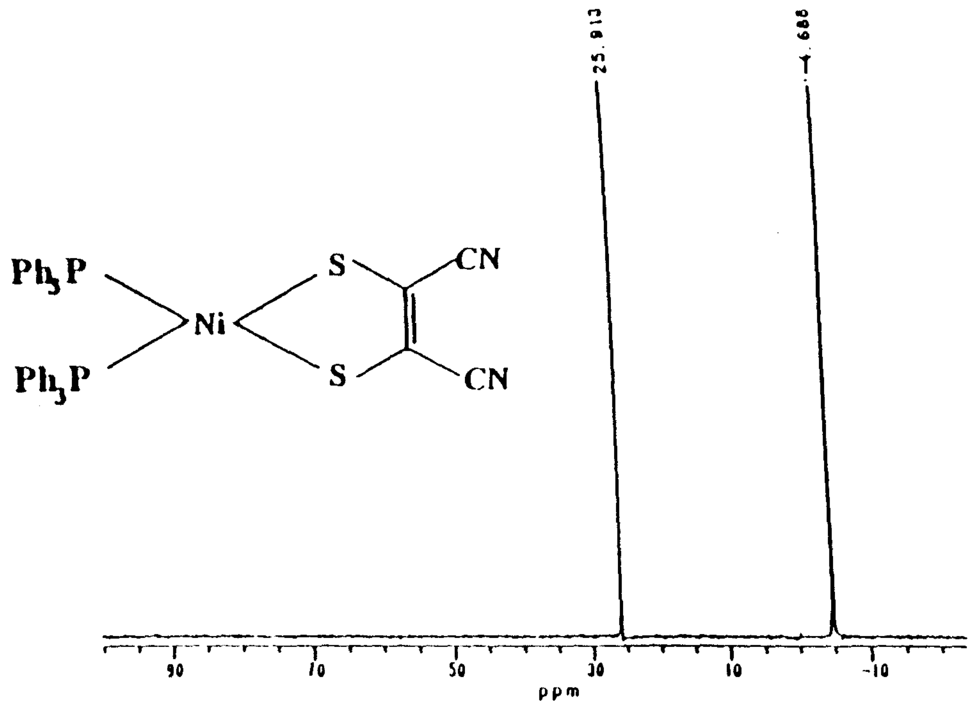
Ph3P
Ph3P
Ni
S
S
CN
CN
25.913
-4.688
90
70
50
30
10
-10
ppm

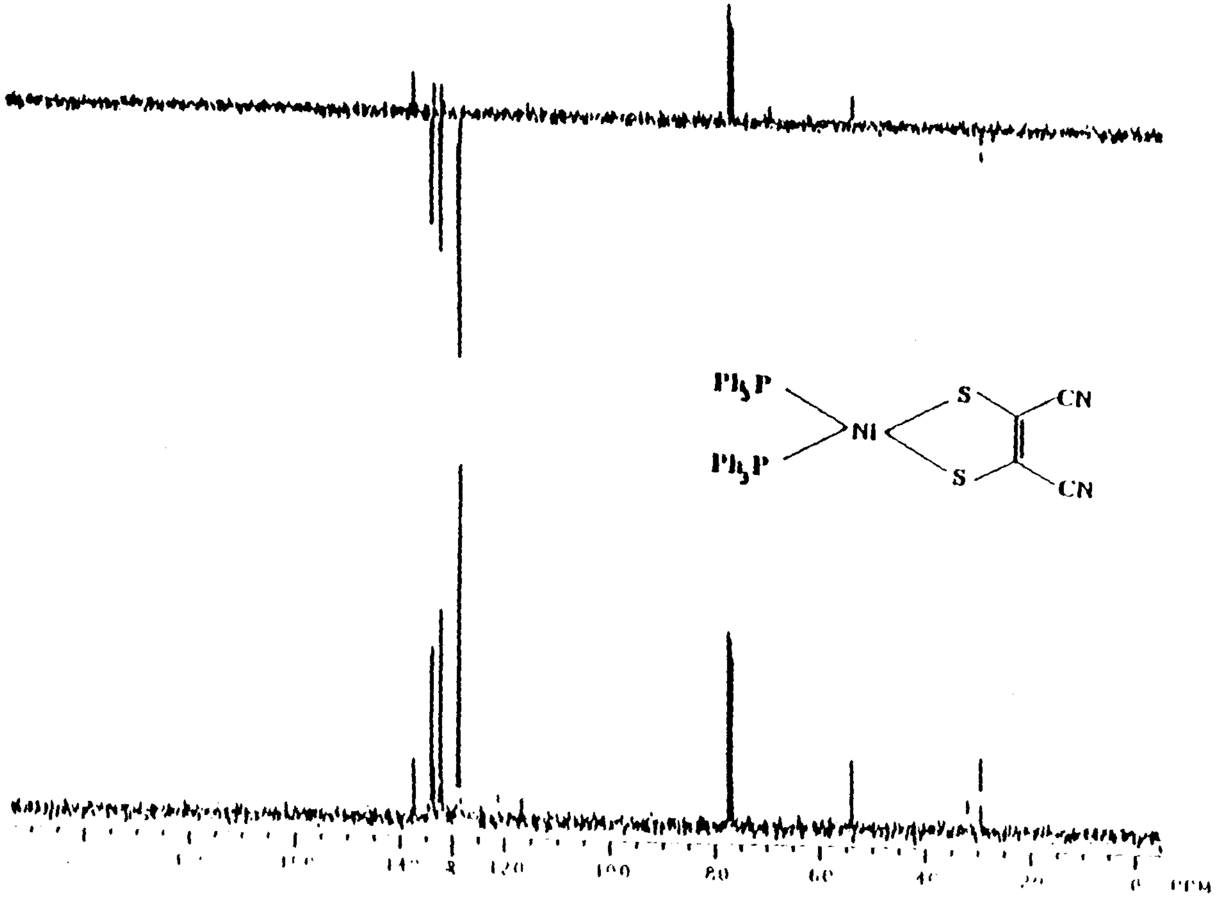
Ph3P
Ph3P
Ni
S
S
CN
CN
140
120
100
80
60
40
0
PPM

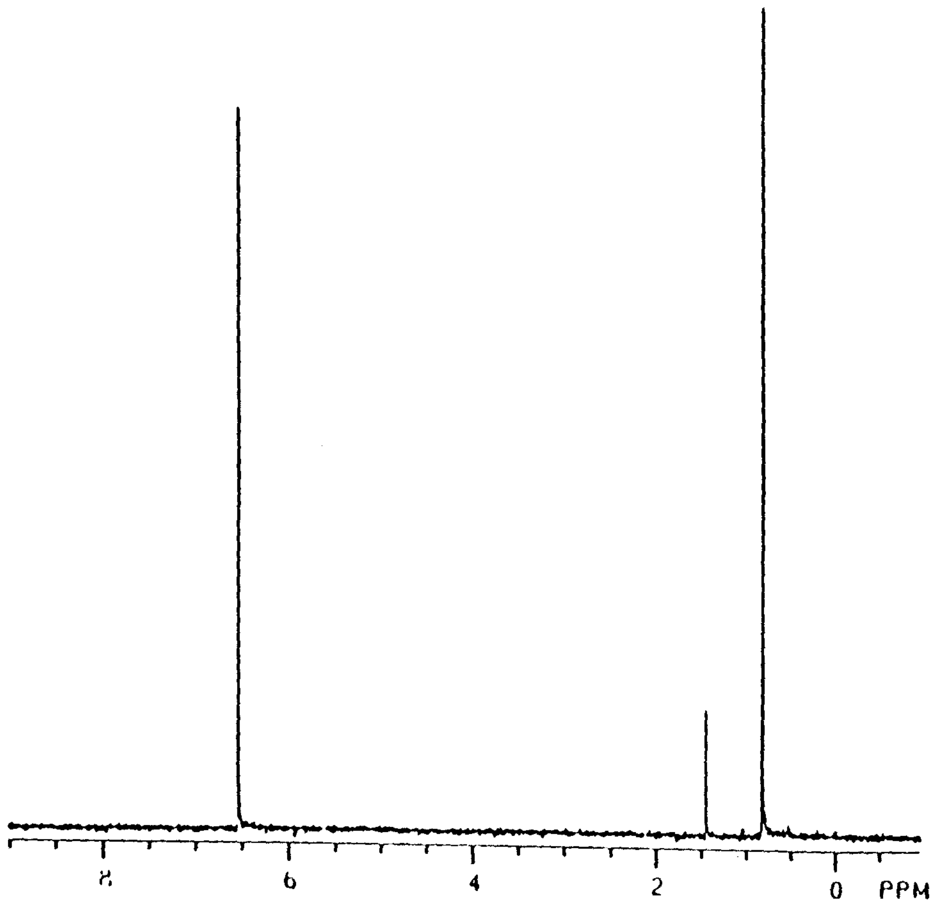
8
6
4
2
0
PPM

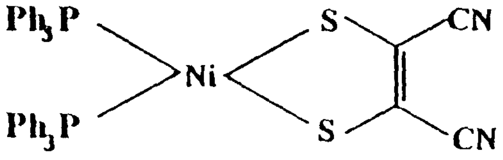
Ph3P
Ph3P
Ni
S
S
CN
CN

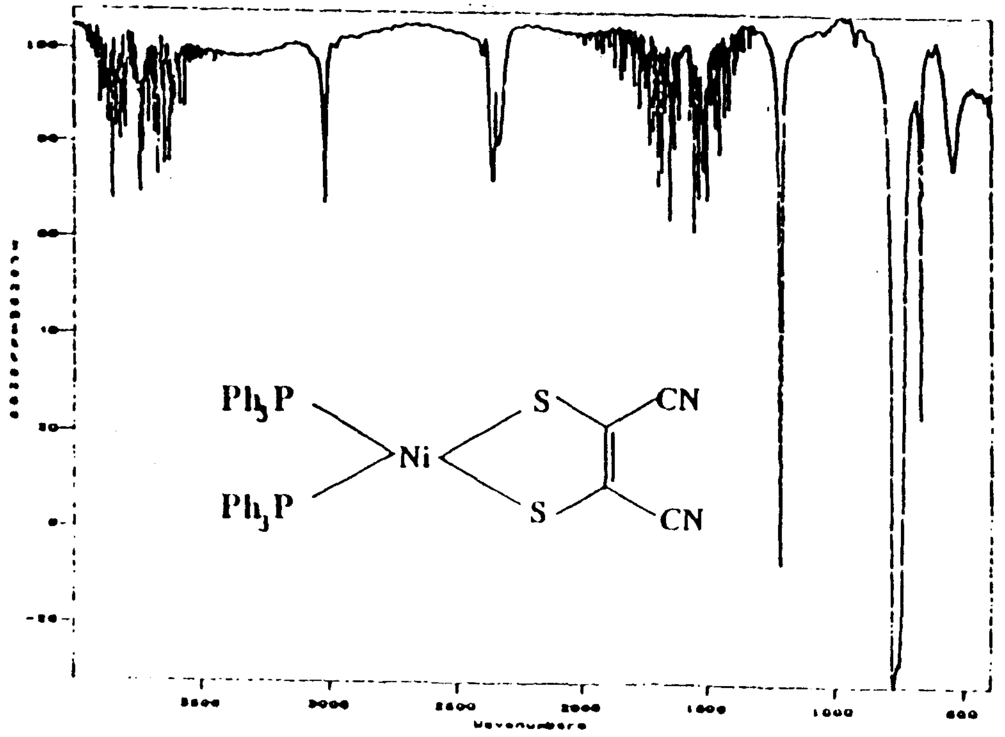
100
80
60
40
20
0
-20
3500
3000
2500
2000
1500
1000
500
Wavenumbers
Ph3P
Ph3P
Ni
S
S
CN
CN

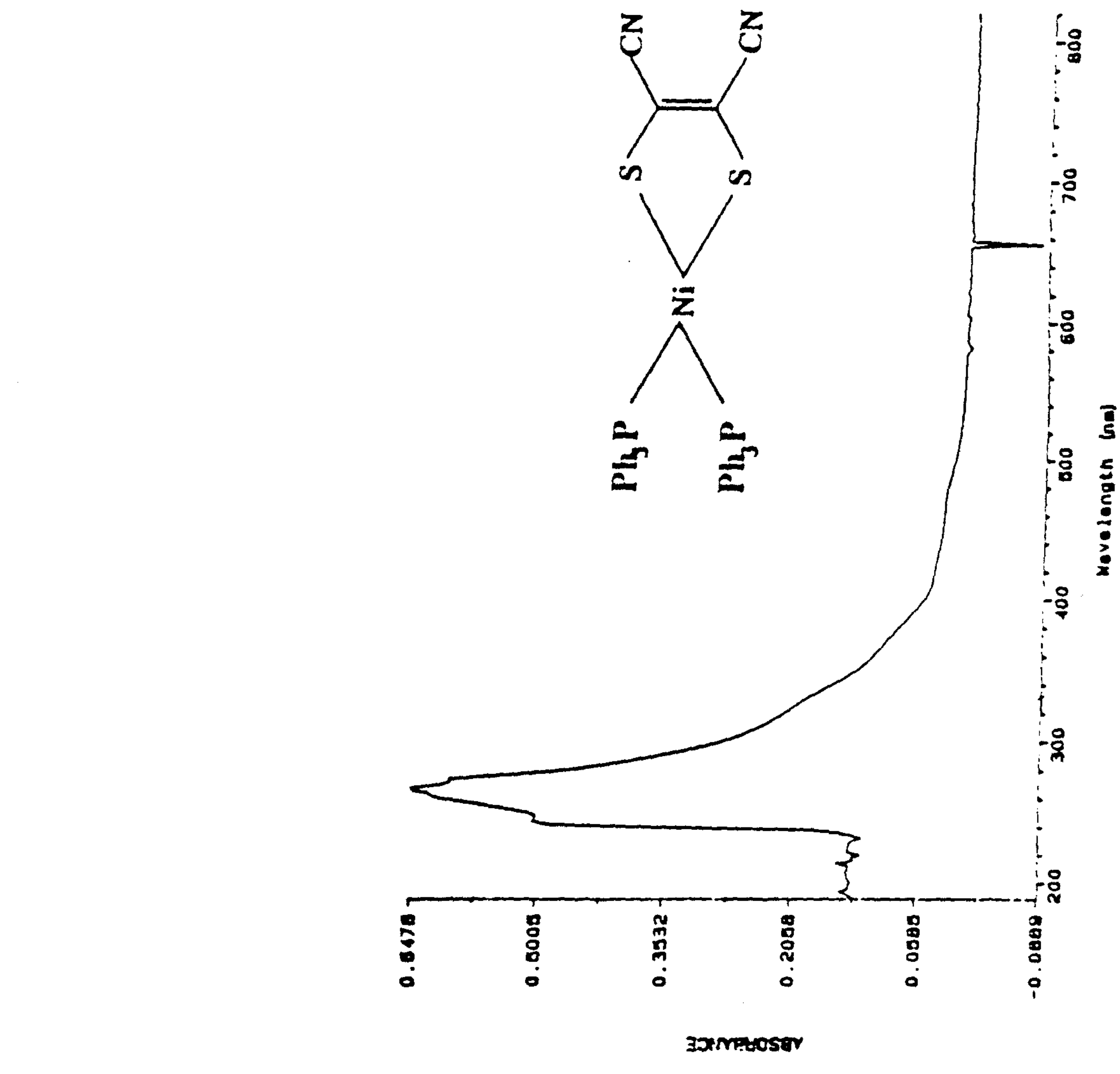
Ph$_3$P
Ph$_3$P
Ni
S
S
CN
CN
ABSORBANCE
0.6478
0.5005
0.3532
0.2058
0.0585
-0.0889
200
300
400
500
600
700
800
Wavelength (nm)